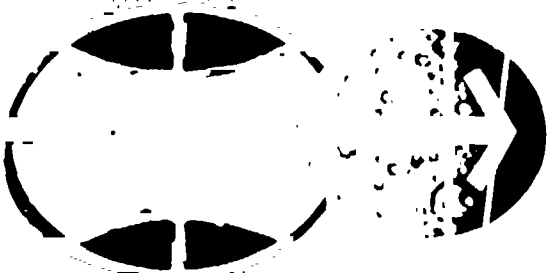NATIONAL AERONAUTICS AND SPACE ADMINISTRATION

APOLLO 13 MISSION REPORT

GUIDANCE, NAVIGATION, AND CONTROL SYSTEMS

PERFORMANCE ANALYSIS

MANNED SPACECRAFT CENTER

HOUSTON, TEXAS

September 1970

APOLLO 13 MISSION REPORT

SUPPLEMENT 1

GUIDANCE, NAVIGATION, AND CONTROL SYSTEMS PERFORMANCE

PREPARED BY

TRW Systems

APPROVED BY

James A. McDivitt
Colonel, USAF
Manager, Apollo Spacecraft Program

NATIONAL AERONAUTICS AND SPACE ADMINISTRATION

MANNED SPACECRAFT CENTER

HOUSTON, TEXAS

September 1970

11176-H586-R0-00

PROJECT TECHNICAL REPORT
TASK E - 38D

APOLLO XIII GUIDANCE, NAVIGATION, AND CONTROL
SYSTEMS PERFORMANCE ANALYSIS REPORT

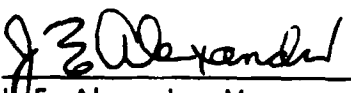NAS 9-8166   24 JULY 1970

Prepared for
NATIONAL AERONAUTICS AND SPACE ADMINISTRATION
MANNED SPACECRAFT CENTER
HOUSTON, TEXAS

Prepared by
Guidance and Control Systems Department

Approved by _____
J. E. Alexander, Manager
Guidance and Control Systems
Department

TRW
SYSTEMS GROUP

CONTENTS

Contents (Continued)

TABLES

Tables (Continued)

ILLUSTRATIONS

Illustrations (Continued)

Illustrations (Continued)

Illustrations (Continued)

NOMENCLATURE

ACA	Attitude Controller Assembly
ACB (X, Y, Z)	Accelerometer bias (channels X, Y, Z)
ADSRA (X, Y, Z)	Gyro drift due to acceleration along the spin reference axis (Channels X, Y, Z)
ADIA (X, Y, Z)	Gyro drift due to acceleration along the input axis (Channels X, Y, Z)
AGS	Abort Guidance System
AOT	Alignment Optical Telescope
APS	Ascent Propulsion System
ASA	Abort Sensor Assembly
BDA	Bermuda (tracking station)
CDU	Coupling Data Unit
COAS	Crew Optical Alignment Sight
CM	Command Module
CMC	Command Module Computer
DAP	Digital Auto Pilot
DEDA	Data Entry and Display Assembly
DPS	Descent Propulsion System
DSKY	Display and Keyboard
EPC	Earth Prelaunch Calibration
FDAI	Flight Director Attitude Indicator
GDA	Gimbal Drive Actuator
GDS	Goldstone (tracking station)
GET	Ground Elapsed Time (Range Time)
G&N	Guidance and Navigation
GSOP	Guidance System Operational Plan
HOPE	Houston Operations Predictor/Estimator
IFC	Inflight Calibration
IMU	Inertial Measurement Unit
IRIG	Inertial Rate Integrating Gyro
JPL	Jet Propulsion Laboratory

Nomenclature (Continued)

LGC	LM Guidance Computer
LM	Lunar Module
LOS	Line-of-sight
LOX	Liquid Oxygen
MCC	Midcourse Correction
MERU	Milli-Earth Rotational Units
MIC	Minimum Impulse Control (mode)
MSC	Manned Spacecraft Center
NASA	National Aeronautics and Space Administration
NAT	NASA Apollo Trajectory
Omega P'error	Rate error about P axis
Omega U'error	Rate error about U' axis
Omega V'error	Rate error about V' axis
P error	Yaw axis error
PGNCS	Primary Guidance, Navigation and Control System
PIC	Pre-Installation Calibration
PIPA	Pulsed, Integrating Pendulous Accelerometer
PPM	Parts per Million
PTC	Passive Thermal Control
RCS	Reaction Control System
REFSMMAT	Reference to Stable Member Matrix
RHC	Rotational Hand Controller
RSS	Root of the Sum of the Squares
RTCC	Real Time Control Center
S/C	Spacecraft
SFE(X, Y, Z)	Scale Factor (Channels X, Y, Z)
SM	Service Module
SODB	System Operational Data Book
SPS	Service Propulsion System
SIVBIU	Saturn IVB Instrumentation Unit

Nomenclature (Continued)

TEI	Trans-Earth Insertion
THC	Translational Hand Controller
TLI	Trans-Lunar Injection
TTCA	Thrust and Translation Controller
U error	Computed Errors
U' error	Computed Errors
V error	Computed Errors
V' error	Computed Errors
VG	Velocity Gained
VO (X, Y, Z)	Velocity Offset (X, Y, Z)
a_x	Measured gravity vector in IMU coordinates (x)
a_y	Measured gravity vector in IMU coordinates (y)
a_z	Measured gravity vector in IMU coordinates (z)
μg	Micro-gravities
P, U, V axis	DAP control axis oriented relative to LM body axes as shown below:
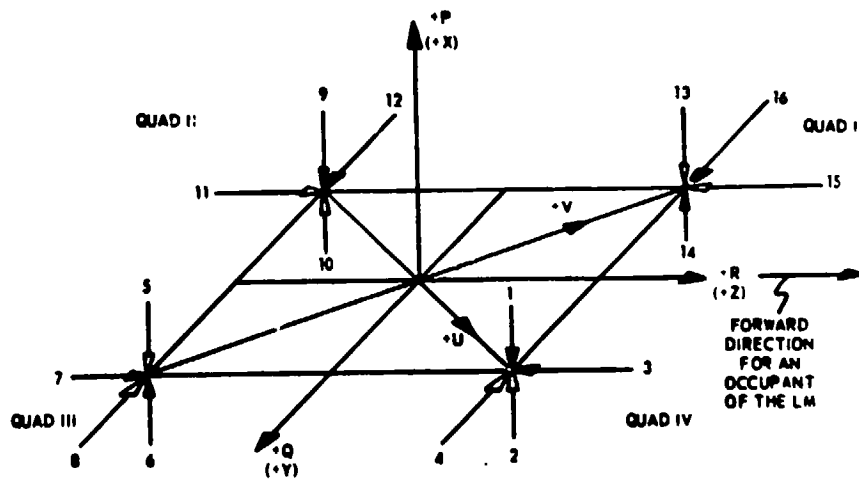
1.0   INTRODUCTION

This report presents the conclusions of the analyses of the inflight performance of the Apollo 13 mission Guidance, Navigation and Control equipment onboard the CSM-109 and LM-7 spacecrafts. This analysis is supplement 1 to the Apollo 13 Mission Report (Reference 1).

2.0 SUMMARY

CM IMU

Analysis of the ascent and TLI burn errors indicated an X-gyro constant drift which was outside of the 1σ specification (2 meru). The derived values were 3.14 meru for ascent and 2.35 meru for TLI. There is evidence that this apparent instrument error actually resulted from an inappropriate gyro drift compensation load. PIPA bias values were reasonably stable during the time the IMU was turned on, but the Z PIPA bias value shifted approximately 1.64 cm/sec^2 across the long power down period and required a CMC compensation update prior to entry.

After the SM LOX tank incident occurred, the IMU power supply underwent degradation. Concurrently, the PIPA's registered a low level acceleration which was first interpreted as venting. However, doppler radar failed to confirm venting of the necessary magnitude. It is now believed that the degradation in power supply voltage induced a corresponding transient in PIPA performance.

CM OPTICAL NAVIGATION

Processing of translunar P23 (star-horizon) data indicates that the actual horizon altitude was about 18 kilometers. However, the apparent altitude (due to small sighting errors) was about 10 kilometers.

LM IMU

IMU performance was good. PIPA bias values were quite stable about their prelaunch values. No direct measurement of gyro drift was obtained, but there is good evidence that total (RSS) misalignment of the IMU at the time of the TEI burn-after 20.5 hours of gyro drift - was of the order of 0.5 to 0.6 degrees. The 1σ value from LM IMU drift alone (ignoring initialization errors) is 1.1 degrees, indicating excellent gyro performance.

LM DIGITAL AUTOPILOT

During the mission, the LM DAP was called upon to control both LM/CSM and LM/CM spacecraft configurations in auto maneuver and attitude hold modes. Performance was satisfactory in all cases although in some instances violations of deadband limits did occur.

The roll GDA was observed to drive approximately -1.3 degrees from its initial position at the start of the TEI burn, stimulating conjecture that the engine gimbal trim function might have been abnormal. Detailed analysis indicated that this position change was necessary to relieve compliance and correct for initial mistrim. Performance is now believed to have been nominal.

Difficulty was encountered when attempting to maneuver the spacecraft into the PTC attitude following the TEI burn. Downlink data were not available for the maneuver, so that investigation was necessarily restricted. One explanation was found by a theoretical examination of cross couplings resulting from various control modes. It was determined that the use of rotational commands would have resulted in significant cross coupling (due to jet impingement forces) and drastic alterations in the intended commands. Although purely translational commands were planned for this maneuver, it is hypothesized that some rotational commands were intermingled and were the source of the problem.

Another possible explanation is that the difficulty arose from the necessity of determining hand controller commands purely by interpreting gimbal angle displays on the DSKY. This was necessary because the FDAI was powered down.

LM ABORT GUIDANCE SYSTEM

The AGS was used for spacecraft control in two burns, MCC 3 and MCC 4. In both cases, performance was satisfactory.

AGS gyro and accelerometer errors were estimated from free flight data and from AGS/PGNCS velocity comparisons obtained during the TEI burn. Instrument static errors showed excellent stability. The TEI burn afforded the only opportunity for observing acceleration sensitive errors. Instrument dynamic performance during that burn was within the 2σ limits determined from the ASA023 error model. This is excellent performance, particularly in view of the fact that the ASA023 dropped 23 degrees F below its specified minimum temperature (60° F) during the 24 hour period in which it was shut down prior to the TEI burn.

LM OPTICAL ALIGNMENT CHECKS

Prior to the TEI burn the LGC was used to aim the AOT line-of-sight in the LGC calculated sun direction. This was done to assess IMU alignment errors and resulted in an estimated misalignment of 0.5 degrees. By its nature, the check could not resolve errors about the line-of-sight. However, the line-of-sight direction was such that misalignments about it had negligible impact on significant state vector errors induced by the IMU during the TEI burn. As conducted, the check determined only the magnitude of the misalignment in one plane - that plane in which misalignments were of greatest consequence. The direction of these errors was not determined, and therefore the appropriate corrective IMU torques could not be calculated. The IMU misalignment generated a burn error of approximately 5.3 feet/second in the TEI burn. Unfortunately, much of this error was in the direction most critical to entry flight path angle; the resultant (potential) error in the post-TEI trajectory entry flight path angle was in excess of -4 degrees. The allowable error in flight path angle is 0.5 degrees. Two midcourse corrections were subsequently required to correct this error.

An alignment of the LM IMU was performed using the sun and moon
as optical targets in preparation for the MCC 4 burn. A star angle dif-
ference of -1.12 degrees was computed by the LGC and displayed on the
DSKY, indicating a very large astronaut sighting error. It was sub-
sequently determined that the actual sighting error was only about .08
degree. The remainder of the apparent sighting error arose from in-
accurate LGC ephemeris data for the moon and sun, and from the LGC
software.

3.0   CM SYSTEMS

3.1   CM INERTIAL MEASUREMENT UNIT

3.1.1   Velocity Comparisons During Ascent and TLI

The Apollo 13 CM IMU performance analysis was based on comparisons
of Apollo (denoted G&N) and Saturn (denoted S-IVB) measured velocities.
Analysis centered around the "sensed" velocities - those resulting
from integration of that portion of the vehicles acceleration which can
be sensed by the accelerometers. Sensed velocities exclude the influence
of the gravitational field. In addition to the sensed velocity com-
parison, a cross check of ascent phase results was obtained by analyzing
"total" velocity differences. Total velocity is the actual vehicle
velocity in inertial space. It is obtained by integrating both sensed
acceleration (due to engine thrusting) and gravitational acceleration.
The cross check was performed because telemetry data dropouts caused
minor discrepancies in the GN sensed velocity estimates. Sensed and
total velocity differences are presented below for the end of the ascent
phase (t = 752 seconds, CMC clock time) and for TLI cutoff (t = 9704.48)

Time	Type of Comparison	Comparison	$\Delta\dot{X}$ (ft/sec)	$\Delta\dot{Y}$ (ft/sec)	$\Delta\dot{Z}$ (ft/sec)
752.0 sec	Sensed	G&N - S-IVBIU	-6.75	87.04	- 3.82
752.0 sec	Total	G&N - S-IVBIU	-5.41	75.51	1.02
9704.48 sec	Sensed	G&N - SIVBIU	-20.50	- 2.50	2.03

IU represents the edited Saturn telemetry data.

The ascent and TLI uncompensated sensed velocity differences (G&N - S-IVBIU) appear in Figures 3-1 through 3-6. Those IMU errors solved for in this analysis are defined in Table 3.1. IMU error sets derived to fit the ascent and TLI velocity differences are presented in Table 3.2. Close agreement was obtained between the results of the sensed and total velocity analyses, so that inclusion of the results for the total was unnecessary. Compensated sensed velocity differences (G&N - S-IVBIU, where the G&N data has been compensated with the derived IMU errors) are presented in Figures 3-7 through 3-12.

3.1.2 Ascent and TLI Error Determination

The Apollo 13 G&C system accuracy analysis was based upon the determination of a common set of errors which resulted in small residuals for both the boost to orbit phase and the translunar insertion phase. The analysis is accomplished with the aid of a Kalman Filter which solves for a "best" set of IMU errors for minimizing the velocity differences in a least squares sense. Several constraints were imposed on the errors used. The bias values for accelerometers (Table 3.3) and gyros were forced to be in close agreement with inflight determined values and the other error terms were chosen to agree favorably with preflight calibration histories. Due to various physical factors such as actual parameter shifts during the boost phase and degradation of the reference data between the two flight phases (2.4 hours of drift between ascent and TLI) it was again recognized that all of the above conditions could not be met at all times. Based on engineering judgement, the approach pursued was to seek two sets of error sources with bounded variations $(\pm 1\sigma)$. The error terms derived for the sensed analyses are presented in Table 3.2, and using these values, the G&N corrected trajectories fit the respective external measurement (S-IVBIU) trajectories. The maximum deviation between the derived ascent and TLI error sources was 0.86σ.

The derived boost and TLI values for NBDX (X Gyro Constant Drift Rate) exceeded the 1σ (2 meru) instrument stability criteria. The derived values were 3.14 meru (ascent) and 2.35 meru (TLI). These represent 1.57σ and 1.18σ values respectively for boost and TLI. Preflight data obtained at Cape Kennedy, from 3 July 1969 to 3 April 1970, revealed a pronounced negative trend which peaked out at -3.3 meru on 6 January 1970. Overall NBDX Cape test results are somewhat erratic. Following the referenced negative peak, NBDX results varied considerably. For the subsequent four calibrations, the quantity began trending positive and the last calibration value on 3 April 1970 was 0.5 meru. The CM computer erasable memory compensation value for NBDX was -0.7 meru. If the term continued to trend positively, it is probable that an effective error on the order of 2-3 meru did exist during ascent and TLI. Consequently, it is understandable that the derived values for NBDX did exceed the 1σ instrument stability criteria. The apparently large shift in drift probably reflects a compensation error rather than instrument degradation. All other error sources were within 1σ limits.

3.1.3 Quick Look Evaluation

It is worthwhile to point out that a technique has been developed for taking a gross "quick look" at IMU performance without recovering individual instrument errors. This was done for the Apollo 13 CM IMU by comparing actual ascent cut-off state errors with standard deviations of these errors. The standard deviations used for this comparison were obtained by integrating an ensemble of 1σ IMU instrument errors along the ascent trajectory. Resultant 1σ state errors formed trajectory bounds from which IMU performance could be gauged in the system sense; i.e., from which it could be determined whether or not overall IMU performance as a navigation instrument was within 1σ bounds. This gross "quick look" technique provided an additional confidence factor in the derived NBDX error source values discussed, inasmuch as it demonstrated that IMU performance was not within specifications during ascent. A comparison of actual with 1σ velocity errors is presented as follows (at t = 752 seconds GET):

	X (Ft)*	Y (Ft)	Z (Ft)	$\Delta\dot{X}$ (Ft/Sec)	$\Delta\dot{Y}$ (Ft/Sec)	$\Delta\dot{Z}$ (Ft/Sec)
1σ:	1434	27630	3542	4.46	61.89	9.88
Actual:	3555.8	32220.6	1316	-5.41	75.51	1.02

*The position and velocity values are totals
(units as noted).

3.1.4 Impact of Power Supply Degradation on CM PIPA Behavior

Immediately following the SM LOX tank incident at 55:54:53 GET,
the CM downlink recorded PIPA pulses which resembled the effect of venting.
However, efforts to reconcile these data with doppler radar measurements
met with failure. Consequently it was theorized that the actual pheno-
menon being observed might be a bias shift in the PIPA's due to power
supply transients, rather than accelerations due to venting. To support
this hypothesis, an effort was made to correlate power supply transients
with observed PIPA data.

Figure 3-13 is a plot of the 28VDC Main A, 120VDC PIPA supply and
the 3.2 KC 28V power supplies at the time of the LO_2 tank event at 55:54:53
GET. The 120V PIPA supply and the 3.2 KC 28V supply began to degrade when
the 28VDC Main A supply reached 26.3 volts. Figure 3.14 is a plot of the
accumulated thrust velocity (V_{SX}, V_{SY}, V_{SZ}) indicated by the PIPA's through
the time of the voltage transient; superimposed on this is a plot of MSFN
doppler radar residuals for the same time period. The change in PIPA
velocities can be directly correlated to the degraded voltage. The reason
for the different PIPA responses (i.e., XPIPA does not show response to the
sharp voltage transient at 56:00 and 56:03 as do Y and Z) is unknown.
Referring to the plot of the Bermuda/Goldstone tracking station doppler
residuals through the period of interest, no appreciable change is noted
between 55:57:56 and 56:03:10, the region of the 120V PIPA supply transient.

3-4

Shifts in the doppler residuals near 55:55:00 and 56:03:30 resemble velocity changes indicated by the X PIPA which is pointed principally along the LOS to Earth. The trend shown by the X PIPA however, is not reflected in the doppler data, thus indicating that X PIPA velocity indications were erroneous.

Following the event, the CSM IMU was powered down (including instrument heaters) at 58:40 GET and remained down until 140:10 GET. At IMU power up, a shift of 1.64 cm/sec^2 was noted on the Z PIPA and as a result a bias update was performed prior to entry. Table 3.3 is a summary of the PIPA bias before and after the event.

3.2 CM OPTICAL NAVIGATION

Prior to the SM LOX tank incident, two batches of navigation sightings were conducted. The data obtained from these sightings is listed in Table 3.4. These data were analyzed for the purpose of estimating sextant trunnion bias and earth horizon bias.

Two basic options were available for analysis of these data. In Option 1, only trunnion angle data is processed. This option assumes that the astronaut was successful in locating the substellar "point" - i.e., in placing his horizon line-of-sight on the line connecting the star with the earth's center. Option two utilizes gimbal and shaft angle data for the purpose of correcting erroneous determinations of the substellar point. In addition to these options, batch one was processed using:

Method 1: Horizon altitude only estimation, and

Method 2: Horizon altitude and trunnion bias estimation, with no a priori estimate of these parameters (i.e., with initial estimates weighted such that they had no effect on the solution).

The combination of methods one and two with options one and two yielded four cases. The output of these cases were used as the input (initialization values) for the processing of batch two. Table 3.5 presents these combined results. Option 1 results from batch 1 were used only with option 1 runs for batch 2. Likewise, option 2 results from batch 1 were used only with option 2 runs for batch 2.

The results indicate that the actual horizon altitude was about 18 kilometers. However, due to small sighting errors the astronaut was actually sighting on an effective altitude of about 10 kilometers.

Accelerometer Errors

Apollo Mnemonic	Accelerometer Errors
ACBX ACBY ACBZ	Bias
SFEX SFEY SFEZ	Scale Factor
MCXX MCYY MCZZ	SF sensitivity to input acceleration squared
MIAK	MIAK is the misalignment of accelerometer "I" about the "K" platform axis.
(not modeled)	SF sensitivity to coupling of acceleration along input and output axes (ppm/g)

Platform Errors

ILM (X, Y, Z)	Platform Misalignment
DT	Timing Error
VO (X, Y, Z)	Velocity Offset

Gyro Errors

Apollo Mnemonic	Gyro Errors
ADIAX ADIAY ADIAZ	Drift rate sensitivity to acceleration along input axis.
ADSRAX ADSRAY ADSRAZ	Drift rate sensitivity to acceleration along spin axis.
ADOAX ADOAY ADOAZ	Drift rate sensitivity to acceleration along output axis.
ADSXX ADSYY ADSZZ	Drift rate sensitivity to acceleration squared along the spin reference axis.
NBDX NBDY NBDZ	Constant drift rate

Table 3.1   IMU ERROR SOURCES - ACRONYM DEFINITIONS

ERROR SOURCE	PREFLIGHT DATA MEAN	FLIGHT LOAD	EXPECTED ERROR	STANDARD DEVIATION	PREFLIGHT EXPECTED 1σ BOUNDS MAXIMUM	PREFLIGHT EXPECTED 1σ BOUNDS MINIMUM	ASCENT OUTPUT ERROR VALUE	TLI OUTPUT ERROR VALUE	$\left\|\left(\dfrac{\text{ASCENT OUTPUT}}{\text{ERROR VALUE}}\right)-\left(\dfrac{\text{TLI OUTPUT}}{\text{ERROR VALUE}}\right)\right\|$	
VOX (FT/SEC)	NA	NA	NA	NA	NA	NA	-0.462	-0.430	NA	NOT COMPARABLE DUE TO STATE VECTOR UPDATE BETWEEN ASCENT AND TLI.
VOY (FT/SEC)	NA	NA	NA	NA	NA	NA	2.120	-0.032	NA	
VOZ (FT/SEC)	NA	NA	NA	NA	NA	NA	-0.175	-0.927	NA	
BI (FT/SEC)	NA	NA	NA	NA	NA	NA	0.0807	0.005	NA	
ADIX (CM SEC²)	-0.17	-0.17	-0.067	0.28	0.193	-0.207	-0.088	-0.084	NA	OUTPUT ERROR VALUES ESTABLISHED FROM INFLIGHT MEASUREMENTS
ADIY (CM/SEC²)	-0.35	-0.35	0.029	0.28	0.229	-0.171	0.029	0.026	NA	
ADIZ (CM/SEC²)	0.057	-0.06	0.057	0.28	0.358	-0.143	0.044	0.07	NA	
SFRU (PPM)	-119	-120	—	116	117	-116	-48	-73	0.045	INSENSITIVE IN ASCENT
SFRV (PPM)	-164	-159	36	116	142	-90	56	77	3.146	
SFRZ (PPM)	-399	-400	21	116	137	-95	-79	-43	0.293	
MIXAZ (ARC SEC)	NA	NA	NA	20	20	-20	0.9	3.7	0.146	
MIXAY (ARC SEC)	NA	NA	NA	20	20	-20	-17.5	0	0.886	
MIYAZ (ARC SEC)	NA	NA	NA	20	20	-20	0.7	-2.4	0.176	
MIYAX (ARC SEC)	NA	NA	NA	20	20	-20	1.4	-3.1	0.236	
MIZAY (ARC SEC)	NA	NA	NA	20	20	-20	14.8	14.7	0.105	
MIZAX (ARC SEC)	NA	NA	NA	20	20	-20	-1.8	-8.5	0.346	
NBDX (HR/HR)	-0.60	-0.7	0.087	2	2.01	-1.99	3.14	2.35	NA	OUTPUT ERROR VALUES ESTABLISHED FROM INFLIGHT MEASUREMENTS
NBDY (HR/HR)	-1.86	-2.3	0.44	2	2.46	-1.54	-0.90	0.36	NA	
NBDZ (HR/HR)	-3.94	-4.9	0.93	2	2.94	-1.06	1.75	1.75	NA	
ADIAX (HR/G/AVG)	24.0	24.0	-1.88	8	6.91	-9.09	4.22	4.34	0.728	INSENSITIVE IN ASCENT
ADIAY (HR/G/AVG)	8.114	1.0	-0.88	8	7.11	-8.89	-1.42	0.1	0.26	
ADIAZ (HR/G/AVG)	19.10	23.0	-3.00	8	4.17	-11.83	-3.79	-3.8	0v	INSENSITIVE IN TLI
ADSMAX (HR/G²/G)	-1.214	-2.0	0.786	5.0	5.79	-4.21	1.00	2.7	0.336	INSENSITIVE IN ASCENT
ADSRAY (HR/G²/G)	-0.86	0.0	-0.88	5.0	4.91	-5.39	-3.35	-1.5	0.375	
ADSRAZ (HR/G²/G)	-5.37	-4.0	0.69	5.0	5.63	-4.37	2.96	3.09	0.036	
ADIOAX (HR/G/AVG)	1.675	NA	1.675	2-5···	6.48	-3.33	-1.45	-1.63	0.045	
ADIOAY (HR/G/AVG)	0.435	1.6	0.435	2-5···	5.43	-4.58	-4.2	-4.1	0.026	
ADIOAZ (HR/G/AVG)	2.95	NA	2.950	2-5···	7.95	-2.05	1.1	1.11	0v	
IRIG X (ARC SEC)	NA	NA	NA	50···	50···	-50···	22	4	NA	NOT COMPARABLE. TLI VALUES BASED ON PLATFORM MISALIGNMENTS AND 24 HOURS DRIFT BEFORE TLI
IRIG Y (ARC SEC)	NA	NA	NA	50···	50···	-50···	-31	372	NA	
IRIG Z (ARC SEC)	NA	NA	NA	50···	50···	-50···	4	218	NA	

* DATA MEAN MINUS FLIGHT LOAD.

** ASCENT UNOFFICIAL MEASUREMENTS BY MIT.

*** BOOST PHASE ONLY.

NA - NOT APPLICABLE

Table 3.2   IMU ERRORS FOR ASCENT AND TLI (DERIVED FROM SENSED VELOCITY COMPARISONS)

3-9

Table 3.3   CM IMU PIPA BIASES

GET	X Bias (cm/sec^2)	Y Bias (cm/sec^2)	Z Bias (cm/sec^2)
10:10	-0.20	-0.21	0.0
12:25	-0.20	-0.20	0.0
13:05	-0.19	-0.21	0.0
14:35	-0.20	-0.20	0.0
16:35	-0.20	-0.20	0.0
35:09	-0.20	-0.21	0.01
42:48	-0.20	-0.20	0.0
57:16	-0.21	-0.12	-0.01
141:00	-0.18	-0.16	-1.66

C

Table 3.4
APOLLO 13 P23 CISLUNAR NAVIGATION SIGHTING MARKS
BATCH 1

TIME (GET) Hr	Min	Sec	CDUX (Deg)	CDUY (Deg)	CDUZ (Deg)	CDUS (Deg)	CDUT (Deg)	STAR/HORIZON
6	1	1.98	147.2388	340.0488	.5273	0	0	(calibration)
6	1	48.01	146.8982	340.0598	.4834	0	-.0027	(calibration)
6	2	23.26	146.6345	340.0708	.4504	0	-.0027	(calibration)
6	2	34.33	146.5466	340.0818	.4395	0	0	(calibration)
6	2	49.54	146.5906	340.0818	.4285	0	-.0027	(calibration)
6	10	10.24	158.9282	297.3340	359.1980	278.1519	38.7817	33(Octal)/EF
6	11	19.73	158.8293	297.2241	359.2200	278.0420	38.8477	33(Octal)/EF
6	12	29.52	158.5547	297.0923	359.2639	278.0090	38.9108	33(Octal)/EF
6	18	21.40	159.1150	297.3560	358.4729	102.5024	34.5218	221(Octal)/EN
6	18	57.82	159.1589	297.2900	358.4290	102.4915	34.4916	221(Octal)/EN
6	19	34.07	159.1919	297.2131	358.3960	102.5024	34.4614	221(Octal)/EN
6	22	49.81	159.5325	298.0151	357.2754	290.5225	34.0357	125(Octal)/EF
6	23	33.53	159.4885	297.8723	357.1326	290.2039	34.0741	125(Octal)/EF
6	24	11.53	159.5874	297.7405	357.0117	289.9072	34.1016	125(Octal)/EF
6	28	14.13	162.9382	302.0691	357.9565	161.9934	34.0082	40(Octal)/EN
6	30	51.82	163.0151	302.0251	357.7808	161.8396	33.9725	40(Octal)/EN
6	32	9.04	162.4768	301.8933	357.7478	162.8064	33.9478	40(Octal)/EN
6	33	4.23	162.6855	301.8384	357.7148	162.4438	33.9340	40(Octal)/EN
6	39	18.12	162.4878	291.0059	359.7583	217.200	25.2850	42(Octal)/EN
6	39	59.30	162.7185	291.0608	359.7034	218.408	25.3070	42(Octal)/EN
6	41	21.98	162.9163	291.0608	359.6594	219.836	25.3400	42(Octal)/EN
6	41	58.64	162.5208	290.9839	359.6594	216.101	25.3180	42(Octal)/EN

Table 3.4

Apollo 13 P23 Cislunar Navigation Sighting Marks (Continued)

Batch 2

TIME (GET)			CDUX (Deg)	CDUY (Deg)	CDUZ (Deg)	CDUS (Deg)	CDUT (Deg)	STAR/HORIZON
Hr	Min	Sec						
31	8	5.81	147.3486	340.4553	359.9561	0	-.0027	(calibration)
31	8	15.57	147.3596	340.4333	359.9561	0	-.0027	(calibration)
31	8	25.27	147.3596	340.4004	359.9561	0	-.0027	(calibration)
31	16	22.69	136.1316	306.9690	0	294.8950	23.8843	37(Octal)/EF
31	17	14.96	136.1206	307.0898	.0330	295.1917	23.8843	37(Octal)/EF
31	17	47.98	135.9558	307.1448	.0879	295.2686	23.8898	37(Octal)/EF
31	20	43.17	135.7690	307.4963	.3406	117.9492	17.2046	221(Octal)/EN
31	21	26.69	135.6152	307.5732	.3955	118.1799	17.2019	221(Octal)/EN
31	22	3.22	135.4944	307.6392	.4504	118.3557	17.1964	221(Octal)/EN
31	24	33.75	135.4285	307.9468	.6812	302.7393	31.7725	212(Octal)/EF
31	25	14.77	135.2856	308.0237	.7361	302.8601	31.7752	212(Octal)/EF
31	26	3.31	135.1318	308.1116	.8020	303.0249	31.7780	212(Octal)/EF
31	28	45.85	135.7690	308.9465	1.2854	162.3779	35.3760	44(Octal)/EN
31	29	32.33	135.8569	308.8806	1.0437	162.1582	35.3760	44(Octal)/EN
31	31	7.93	136.1316	308.7158	.6152	161.5540	35.3650	44(Octal)/EN
31	34	19.68	135.8459	307.3865	.5273	301.7725	31.7999	212(Octal)/EF
31	35	10.15	136.0437	307.1887	.2637	301.4209	31.8054	212(Octal)/EF
31	35	52.41	136.2305	307.0459	359.9890	301.2122	31.8137	212(Octal)/EF
31	41	54.48	136.7798	306.9690	359.4287	309.8914	31.9675	77(Octal)/EF
31	42	38.89	136.9995	306.8811	359.4287	309.8254	31.9647	77(Octal)/EF
31	43	35.78	136.8347	306.8372	359.3188	309.6497	31.9757	77(Octal)/EF

EN = EARTH NEAR HORIZON

EF = EARTH FAR HORIZON

Table 3.5 COMBINED RESULTS OF PROCESSING
BATCHES 1 AND 2 OF P23 DATA

	Initialization	Option 1 Results	Option 2 Results
Run 1			
Method 2			
h	10.61 km	10.13	
b	0.00952 mrad	-0.02236	
σ_h	4.88 km	4.57	
σ_b	0.07975 mrad	0.05386	
ρ	0.27406	0.12275	
Run 2			
Method 2			
h	17.42		17.55
b	-0.02827		-0.03093
σ_h	4.88		4.57
σ_b	0.07975		0.05386
ρ	0.27406		0.12276
Run 3			
Method 1			
h	9.61	9.86	
b	-0.05236	-0.05236	
σ_h	4.69	4.53	
σ_b	10^{-5}	10^{-5}	
ρ	0.0	-0.00001	
Run 4			
Method 1			
h	17.04		17.35
b	-0.05236		-0.05236
σ_h	4.69		4.53
σ_b	10^{-5}		10^{-5}
ρ	0.0		-0.00001

where,

h = estimate of altitude bias

b = estimate of trunnion angle bias

σ_h = standard deviation of estimate of altitude bias
from covariance matrix

σ_b = standard deviation of estimate of trunnion bias
from covariance matrix

ρ = correlation coefficient of estimates of altitude and
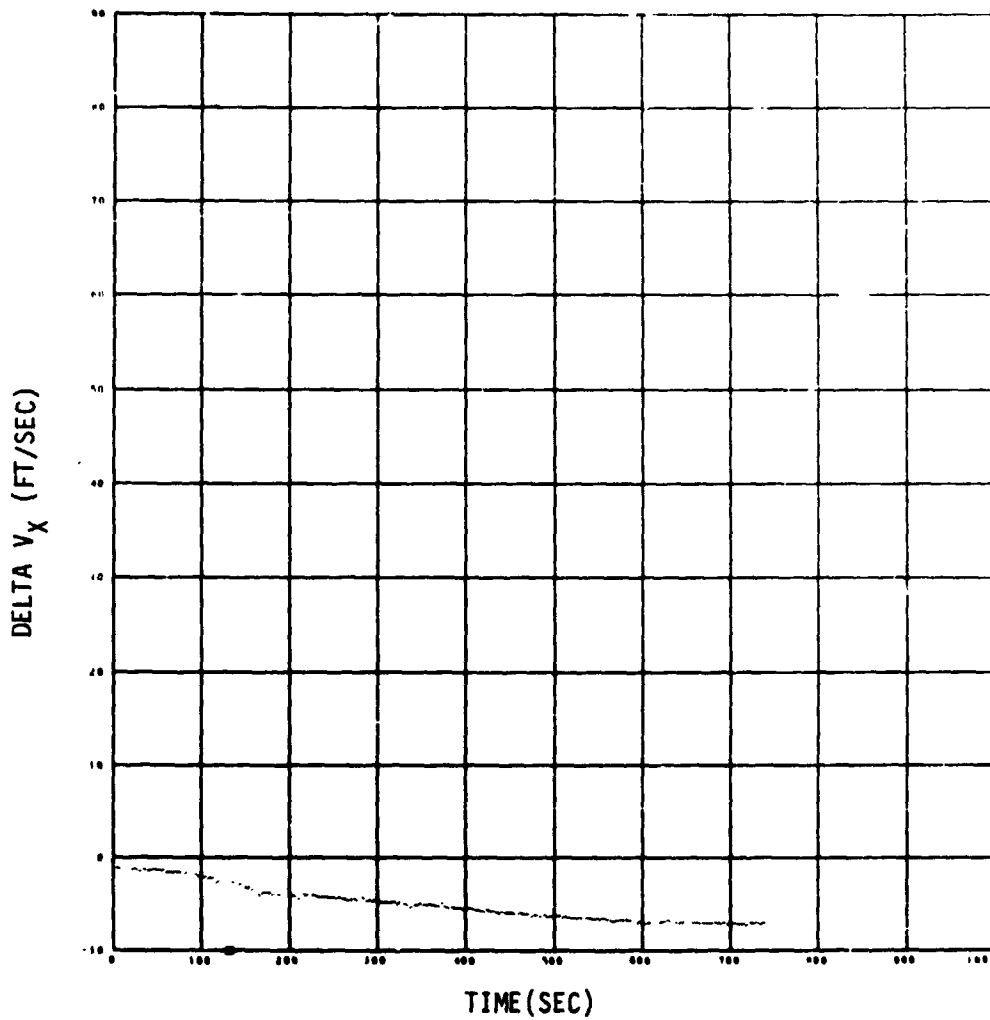trunnion bias from covariance matrix

Figure 3-1   UNCOMPENSATED ASCENT VELOCITY
              COMPARISON (G&N - S-IVB)

Figure 3-2   UNCOMPENSATED ASCENT VELOCITY
COMPARISON (G&N - S-IVB)
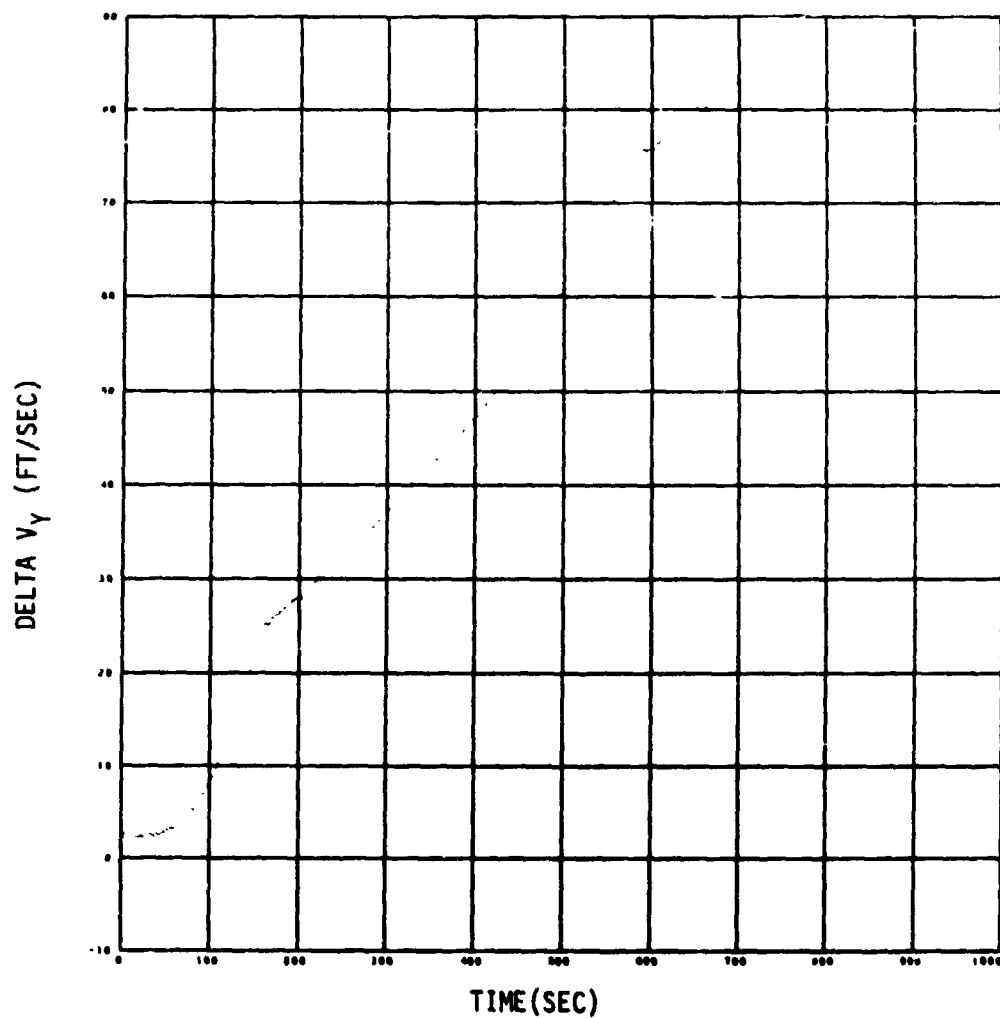
Figure 3-3   UNCOMPENSATED ASCENT VELOCITY
              COMPARISON (G&N - S-IVB)

Figure 3-4   UNCOMPENSATED TLI VELOCITY
COMPARISON (G&N - S-IVB)
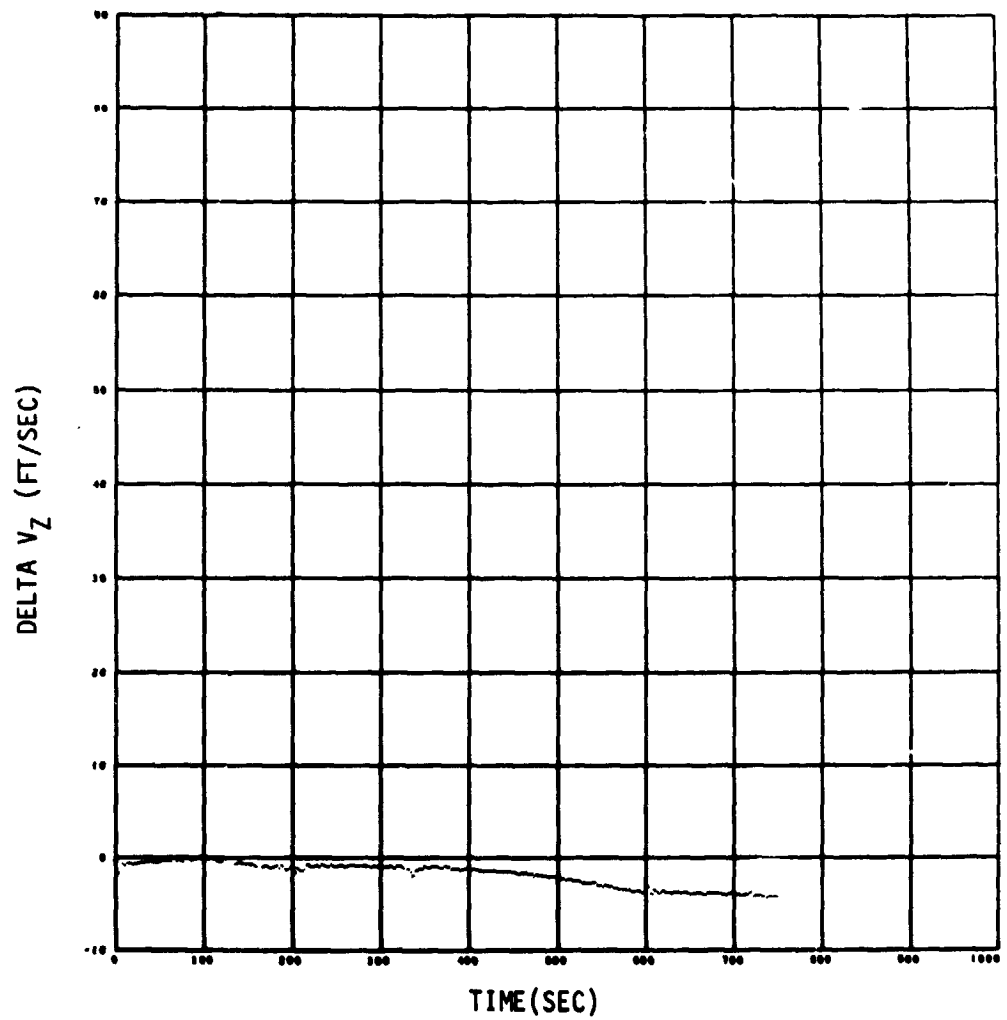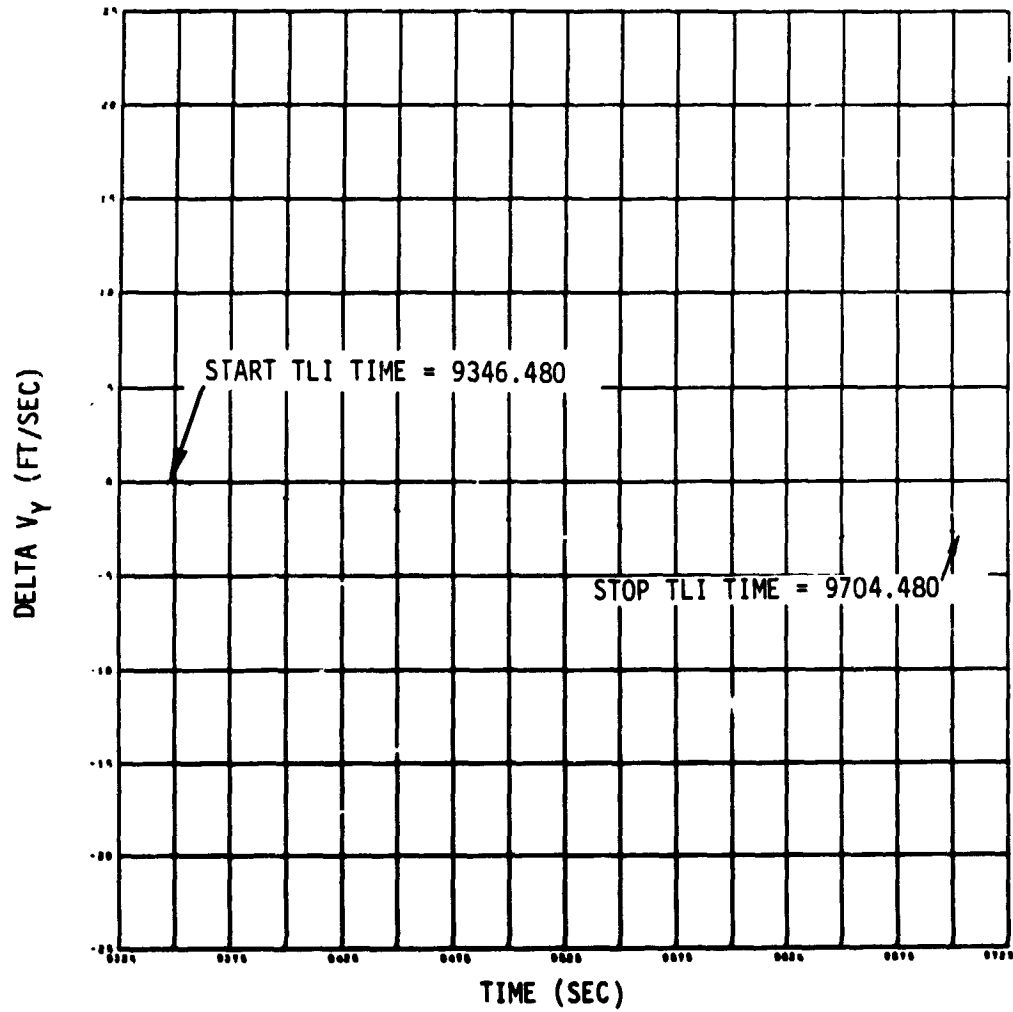
Figure 3-5   UNCOMPENSATED TLI VELOCITY
             COMPARISON (G&N - S-IVB)
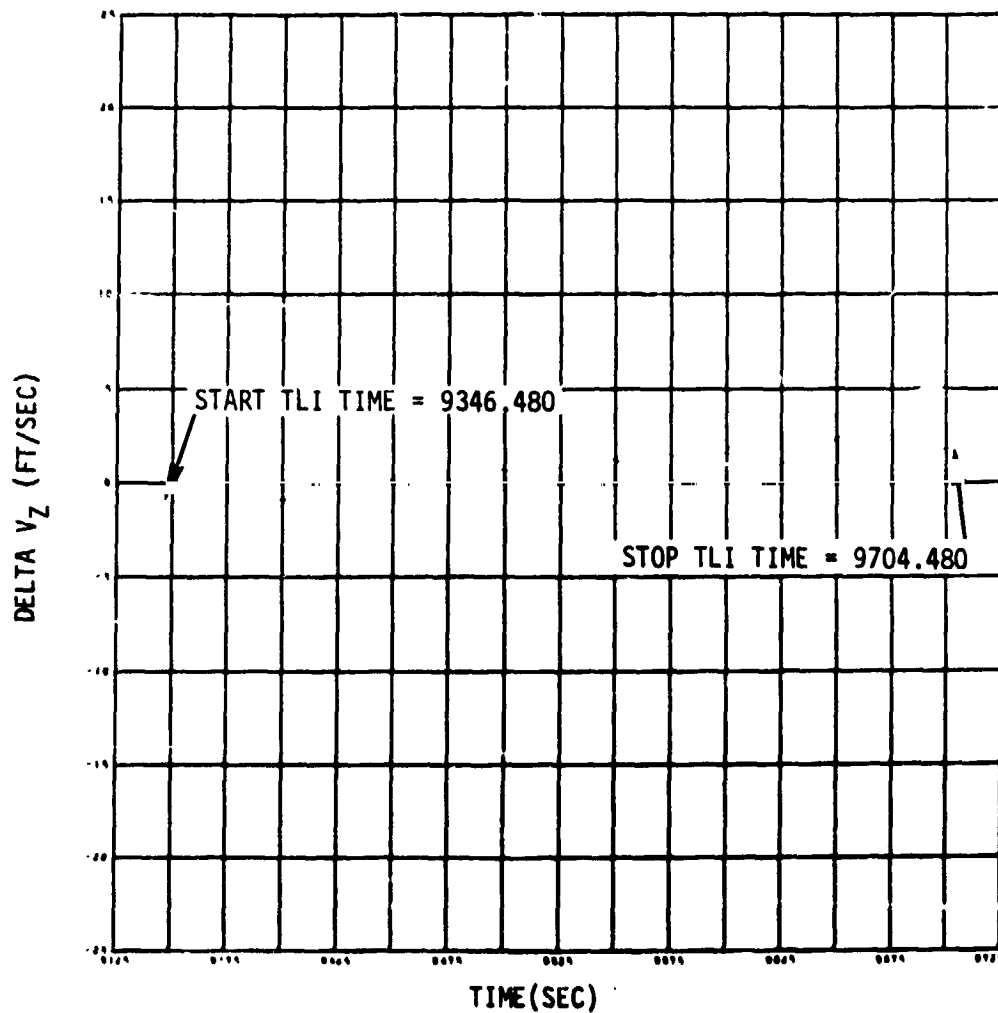
Figure 3-6   UNCOMPENSATED TLI VELOCITY
              COMPARISON (G&N - S-IVB)
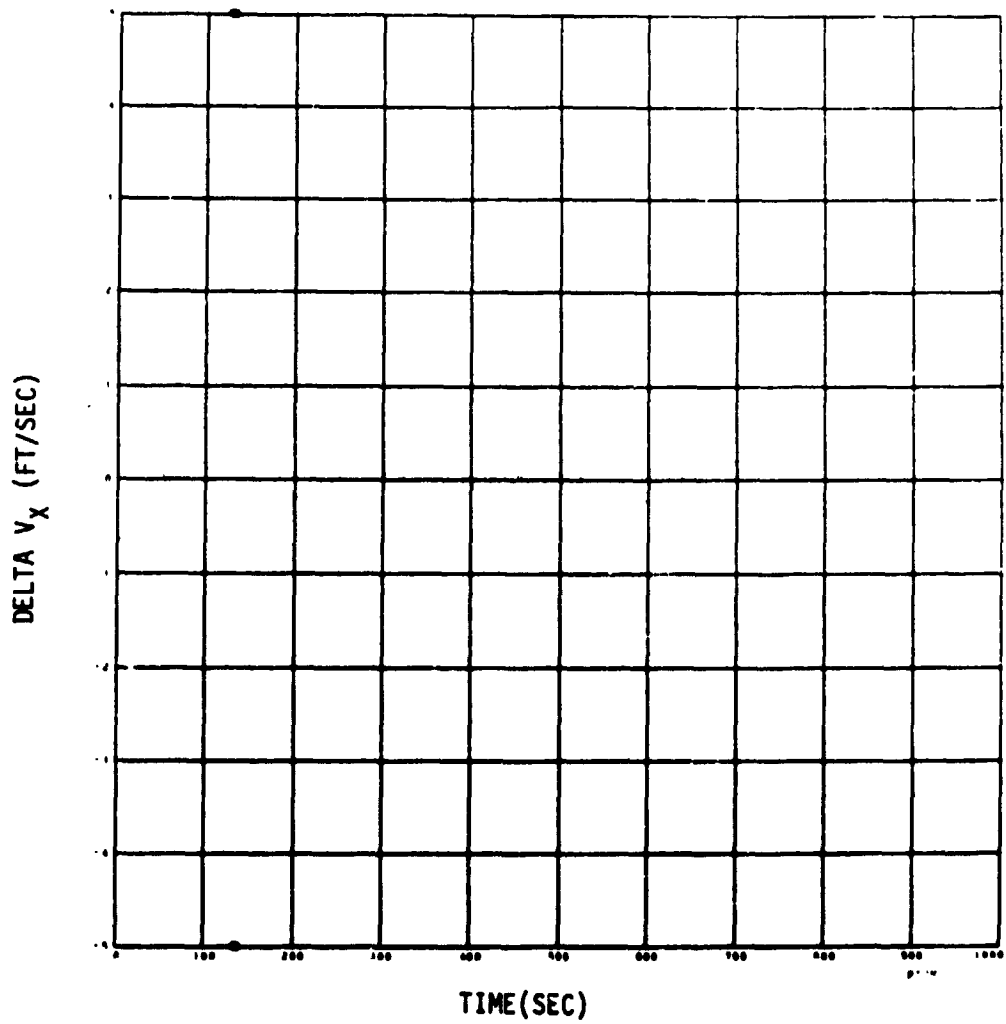
Figure 3-7   COMPENSATED ASCENT VELOCITY
COMPARISON (G&N - S-IVB)

DELTA V_Y (FT/SEC)

TIME(SEC)
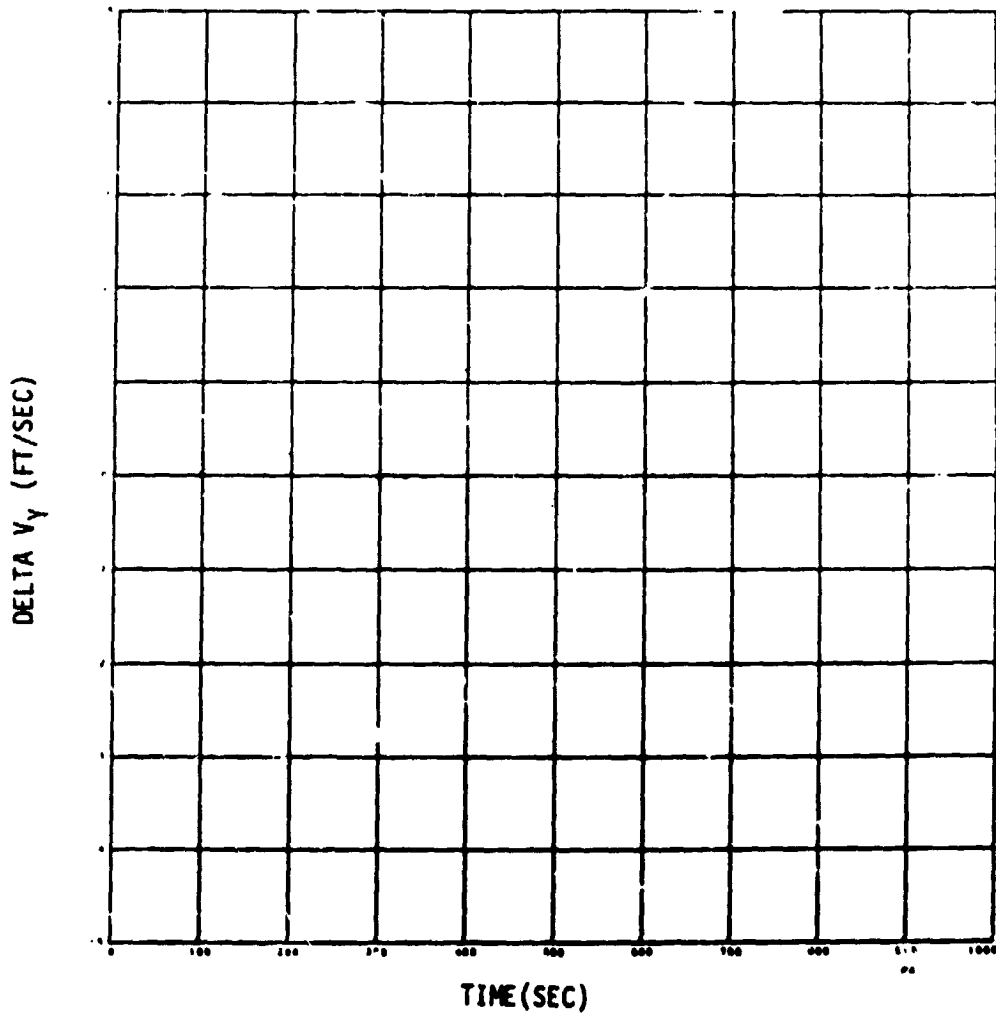
Figure 3-8   COMPENSATED ASCENT VELOCITY
COMPARISON (G&N - S-IVB)
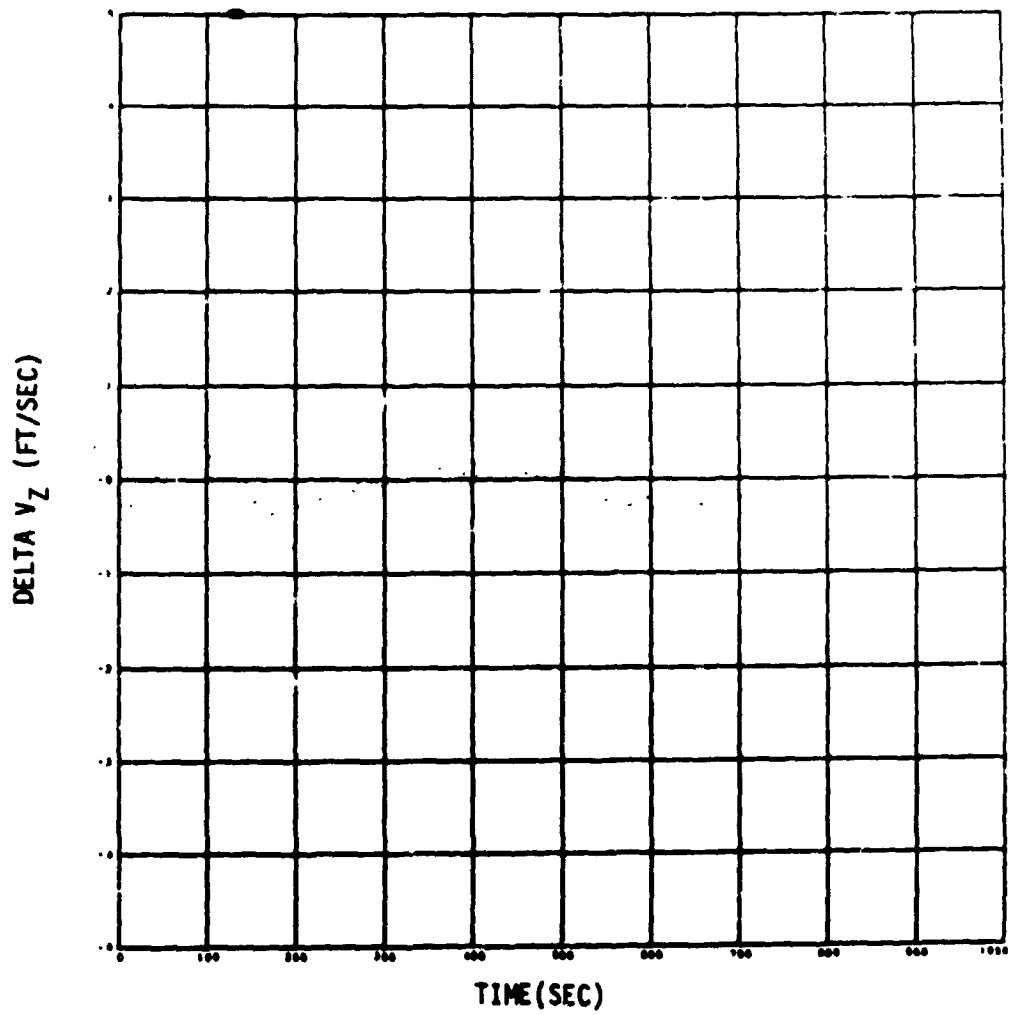
Figure 3-9 COMPENSATED ASCENT VELOCITY
COMPARISON (G&N - S-IVB)

DELTA V_X (FT/SEC)
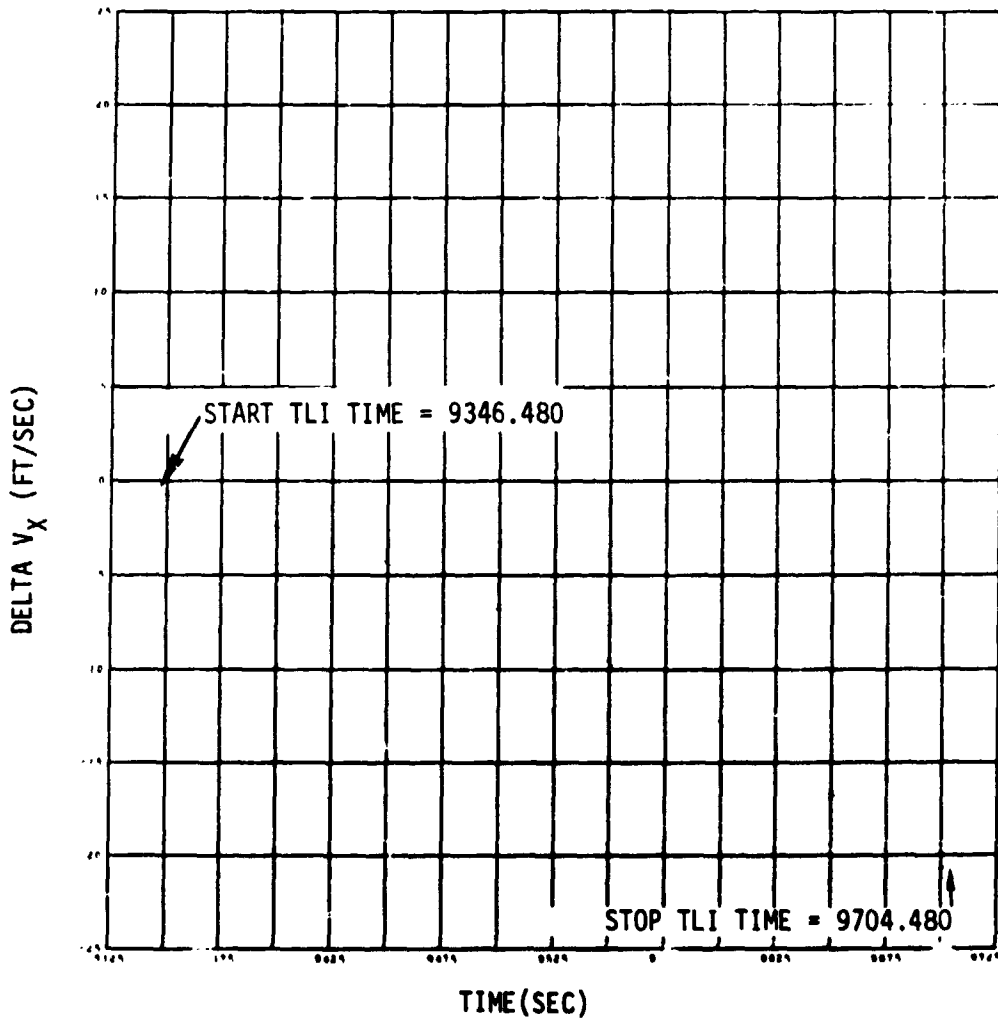
START TLI TIME = 9346.480

STOP TLI TIME = 9704.480

TIME (SEC)
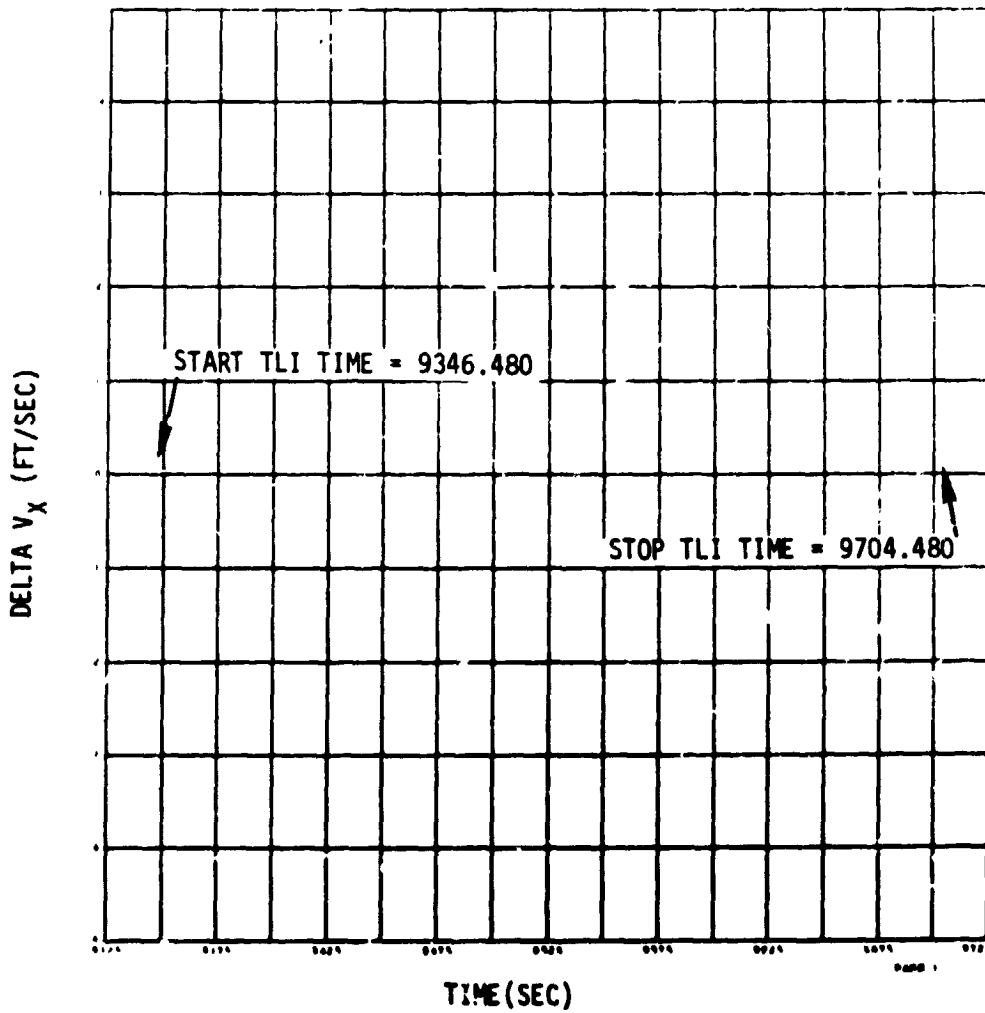
Figure 3-10   COMPENSATED TLI VELOCITY
COMPARISON (G&N - S-IVB)
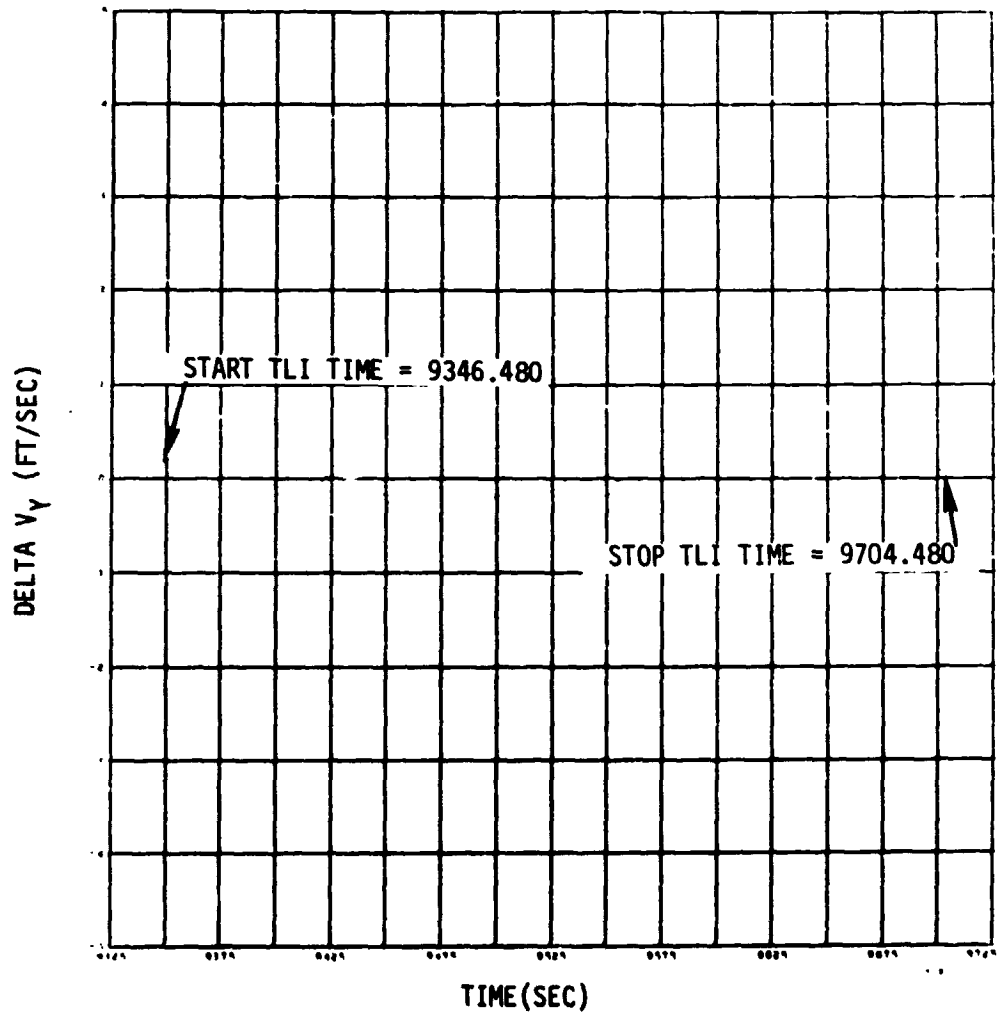
Figure 3-11   COMPENSATED TLI VELOCITY
COMPARISON (G&N - S-IVB)

START TLI TIME = 9346.480

STOP TLI TIME = 9704.480

DELTA V_Z (FT/SEC)
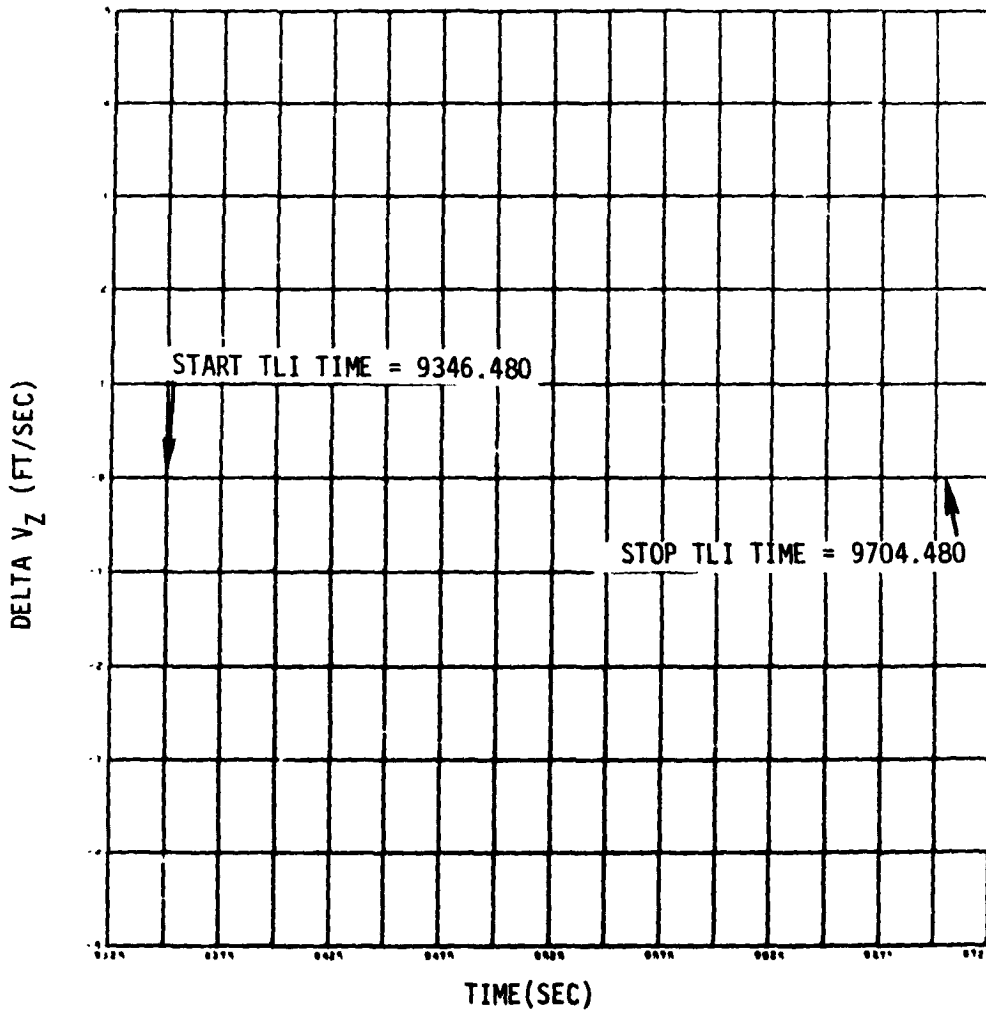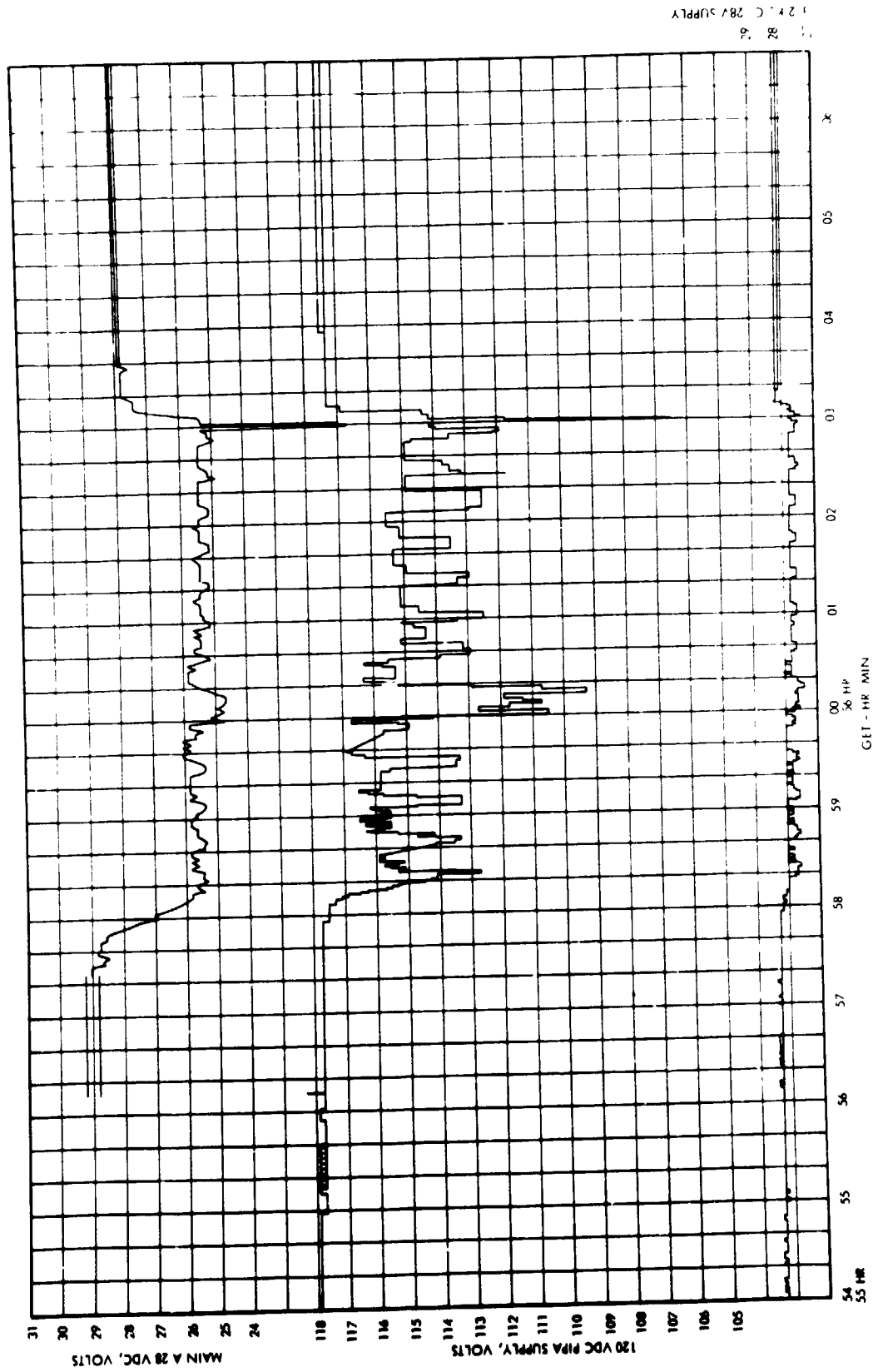
TIME(SEC)

Figure 3-12 COMPENSATED TLI VELOCITY
COMPARISON (G&N - S-IVB)

Figure 3-13   CM PIPA POWER SUPPLY
VOLTAGES

3-27
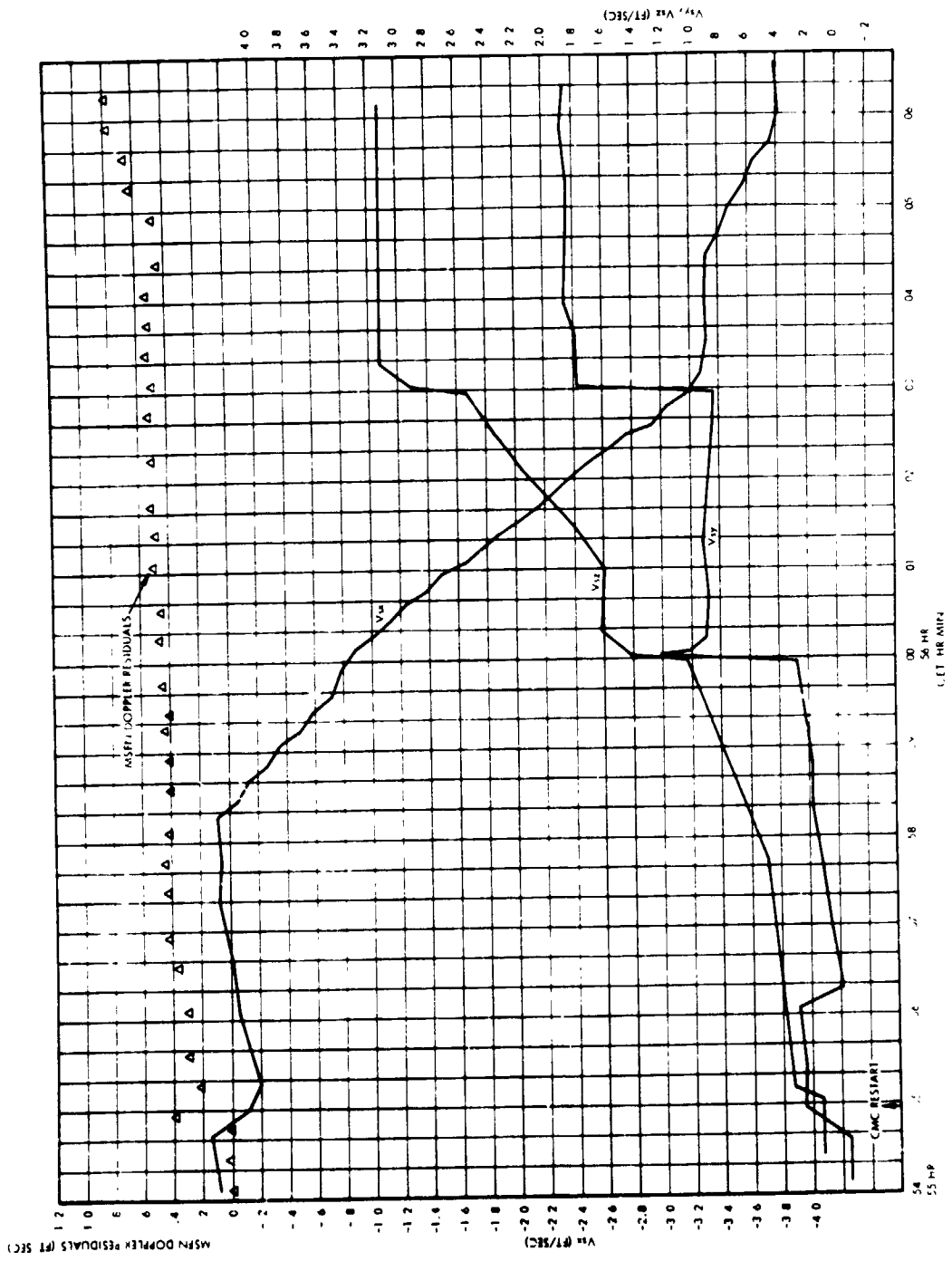
Figure 3-14   PIPA OUTPUTS & MSFN DOPPLER
DATA AFTER SM LOX TANK
INCIDENT

PRECEDING PAGE BLANK NOT FILMED

3-29

4.0 LM SYSTEMS

4.1 LM INERTIAL MEASUREMENT UNIT

4.1.1 Transearth Injection Burn: Cut-Off Velocity Errors

4.1.1.1 Velocity Errors

Velocity errors generated by the IMU during the TEI burn were in-
vestigated. To do this, "best" ignition and cut-off vectors were deter-
mined from free flight data. Three such vectors were determined for the
time of ignition; one was determined for the time of cut-off. These
vectors are presented in Table 4.1. The ignition vectors were extra-
polated to the time of cut-off using accelerometer data from the LGC
downlink. These extrapolated vectors may be thought of as LGC "best
guesses" as to the vehicle state at time of cut-off. They were differ-
enced with the free flight cut-off vector (assumed correct) to obtain
estimates of the IMU induced trajectory errors. Only the velocity
components were calculated, and the results of these calculations are
presented below for each ignition vector and each of three coordinate
frames. The coordinate frames chosen were: BRCS (Basic Reference
Coordinates); IMU, and; local. All reference frames were moon centered.
The local frame is defined to agree with MIT's convention, as follows:

> X: completes the right hand set
> Y: along the negative angular momentum vector ($-\underline{R} \times \underline{V}$)
> Z: along the negative of the radius vector ($-\underline{R}$)

	ΔV ("Best" - NBEX343)			ΔV (GYMX289 - NBEX343)			ΔV (HAWX300 - NBEX343)		
	X	Y	Z	X	Y	Z	X	Y	Z
BRCS	(+3.85;	+3.02;	+2.52)	(+2.92;	-1.21;	+9.62)	(+3.53;	-0.14;	+8.44)
IMU	(-3.77;	-3.83;	-1.07)	(-2.72;	-2.92;	-9.31)	(-3.23;	-3.53;	-7.80)
LOCAL	(+5.46;	+0.41;	-0.56)	(+5.10;	+8.72;	-0.72)	(+5.70;	+7.12;	-0.66)
Magnitude	5.48ft/sec			10.13 ft/sec			9.15 ft/sec		

The GYMX 289 and HAWX 300 ignition vectors yield similar velocity errors whereas errors for the "best" ignition vector differ from these markedly. The first two vectors were obtained by the RTCC in real time. GYMX 289 was the vector with which the TEI burn was targeted. However, both vectors contain only data obtained prior to perilune. The "best" vector was obtained at TRW by fitting data on both sides of perilune. It provided much more satisfactory range and doppler residuals after perilune and consequently has been chosen as the preferred vector for purposes of this report. The disagreement between the preferred vector and the other two vectors lie almost entirely in the out of plane ("Y", in local coordinates) direction; this is the direction in which velocity is least accurately determined by ground based radar (and, therefore, the one in which the greatest uncertainties are experienced).

4.1.1.2 Error Sources

The principal sources of velocity error are likely to have been IMU misalignments (0.7 degrees/axis, due to 1σ drifts alone) and discrepancies in the ignition and cut-off vectors obtained from free flight data. These free flight vector uncertainties are not known explicitly. However, the ignition vector is credited with very good accuracy; on the order of .1 ft/sec, out-of-plane, and less than .1 in the other two axes. The cut-off vector is suspected of greater errors, but these may well be less than one ft/sec (total). With that hypothesis, it was concluded that the majority of the error could be attributed to IMU misalignments. Since alignment errors are perpendicular to the velocity gained, it was of interest to determine how much of the observed error satisfied that condition. This was done as follows:

$$V_p \text{ (parallel to VG)} = (V) \cdot (\text{unit VG}) = -1.47 \ \text{ft/sec}$$

$$\underline{V}_p = V_p \ (\text{unit } \underline{VG}) = [-1.27; +0.73; -0.16], \text{ in IMU coordinates}$$

$$\underline{V}_n \text{ (normal to VG)} = \underline{V} - \underline{V}_p = [-2.50; -4.56; -0.91], \text{ IMU coordinates}$$

$$V_n = 5.27 \ \text{ft/sec}$$

Most of the error was perpendicular to VG, tending to support the argument for IMU misalignments as the principal factor. The -1.45 ft/sec of error parallel to VG cannot be attributed to IMU misalignments and since other IMU contributions can reasonably be expected to have been much less than this, it seems probable that the free flight cut-off vector contained a -1.47 ft/sec error along VG (and an unknown, but presumably small component perpendicular to it).

4.1.2 IMU Misalignments at Time of TEI Burn

Three approaches were taken to determine the IMU alignment errors which existed at the time of the burn. These are described in the following paragraphs.

4.1.2.1 Sun Check

The crew sun check (discussed in Section 4.4.1) performed at 73:47 GET provided information concerning IMU misalignments perpendicular to the line-of-sight. Unfortunately, there were insufficient data to determine the direction of those errors which were observed. However, it was determined that the magnitude of observable errors was approximately 0.51 degrees. This provided a useful method of testing the validity of other estimates.

4.1.2.2 Drift Check

An effort was made to determine alignment errors from gyro drift data. These data included LM prelaunch and CM inflight measurements. Basically, it was assumed that LM IMU error at any given time was the sum of:

o CM IMU drift prior to the docked alignment, plus

o LM IMU drift subsequent to the docked alignment.

The uncertainty in the estimate thus obtained was taken to be the RSS of CM and LM initialization errors. Uncertainties in the drift rates were ignored. The point of this was to determine whether misalignments could have been reliably deduced from existing instrument performance data and eliminated prior to the midcourse burn. Table 4.2 presents the results of these estimates.

4-3

From the table it can be determined that the magnitude of misalignment estimated from drift data is 0.60 degrees, with a 1σ uncertainty due to initialization of $\pm.28$. Almost all of this would have been visible to the sun check. Thus, the magnitude of the predicted error agrees rather well with that observed in the sun check, and the disagreement lies well within the bounds of predicted uncertainty.

4.1.2.3 Velocity Error Check

Once the velocity error at TEI cut-off was determined, it was possible to determine in two steps a unique set of alignment errors which satisfied the constraint that the sum of the squares of the error angles was minimized. Step one consisted of determining that component of velocity error perpendicular to the velocity gained vector. This was done because IMU misalignments can be shown to produce only perpendicular errors. The procedure and results were described in Section 4.1.1.2. The second step consisted of solving for a "minimum" set of error angles. The constraint equations are:

Minimize $\underline{\epsilon} \cdot \underline{\epsilon} = |\underline{\epsilon}|^2$, subject to

$(VG) \times (\underline{\epsilon}) = \underline{\Delta V}_n$, where

$\underline{\epsilon}$: the vector of error angles

$\underline{VG}$: the velocity gained in the burn

$\underline{\Delta V}_n$: that component of burn velocity error perpendicular to $\underline{VG}$.

The solution obtained from these constraints is:

$$\underline{\epsilon} = \left(\frac{1}{VG}\right)^2 (\underline{\Delta V})_n \times (\underline{VG})$$

Applying this relationship to the quantities generated in Section 4.1.1 yields:

$\underline{\epsilon} = [-.062; -.035; +.344]$ degrees

$|\underline{\epsilon}| = .351$ degrees

It must be understood that, assuming a correct measure of $\underline{\Delta V}_n$, these are the errors which generated $\underline{\Delta V}_n$ (moreover, most of this would have been visible in the sun check). However, these errors do not necessarily reflect total IMU misalignment. Platform misalignments about VG would generate no velocity error. Consequently, that component of total IMU misalignment which was about VG cannot be determined by an analysis of $\underline{\Delta V}_n$. It is to be expected that total IMU misalignment magnitude would be no less than .351 and would probably be greater. The discrepancy would arise from the irresolvable component about VG.

A pattern of reasonably good agreement emerged from the above error estimates as evidenced in the summary below:

Source of Estimate	ϕ_x	σ_x	ϕ_y	σ_y	$\ddagger_z$	σ_z	$|\ddagger|$	$\sigma_{\ddagger}$
Sun Check	-----	-----	-----	-----	-----	-----	0.51	-----
Drift Check	-0.26	+0.24	-0.07	+0.14	+0.54	+0.04	0.60	+0.28
Velocity Check	-0.06	-----	-0.04	-----	+0.34	-----	0.35	-----

Agreement between the three methods in the Z component, and in magnitude, is fairly good. Also, agreement in magnitude and in the "X" and "Y" estimates lies within the 1σ uncertainty band.

4.1.3 PIPA Bias and IRIG Drift

LM PIPA biases were stable throughout the periods the LM IMU was activated. The LM IMU was turned on for the first time shortly after the CSM incident and remained powered up until after the TEI burn. Heater power was always maintained in the system. The system was activated for the second time at 134 hours GET in preparation for the MCC 4 maneuver. Samples of PIPA bias during the periods the system was activated indicated the following mean values and data variations.

PIPA	Number of Samples	Mean Value	Sample* Standard Deviation
X	19	1.494 cm/sec^2	0.014 cm/sec^2
Y	19	-1.427 cm/sec^2	0.038 cm/sec^2
Z	19	1.573 cm/sec^2	0.011 cm/sec^2

*Design Specification Uncertainty (1σ) = 0.2 cm/sec^2.

Insufficient data were available to evaluate IMU IRIG drift on this mission. However, based on the small values of LM IMU misalignment at the time of the TEI burn determined from the error separation study in Section 4.1.2.3, it can be deduced that the gyro drifts were small and easily within the 3σ design uncertainty of 0.09 deg/hr.

4.2 LM DIGITAL AUTOPILOT

An analysis of the DAP control functions during the Apollo 13 mission was performed to verify proper DAP performance. The following items were considered:

o The MCC 2 DPS free return maneuver

o The TEI (pericynthion + 2 hour) DPS maneuver

o The maneuver to the LM PGNCS PTC attitude.

o The attitude hold capability of the LM DAP in the LM/CSM and LM/CM configuration.

o The automatic maneuver capability of the LM DAP in the LM/CSM configuration.

o The manual maneuver capability of the LM DAP in the LM/CSM and LM/CM configuration.

4.2.1 MCC 2 DPS Free Return Maneuver Analysis

A four jet, 8.01 second ullage was initiated prior to the MCC 2 - DPS burn at 61:29:36.06 GET. DPS ignition occurred at 61:29:42.84 GET. Prior to the DPS burn the U-V rotational jets (i.e., X translation jets) were not manually inhibited as is usually the procedure. Manual throttle-up from 11.9% to 36.8% occurred at approximately 61:29:50 GET. Program sequencing prior to and during the burn was nominal. Manual throttle-up

to 36.8% was nominal and required ΔV of approximately 38 ft/sec was achieved. The burn residuals were 0.2, 0, and 0.3 ft/sec for the X, Y, and Z components, respectively. No manual nulling of these residuals was necessary. Table 4.3 shows the magnitudes of the maximum estimated rates and the rate gyro signal maximum values during this burn. The low magnitudes indicate good burn performance and no discernible sloshing effects. Little or no slosh would be expected since the APS and SPS were fully loaded during the burn and the DPS was fully loaded at the start of the burn. Table 4.4 shows the magnitudes of the maximum attitude errors and rate errors obtained during this burn. Figures 4-1, 4-2, and 4-3 show the phase plane plots for the P, U, and V axes, re-spectively, for the MCC 2 burn (Relationship between P, U, V and X, Y, Z axes is shown in nomenclature). These plots indicate nominal DAP perfor-mance. Table 4.5 shows the RCS fuel consumption required to maintain attitude control during this burn. The total RCS propellant (excluding ullage) required during MCC 2 was 12.90 lbs. Figures 4-4 and 4-5 show the pitch and roll GDA positions throughout this burn and indicate satisfactory GDA performance. During the manual throttle-up from 11.9% to 36.8%, the effects of a transient due to the compliance of the DPS gimbal system can be seen. This compliance effect results in the GDA's driving in + pitch and a - roll direction. After relieving this compliance, the GDA movement is as expected in trying to track the c.g.

4.2.2 TEI DPS Maneuver Analysis

Prior to the TEI burn, jets 6 and 14 were used for a two jet, 11.1 second ullage which began at 79:27:29.43 GET. DPS ignition occurred at 79:27:38.30 GET. Prior to the burn, the U-V rotational jets were manually inhibited as required by the preburn checklist. A nominal manual throttle-up from 11.4% to 37.7% occurred at approximately 79:27:45 GET. The automatic throttle-up to 93.9% occurred at approxi-mately 79:28:05 GET. The burn residuals were 1.0, 0.3, and 0 ft/sec for the X, Y, and Z components, respectively. No manual nulling of these residuals was performed. Table 4.6 shows the magnitudes of the maximum estimated rates and the rate gyro signals maximum values during this burn.

The values indicate nominal performance and very small slosh effects, as would be expe ..ed with the propellant loadings that were present, i.e., APS full and DPS and SPS nearly full. Table 4.7 presents the magnitude of the maximum attitude errors and rate error which occurred during this burn. Figures 4-6, 4-7, and 4-8 show the phase plane plots for the P, U, and V axes, respectively. The time period plotted begins 10 seconds before ullage and extends 20 to 30 seconds beyond the start of automatic throttle-up. The plots indicate nominal DAP performance. The U and V axes plots indicate two large excursions beyond the dead-band. In each case, the first excursion is smaller and is associated with manual throttle-up. The second excursion is associated with auto-matic throttle-up. Table 4.5 presents the RCS fuel consumption required to maintain attitude control during the burn. The total RCS propellant (excluding ullage) was 4.90 lbs (all expended in P-axis control). Figures 4-9 and 4-10 show the pitch and roll GDA positions from DPS ignition through the automatic throttle-up maneuver and indicate nominal GDA performance. Some concern was expressed about the fact that the roll GDA drove approximately -1.3 degrees from its initial position at the start of the TEI burn. This appears to be nominal behavior caused by relieving compliance and perhaps correcting for some mistrim. The following facts are known.

a) The preferred direction for compliance is in a "+ pitch" and a "- roll" direction.

b) Compliance appears to be highly non-linear and transient effects cannot always be observed.

c) Previous simulations using the now-inoperative MSC bit-by-bit simulation have shown similar transient compli-ance effects on all tests.

d) For the MCC 2 burn the pitch GDA drove +1.05 degrees during throttle-up from 11.9% to 36.8% and the roll GDA drove -0.75 degree during throttle-up from 11.9% to 36.8%. These effects were apparently due to the effects of compliance.

e) At the end of the MCC 2 burn both the pitch and roll GDA's were driving in a positive direction in trying to track the c.g.

4-3

f) For the TEI burn the pitch GDA drove +0.435 degree during throttle-up from 11.4% to 37.7% and the roll GDA drove -1.335 degrees during this throttle-up period.

g) The root-sum-square GDA change due to compliance was approximately 1.29 degrees for the MCC 2 burn and 1.402 degrees for the TEI burn.

h) For the TEI burn the pitch GDA showed no noticeable change during throttle-up from 37.7% to 93.9%. The roll GDA drove -1.245 degrees during this throttle-up period. The root-sum-square GDA change of 1.245 degrees agrees closely with the previously discussed values of 1.29 degrees and 1.402 degrees.

Evaluation of the facts discussed above leads to the conclusion that the GDA behavior for both the MCC 2 burn and the TEI burn was nominal.

4.2.3 Maneuver To PTC Attitude

The difficulties encountered in maneuvering to the PTC attitude subsequent to the TEI burn prompted an investigation of the torques associated with each LM reaction control jet and with the various rotational and translational firing policies available in the LGC. This investigation included the effects of impingement forces on the plume deflectors.

At the time of the maneuver, the best estimate of LM and CSM weights were 25666.2 lbs and 62489.7 lbs, respectively, or a total weight of 88155.9 lbs. This value was referred to in the SODB (Reference 2) which defined the combined vehicle c.g. location in the CSM body frame as follows: X_A = +1049.38 inches; Y_A = +2.49 inches; and Z_A = +3.59 inches. These values were obtained by linear inter-polation of the values recorded in the SODB. These data were used to transform the c.g. location into LM body axes.

The SODB also defined the locations of the points at which the re-
action control jet forces are applied. The location of the impingement
forces on the plume deflectors was defined by Reference 3. Based on the
location of each of the sixteen reaction jets with respect to the c.g. and
the thrust vector, the torque for each jet was calculated. Using the data
from Reference 3, torques were calculated for the impingement forces result-
ing from each of the downward firing thrusters.

The GSOP (Reference 4) gives the jet policies to be used in the
various translation and U-V rotational maneuvers that can be performed.
Tables 4.8 and 4.9 indicate the torques which result from the use of
each of these policies. In addition, there are possible jet policies
associated with Q and R axes rotations in the minimum impulse mode.
These are not defined in the GSOP. However, the various policies have
been determined and the torques resulting from each policy are defined
in Table 4.10.

The maneuvering problem reported by the astronauts primarily was
a cross-coupling effect between the pitch (Y or Q) axis and the roll
(Z or R) axis. No downlink data is available for the period of the
maneuver. However, certain assumptions can be made.

a) All jets were functioning; this implies that primary
    jet-policies were in effect at all times.

b) The maneuver was conducted manually using either:

    1) Y-axis and Z-axis translation commands through
        the TTCA; or

    2) Three-axis (X, Y, and Z) rotational commands
        through the ACA.

Examination of Table 4.8 reveals that Y-axis and Z-axis translation com-
mands produce only minor cross-coupling around the yaw axis. Pitch-roll
cross-coupling is non-existent. Examination of X-axis rotational policies
in Table 4.9 reveals that primary jet-policies, using either four jets
or two, produce only X-axis rotations. Data for Y-axis and Z-axis rota-
tions are shown in Table 4.10. The use of four jets for any rotational
maneuver produces very minor cross-coupling. However, the GSOP states
that pitch and roll maneuvers in the minimum impulse mode will be

4-10

accomplished with two jets. Examination of the jet-policies which use two jets reveals cross-coupling torques that have the same magnitude as the primary torques. This occurs because each of these jet-policies employs one downward firing jet. The resulting impingement force acts equally about the Y-axis and the Z-axis using the long X-axis moment arm. The result is to reduce the primary torque by a factor of two and produce the large cross-coupling force.

Although data for this time period is lacking, examination of data for a later period revealed that these rotational firings took place. Data indicated a +R (+Z) rotational command at 137:22.49.616 and -Q (-Y) rotational command at 137:23:01.616. Examination of jet firings data showed corresponding 60 millisecond firings of jets 5 and 10 at 137:22:50.434 and of jets 10 and 13 at 137:23:01.234. Analysis has shown that jets 5 and 10 produce a primary +R torque and jets 10 and 13 produce a primary -Q torque. Since two jet Y and Z axes torques occurred at these times, it is not unreasonable to infer that they also occurred during the maneuver to PTC attitude and that they produced not only the primary torque but a cross-coupling torque of equal magnitude as well. If the THC was used to perform maneuvers in the LM/CSM docked configuration, no unexpected problems should be encountered if the crew is familiar with this type of operation. However, use of the RHC or the MIC can produce results which would be very unexpected.

It is recognized that the above analysis represents only one of a number of possible explanations of the control difficulties encountered. Another probable source of difficulty is the fact that the FDAI was powered down during the maneuver. Without that source of attitude information, it was necessary to monitor attitude by observing gimbal angles displayed on the DSKY. Because the spacecraft yaw axis was not coincident with that of the platform, either a pitch or a roll command would cause a change in both of the corresponding gimbal angle displays. That this was a factor is supported by the fact that, after the vehicle's and platform's corresponding axes were brought into closer alignment, passive thermal control was established satisfactorily.

4-11

4.2.4 DAP Control of the LM/CSM Configuration

DAP attitude control was evaluated for periods of attitude hold, and for periods of automatic and manual maneuvers. The available data were for a 5 degree deadband. Figures 4-11, 4-12 and 4-13 (P, U, and V axes, respectively) present both periods of auto maneuver and attitude hold. The auto maneuver period was 61:25:17 to 61:25:20 GET. The attitude hold period began at 61:25:21 GET and was plotted for approximately 2 minutes. This period precedes the MCC 2 maneuver and nominal DAP performance is indicated. An auto maneuver prior to the TEI burn is presented in Figures 4-14, 4-15, 4-16 (P, U, and V axes, respectively). The maneuver began at 79:21:43 and was terminated 3 seconds later. Nominal DAP performance is indicated. A five minute period of attitude hold subsequent to this maneuver is plotted in Figures 4-17, 4-18, and 4-19 (P, U, and V axes, respectively). The period covered is 79:22:00 to 79:27:00. The U and V axes phase planes are plotted for the entire time period. The P axis was functioning in a much faster duty cycle of which one complete cycle has been plotted. Manual maneuvers were performed in the minimum impulse mode where the desired CDU angles are set equal to the actual CDU angles. Since no attitude errors exist, it is not possible to generate a meaningful phase plane plot. However, it was determined that the rate errors did not exceed the deadband limits.

4.2.5 DAP Control of the LM/CM Configuration

DAP attitude control was evaluated for a time period that contained both attitude hold and a manual maneuver. The P, U, and V axes phase plane plots are presented in Figures 4-20, 4-21 and 4-22, respectively. The attitude hold period presented began at 140:49:12 GET and terminated at 140:51:25 GET at which time the manual maneuver began. Since the manual maneuver was performed in the minimum impulse mode, the attitude error remained approximately zero as shown by the three figures.

4.3 LM ABORT GUIDANCE SYSTEM

Investigation of AGS performance was conducted with the objectives
of:

o Determining the stability of AGS sensor static errors
   (accelerometer bias; gyro static, or bias drift).

o Determining AGS sensor dynamic errors from comparisons
   of AGS and PGNCS measurements during the TEI burn.

o Comparing AGS and PGNCS measurements of velocity gained
   and vehicle attitude during midcourse burns.

After the Service Module LOX tank incident, four burns were made to
return the spacecraft to earth as quickly and safely as possible. The
first and second burns were made under PGNCS control with the LM DPS;
the AGS was powered up for the second burn and used in the "back-up"
mode in case of PGNCS failure. The AGS was used to perform the last
two burns, a DPS burn of 7.8 ft/sec and an RCS burn of 2.8 ft/sec.

4.3.1   Burn Analysis

TEI (AGS in Follow-Up)

The second LM DPS burn was initiated at approximately 79:27:41
following an X-axis RCS burn for ullage. This burn was performed with
PGNCS control and the AGS in follow-up. Although the AGS was not tar-
geted for the maneuver, its indication of sensed velocity and attitude
were available to confirm success of the burn. After AGS power-up,
a Body Axis Align was performed. Throughout most of the burn, the astronauts
monitored "X" sensed velocity in body coordinates on the DEDA and PGNCS sensed
velocity on the DSKY. These velocities are plotted in Figure 4-23 and
indicate good agreement between the AGS and PGNCS.

Following the burn, AGS power-down (including heaters off) began at
approximatley 79:51:00.

4-13

MCC 3 (AGS Controlled - DPS)

This burn, a small maneuver to increase the entry flight path angle, was performed under AGS control. Plots of sensed velocities are shown in Figure 4-24. Since the burn was insensitive to burn time cut-off errors and attitude errors, the primary burn rule was to avoid excessive rates (more than 10 leg/sec) about any axis.

System power-up for the burn was initiated at approximately 104:40:00. At approximately 104:58:20, the ASA temperature had risen above 115 degrees F and the AGS was activated.

DPS burn time was voiced up as 15 sec although the astronauts were told to shut-down after 14 sec to avoid an overburn, which would require an RCS trim, impinging on the command module.

Figures 4-25, 4-26, and 4-27 show the attitude rates and attitude errors. Rate and attitude error data indicate no appreciable disturbances since all three channels appeared to be in normal limit cycle operation.

Because of the planned early shutdown, the maneuver was a slight underburn. An RCS trim burn was performed approximately one minute later, increasing the burn ΔV by 0.2 ft/sec to 7.8 ft/sec. Subsequently, the AGS was powered-down including heater power off.

MCC 4 (AGS Controlled - RCS)

PGNCS and AGS were powered-up at approximately 136 hours and the maneuver to burn attitude for this midcourse correction was with the PGNCS.

In Figures 4-29, 4-30, and 4-31 comparisons between the AGS and PGNCS indicated attitudes are made for the period of manual maneuvering to acquire the appropriate spacecraft attitude for MCC 4. (An AGS to PGNCS align preceded the re-orientation.) Following acquisition of the burn attitude, Guidance/Control was switched to AGS.

The burn was initiated at approximately 137:39:52 with the X-axis RCS. The DSKY was used to observe the accumulated velocity. After about 23 seconds, the RCS was turned off after achieving a ΔV of 2.7 ft/sec. A partial trim was effected 15 sec later, bringing the total ΔV to 2.8 ft/sec. This was short of the desired value of 3.1 ft/sec, but was indicated as acceptable by the ground. The ΔV's are shown in Figure 4-28.

No attitude control problems were noted during the burn, with manual pitch and roll provided by the TTCA and AGS yaw control by the AGS attitude hold mode as seen in Figure 4-32.

4.3.2   Sensor Performance (ASA 023)

4.3.2.1   Accelerometer Errors

Free Flight Performance - Free flight accelerometer static bias data were obtained for two time periods, pre-TEI and post-MCC 4. Bias estimates obtained from these data appear in Table 4.11. Table 4.12 compares the shifts undergone by this parameter after prelaunch calibration with standard deviations of this shift. The AGS Capability Estimate one sigma values result from data samples taken from a number of AGS systems; as such, they are representative of general AGS performance. The table reveals that static bias performance was easily within 1σ of AGS Capability Estimate. This is excellent performance in view of the fact that the ASA dropped 23 degrees F below the specified minimum (60° F) during the 24 hour period in which it was shutdown prior to the TEI burn.

Powered Flight Performance - The TEI burn was the only one performed during Apollo Mission 13 of sufficient duration and thrust to permit estimation of AGS dynamic sensor performance. Figures 4-33, 4-34, and 4-35 show the accumulated sensed velocity along the body axes. The ΔV magnitude was about 860 ft/sec.

Accelerometer errors were found from AGS/PGNCS sensed velocity comparisons. The PGNCS velocities were compensated for known static

bias errors, interpolated to AGS times, transformed to body coordinates, and subtracted from the corresponding AGS velocities. The differences are shown i.. Figures 4-36, 4-37, and 4-38. Since PGNCS gimbal angles were used to transform the velocities, these differences reflect only accelerometer errors (plus noise due to AGS downlink and PGNCS gimbal angle quantizations).

The estimates of dynamic and total accelerometer error are listed in Table 4.13. The total errors were derived with a digital computer program which determines a set of "best" AGS errors for the purpose of minimizing the AGS-PGNCS velocity residuals in a least squares sense. The dynamic errors were obtained by subtracting the static bias (measured over a 15 minute interval just before the burn) from the totals. Table 4.15 presents ratios of the shifts (from prelaunch values) in these parameters to shif⁺s predicted by the ASA 023 error model. The table shows that all of these errors were within the error model 2σ limits. Plots of the velocity residuals, compensated for the recovered errors, are shown in Figures 4-39, 4-40, and 4-41.

4.3.2.2 Gyro Errors

Free Flight Performance - Free flight gyro static drift data were obtained during two time periods, pre-TEI and post-MCC 4 (the interval ' ˉom 140:29 to 140:51 GET). Drift estimates obtained from these data appear n Table 4.11. X channel data were noisy and interpretation was correspondingly difficult. Thus it was necessary to specify a range of possible performance values. Instrument performance was within 1σ AGS Capability Estimate tolerances, so that it may be said that the static drift performance was quite satisfactory.

Powered Flight Performance - Gyro error was obtained from AGS/PGNCS attitude differences obtained just before and during the burn. These differences are shown in Figure 4-42, 4-43, and 4-44. Because of relatively constant inertial attitude and thrust level, the effects of dynamic drift, scale factor error, input axis misalignment, and mass

unbalance cannot be separated. However, since the burn was performed in the "attitude hold" mode, the effect of a significant scale factor error or input axis misalignment would have been negligible. Because of the low thrust level (about 0.1 g), mass unbalance probably contributed very little error. Thus most of the error was attributed to gyro static and dynamic drift. The total errors were determined by measuring the slopes of the attitude differences during the burn. The dynamic error was obtained by subtracting the static values from the totals. The dynamic and total errors are presented in Table 4.14.

Listed in Table 4.15 are ratios of the shifts in measured parameters to their 1σ values. None of the errors exceeded 2σ with respect to ASA 023 prelaunch performance.

4.4 LM OPTICAL ALIGNMENT CHECKS

4.4.1 Sun Check for TEI Alignment

Shortly after the service module LOX tank incident, the crew performed a docked LM IMU alignment to the CM IMU. At 73:47 GET a check of this alignment was performed. At the time of the check, visibility through the optical instruments was extremely poor due to an agregation of debris surrounding the spacecraft. In addition it was desired that maneuvering be held to a minimum to conserve RCS propellant. Consequently the decision was made to limit the initial check to one celestial body. The sun was chosen because of the visibility conditions. The check consisted of pointing the AOT line-of-sight toward the LGC calculated sun direction and then noting the approximate magnitude of the offset. The LGC was placed in P52 and routine R52 (Auto Optics Positioning) was used to establish the LGC-estimated pointing vector. The FDAI attitude error displays were used to hold this spacecraft attitude while the position of the sun in the field of view was determined. It was determined on the ground that the solar disc would subtend approximately one-half of a degree in the AOT field of view. From that fact and the observed sun image the crew determined an image (and therefore an IMU) misalignment of approximately one-half of a degree in an undetermined direction. Since this single target optical check could not resolve errors about the line-of-sight, no estimate of possible misalignments in that direction was obtained. The mission rule established for this

check was that any observed error of less than one degree was tolerable. No effort was made to correct the error observed, or to determine the error about the line-of-sight, prior to the TEI burn.

In conducting a single target alignment check such as this it is important to select a line-of-sight which reveals those alignment errors of consequence in subsequent powered flight phases. More explicitly, it should be chosen to measure all misalignments having a significant impact on trajectory parameters of importance to a safe re-entry. One very crucial parameter is entry flight path angle, and during the deep space phases of transearth flight this is governed largely by inplane velocity perpendicular to the earth centered radius vector. The sun was an excellent choice of targets for detecting misalignments as they effected Apollo 13's post-TEI entry corridor. This is demonstrated by the results presented below:

Let $\quad$ = entry flight path angle

V = velocity error in the direction which effects flight path angle

$\underline{V}$ = velocity gained in the TEI burn

Unit $(\underline{LOS})$= the unit line-of-sight vector to the sun at the time of the sun check.

$\ddagger_{LOS}$= IMU misalignment about the line-of-sight vector

Then $\dfrac{\partial \gamma}{\partial \phi_{LOS}} = \dfrac{\partial \gamma}{\partial V} \left[\dfrac{\partial V}{\partial \underline{V}} \cdot (\underline{V} \times \text{Unit } \underline{LOS}) \right] = -.088$

This quantity is unitless and serves to show that a one degree misalignment (for example) of the IMU about the line-of-sight vector would have produced only -.088 degrees of error in the entry angle of the post-TEI trajectory. Restated, entry flight path angle errors were extremely insensitive to misalignments which the sun check could not resolve.

Conversely, α was quite sensitive to those errors which could be observed by the sun check, as illustrated below:

$\dfrac{\partial \alpha}{\partial \phi_n}$ = -10., where ϕ_n is misalignment observed in the sun check.

Based on the above study, it is concluded that:

o ʿhe choice of the sun as the target for this optical check was an excellent one, and;

o Compensative torquing of the IMU to eliminate the error observed in the sun check would have resulted in a much safer post·TEI trajectory.

4.4.2 Sun/Moon Alignment Star Angle Difference

During the time interval from 134:45 through 135:02 of ground elapsed time the Apollo 13 crew performed a P52 alignment of the LM IMU. The sun and moon (centers) were the optical targets. A star angle difference of -1.12 degrees was calculated by routine R54, indicating a very large astronaut sighting error. However, a postflight investigation shows the actual star angle difference to have been approximately 0.08 degree.

The LGC has an algorithm and associated ephemeris data stored within it for computing pointing vectors to various celestial bodies, including the sun and moon. For the star angle difference calculations, this algorithm is used and the scalar product of the resulting vectors is computed. The arc cosine of this quantity forms the LGC's best estimate of the angle between the sighting vectors. The LGC also computes the angle between the measured vectors, and these two angles are differenced to obtain an error (stored - measured) for presentation to the crew. After the above mentioned Apollo 13 sightings, the crew display showed an angular error of -1.12 degrees. In order to check this value, the two angles and their differences were recomputed independently as described below.

Procedurally, the crew can make as many as five measurements of each vector. The LGC averages these measurements and transmits the two average vectors on the downlink. These vectors (unitized) together with the time interval in which they were taken, are presented below in platform coordinates (before realignment).

4-19

Sun	X	Y	Z
(134:45 - 134:48)	+.80789816	-.00424996	+.58930660

Moon			
(134:57 - 135:02)	-.16146112	-.02178924	-.98663840

The angle subtended by these two vectors is 135.38 degrees.

In order to determine the actual subtended angle at the time of mark, two sources of data were used. The first was the NASA Apollo Trajectory (NAT), from which a spacecraft state vector was obtained for an epoch immediately prior to the sightings. This vector and time were:

Time: 17 April 1970, 09:50:00.00 GMT (134:37:00.00 GET)
$\quad$ X: -.28228044E9 ft
$\quad$ Y: +.18416553E9
$\quad$ Z: +.83610975E8
$\quad$ $\dot{X}$:   +.533054E4 ft/sec
$\quad$ $\dot{Y}$:   -.581689E4
$\quad$ $\dot{Z}$:   -.294957E4

This vector and the TRW Houston Operations Predictor Estimator program were used to obtain spacecraft-centered sun and moon vectors from the most recent JPL ephemeris tape (JPL DE69D) at the start and stop times of each measurement interval. These vectors were then unitized and averaged. They are presented in Basic Reference Coordinates.

Sun	X	Y	Z
(134:46.5)	+.89145748	+.41570609	+.18025559

Moon			
(134:59.0)	-.95321902	+.27595070	+.12338832

The angle subtended by these vectors is 135.46 degrees. Therefore, the actual difference in the angles is seen to be 135.46 - 135.38 = .08 degree. Therefore, an LGC calculated angular discrepancy of -1.12 - (.08) = -1.20 is seen to exist and is attributed to the LGC ephemeris data and software.

Table 4.1   TEI IGNITION AND CUTOFF VECTORS

Source	Time (GET)	Feet			Feet/Second		
		X	Y	Z	$\dot{X}$	$\dot{Y}$	$\dot{Z}$
Refit of pre- and post-Perilune data; best residuals	Ignition; 79:27:39.00	+.37489659E8	+.8689836E7	+.5790658E7	+.454390E4	-.19432E3	+.5086E2
RTCC (GYMX 289) (PC+2 Burn Vector for the Mission)	Ignition; 79:27:39.00	+.37480812E8	+.8658677E7	+.5848097E7	+.454299E4	-.19857E3	+.5800E2
RTCC (HAWX 300)	Ignition; 79:27:39.00	+.37488500E8	+.8675873E7	+.5817899E7	+.45439E4	-.19790E3	+.5654E+2
RTCC (MBEX343)	Cut-Off; 79:32:02.8	+.38734395E8	+.854177E7	+.5788384E7	+.493695E4	-.84713E3	-.33399E3

Table 4.2   LM IMU PREDICTED MISALIGNMENTS (DEGREES)

	X Axis	Y Axis	Z Axis
CM IMU Drift (Δt = 10 hours)	-0.200	-0.040	-0.020
LM IMU Drift at Sun Check (Δt = 15 hours)	-0.045	-0.022	+0.382
Total Drift at Sun Check (Δt = 25 hours; t = 73:47 GET))	-0.245	-0.062	+0.402
IMU Drift—Sun Check to TEI (Δt = 5.5 hours)	-0.016	-0.008	+0.138
Total Drift at TEI (Δt = 30.5 hours; t = 79:27)	-0.261	-0.070	+0.540
Uncertainty Due to CM IMU Initial Alignment (1σ)	±0.011	±0.011	±0.011
Uncertainty Due to LM IMU Initial Docked Alignment (1σ)	±0.237	±0.144	±0.038
Total Initialization Uncertainty (1σ)	±0.237	±0.144	±0.040

Table 4.3 MAXIMUM BODY RATES (MCC 2 BURN)

Phase	Maximum Estimated Body Rate (Magnitude)			Maximum Rate Gyro Signal (Magnitude)		
	OMEGAP (deg/sec)	OMEGAQ (deg/sec)	OMEGAR (deg/sec)	Yaw (deg/sec)	Pitch (deg/sec)	Roll (deg/sec)
DPS On (Minimum Throttle)	.0220	.1208	.0577	.2964	.2964	.2964
Manual Throttle-Up to ?.8%	.0165	.2719	.1291	.2964	.0988	.0988
Post Throttle-Up	.1263	.4477	.5960	.4941	.6917	.4941

Table 4.4 DAP CONTROL AXES ATTITUDE ERRORS
AND RATE ERRORS (MCC 2 BURN)

Phase	Maximum Attitude Errors (Magnitude)			Maximum Rate Errors (Magnitude)		
	PERROR (deg)	UERROR (deg)	VERROR (deg)	OMEGAP ERROR (deg/sec)	OMEGAU ERROR (deg/sec)	OMEGAV ERROR (deg/sec)
DPS ON (Minimum Throttle)	1.231	1.317	.779	.022	.115	.062
Manual Throttle-Up to 36.8%	1.213	1.107	.149	.022	.070	.062
Post Throttle-Up	1.129	1.469	1.037	.126	.703	.326

Table 4.5 RCS FUEL CONSUMPTION REQUIRED TO
MAINTAIN ATTITUDE CONTROL

Burn	+P Control (lbs) (jet-seconds)	-P Control (lbs) (jet-seconds)	+U Control (lbs) (jet-seconds)	-U Control (lbs) (jet-seconds)	+V Control (lbs) (jet-seconds)	-V Control (lbs) (jet-seconds)
MCC2(DPS)	0	0.1462	4.5488	6.0111	0	2.1934
Free Return	0	0.3985	12.3946	16.3789	0	5.9766
TEI (DPS)	2.6321	2.2665	0	0	0	0
	7.1719	6.1758	0	0	0	0

Table 4.6   MAXIMUM BODY RATES (TEI BURN)

Phase	Maximum Estimated Body Rate (Magnitude)			Maximum Rate Gyro Signal (Magnitude)		
	OMEGAP (deg/sec)	OMEGAQ (deg/sec)	OMEGAR (deg/sec)	Yaw (deg/sec)	Pitch (deg/sec)	Roll (deg/sec)
DPS On (Minimum Throttle)	.0439	.0055	.0851	.2964	.2964	.4941
Manual Throttle-Up	.1071	.0275	.3873	.4941	.2964	.4941
10-seconds After Manual Throttle-Up	.1071	.0577	.4477	.4941	.2964	.2964
Auto Throttle-Up	.1730	.1044	.7938	.4941	.2964	1.0870
23-Seconds After Auto Throttle-Up	.2197	.2142	.4559	.4941	.2964	.6917

Table 4.7 DAP CONTROL AXES ATTITUDE ERRORS
AND RATE ERRORS (TEI BURN)

Phase	Maximum Attitude Errors (Magnitude)			Maximum Attitude Rate Errors (Magnitude)		
	PERROR (deg)	UERROR (deg)	VERROR (deg)	OMEGAP ERROR (deg/sec)	OMEGAU ERROR (deg/sec)	OMEGAV ERROR (deg/sec)
DPS On (Minimum Throttle)	.351	1.160	.844	.044	.064	.103
Manual Throttle-Up	1.093	2.323	2.108	.107	.157	.239
10-Seconds After Manual Throttle-Up	.849	2.054	1.824	.107	.241	.264
Auto Throttle-Up	.938	4.429	4.953	.173	.439	.528
23-Seconds After Auto Throttle-Up	1.088	.672	1.831	.220	.181	.297

Table 4.8   BODY TORQUES CREATED BY TRANSLATIONAL
POLICIES DEFINED IN GSOP (Reference 4)

Axis	Jets	Body Axis Torque		
		T_x (in-lb)	T_y (in-lb)	T_z (in-lb)
+X (+P)				
4 jet	2,6,10,14	0	-128.2	+ 1559.2
2 jet,sys A	2,10	0	- 64.1	+ 779.6
2 jet,sys B	6,14	0	- 64.1	+ 779.6
-X (-P)				
4 jet	1,5,9,13	0	-144	- 1740
2 jet,sys A	5,13	0	+ 72	- 870
2 jet,sys B	1,9	0	+ 72	- 870
+Y (+Q)				
2 jet, pri *	12,16	+ 72	0	-23,874
1 jet, tack**	16,15/16,7	+ 36	0	-11,937
	12,3/12,11	+ 36	0	-11,937
-Y (-Q)				
2 jet, pri	4,8	- 72	0	+23,874
1 jet, tack	8,7/8,15	- 36	0	+11,937
	4,3/4,11	- 36	0	+11,937
+Z (+R)				
2 jet, pri	7,11	-870	+23,874	0
1 jet, tack	7,8/7,16	-435	+11,937	0
	11,4/11,12	-435	+11,937	0

*Pri = Primary Mode

**Tack = Tacking Mode

4-27

Table 4.8   (Continued)

Axis	Jets	Body Axis Torque		
		T_x (in-lb)	T_y (in-lb)	T_z (in-lb)
-Z (-R)				
2 jet, pri *	3,15	+870	-23,874	0
1 jet, tack	15,8/15,16	+435	-11,937	0
	3,4/3,12	+435	-11,937	0
+U (=+Y, +Z)				
4 jet, pri	7,11,12,16	-798	+23,874	-23,874
2 jet, alt**	7,16	-399	+11,937	-11,937
	11,12	-399	+11,937	-11,937
-U (=-Y, -Z)				
4 jet, pri	3,4,8,15	+798	-23,874	+23,874
2 jet, alt	8,15	+399	-11,937	+11,937
	3,4	+399	-11,937	+11,937
+V (=-Y, +Z)				
4 jet, pri	4,7,8,11	-942	+23,874	+23,874
2 jet, alt	7,8	-471	+11,937	+11,937
	4,11	-471	+11,937	+11,937
-V (=+Y, -Z)				
4 jet, pri	3,12,15,16	+942	-23,874	-23,874
2 jet, alt	15,16	+471	-11,937	-11,937
	3,12	+471	-11,937	-11,937

*Pri = Primary Mode

**Alt = Alternate Mode

Table 4.9   BODY TORQUES CREATED BY ROTATIONAL
POLICIES DEFINED IN GSOP (Reference 4)

Axis	Jets	Body Axis Torque		
		T_X (in-lb)	T_Y (in-lb)	T_Z (in-lb)
+X(+P)				
4 jet	4,7,12,15	+26,440	0	0
2 jet, pri *	4,12	+13,220	0	0
	7,15	+13,220	0	0
2 jet, alt **	4,7	+12,749	+11,937	+11,937
	7,12	+12,821	+11,937	-11,937
	12,15	+13,691	-11,937	-11,937
	4,15	+13,619	-11,937	+11,937
-X(-P)				
4 jet	3,8,11,16	-26,440	0	0
2 jet,pri	3,11	-13,220	0	0
	8,16	-13,220	0	0
2 jet,alt	8,11	-13,691	+11,937	+11,937
	11,16	-13,619	+11,937	-11,937
	3,16	-12,749	-11,937	-11,937
	3,8	-12,821	-11,937	+11,937
+U(= +ᵛ,+Z)				
2 jet, pri	5,14	+ 196.4	+ 6,236.8	+ 6,187.9
1 jet, alt	14	+ 196.4	- 409.2	+ 12.9
	5	0	+ 6,646	+ 6,175
-U(= -Y,-Z)				
2 jet, pri	6,13	- 196.4	- 6,229.4	- 6,278.3
1 jet, alt	6	- 196.4	+ 344.6	+ 766.7
	13	0	- 6,574	- 7,045

* Pri = Primary Mode
** Alt = Alternate Mode

4-29

Table 4.9 (Continued)

Axis	Jets	Body Axis Torque		
		T_X (in-lb)	T_Y (in-lb)	T_Z (in-lb)
+V(= -Y, +Z)				
2 jet, pri	1,10	- 166.4	- 6,229.4	± 6,187.9
1 jet-alt	1	0	- 6,574	+ 6,175
	10	- 166.4	+ 344.6	+ 12.9
-V(=+Y,-Z)				
2 jet, pri	2,9	+ 166.4	+ 6,236.8	- 6,278.3
1 jet,alt	9	0	+ 6,646	- 7,045
	2	+ 166.4	- 409.2	+ 766.7

Table 4.10 BODY TORQUES CREATED BY POSSIBLE PITCH ROLL ROTATIONAL POLICIES

Axis	Jets	T_X (in-lb)	T_Y (in-lb)	T_Z (in-lb)
+Y (+Q)				
4 jet	2,5,9,14	+362.8	+12,473.6	− 90.4
2 jet	2,5	+166.4	+ 6,236.8	+ 6,941.7
	9,14	+196.4	+ 6,236.8	− 7,032.1
−Y (−Q)				
4 jet	1,6,10,13	−362.8	−12,458.8	− 90.4
2 jet	1,6	−196.4	− 6,229.4	+ 6,941.7
	10,13	−166.4	− 6,229.4	− 7,032.1
+Z (+R)				
4 jet	1,5,10,14	+ 30.0	+ 7.4	+12,375.8
2 jet	1,14	+196.4	− 6,983.2	+ 6,187.9
	5,10	−166.4	+ 6,990.6	+ 6,187.9
−Z (−R)				
4 jet	2,6,9,13	− 30.0	+ 7.4	−12,556.6
2 jet	2,13	+166.4	− 6,983.2	− 6,278.3
	6,9	−196.4	+ 6,990.6	− 6,278.3

TABLE 4.11
Sensor Static Bias Errors

		PIC (3/17/70)	TEI (4/14/70)	MCC 4 (4/15/70)
Gyro Static Bias Errors	X	0.06°/hr	*(-0.11 to -0.19)°/hr	-0.12°/hr
	Y	-0.30°/hr	-0.34°/hr	-0.23°/hr
	Z	-0.47°/hr	-0.52°/hr	-0.61°/hr
Accelerometer Static Bias Errors	X	60.0 μg	- 5.0 μg	-16.8 μg
	Y	-31.0 μg	-59.0 μg	-59.4 μg
	Z	47.0 μg	57.0 μg	47.0 μg

* Reasonable range derived from noisy data

TABLE 4.12
Sensor Static Bias Stability

		Shift from PIC to TEI (30 days)	Expected 1σ	Shift from TEI to MCC 4 (1 day)	Expected 1σ
Gyros	X	(-0.17 to -0.25)*°/hr	0.28°/hr	(-0.01 to 0.07)*°/hr	0.22°/hr
	Y	- 0.04°/hr	0.23°/hr	0.11°/hr	0.22°/hr
	Z	- 0.05°/hr	0.28°/hr	- 0.09°/hr	0.22°/hr
Accelerometer	X	-65.0 μg	77 μg	-11.8 μg	30 μg
	Y	-28.0 μg	77 μg	- 0.4 μg	30 μg
	Z	10.0 μg	77 μg	-10.0 μg	30 μg

* Range determined from noisy data.

TABLE 4.13

Equivalent Accelerometer Bias Errors (μg)

		ASA 023 Inflight Estimate (TEI)	ASA 023 Preflight Estimate	
			Mean	3σ
Accelerometer Bias and Nonlinearity	X	-65 (1)	0	135
	Y	-28 (1)	0	125
	Z	10 (1)	0	147
X-Scale Factor and Dynamic Errors	X	- 1 (2)	6	22
Y and Z Dynamic Errors, ASA Accelerometer Internal Misalignment and ASA to IMU Mounting Points Misalignment	Y	- 4 (2)	- 3.3	60
	Z	-58 (2)	-21.5	59
Total (μg)	X	-66	6	137
	Y	-32	- 3.3	138
	Z	-48	-21.5	158

NOTES: 1. Inflight Estimate: Shift between freeflight period and last compensation value.

2. Inflight Estimate: Difference between measured total error and measured fixed bias.

TABLE 4.14
Equivalent Gyro Bias Errors (deg/hr)

		ASA 023 Inflight Estimate (TEI)		ASA 023 Preflight Estimate	
				Mean	3σ
Gyro Fixed Drift	X	(-.17 to -0.25)*	(1)	0	0.59
	Y	-0.04	(1)	0	0.66
	Z	-0.05	(1)	0	0.67
X-Gyro Dynamic Drift	X }	(0.0 to 0.08)*	(2)	{ -0.14	0.35
X-Gyro Spin Axis Mass Unbalance	X }			{ 0	0.07
Y and Z Gyro Dynamic Drift	Y	0.04	(2)	-0.08	0.34
	Z	-0.15	(2)	-0.09	0.30
Total (deg/hr)	X	-0.17		-0.14	0.69
	Y	0.0		-0.08	0.73
	Z	-0.20		-0.09	0.73

NOTES: 1. Inflight Estimate: Shift from last freeflight period and last compensation value.

2. Inflight Estimate: Difference between measured total error and measured fixed bias.

* Possible range derived from noisy data.

TABLE 4.15

Ratios of Shifts in Dynamic and total Errors to Expected 1·
Values* of these Shifts at time of TEI

	X	Y	Z
Gyro Dynamic Error	(1.17 to 1.83)**	1.18	-0.60
Total Gyro Powered Flight Error	-.13	0.33	-0.45
Accelerometer Dynamic Error (Y&Z misalignment, X scale factor)	-0.95	-0.04	-1.86
Total Accelerometer Powered Flight Error	-1.58	-0.62	-0.50

* From ASA 023 Preflight Estimate.
** Range Determined from Noisy Data. Includes spin axis mass unbalance.

Figure 4-1 MCC 2 Burn P Axis Phase
Plane Plot

PERROR (DEG)

OMEGA ERROR (DEG/SEC)

4-37
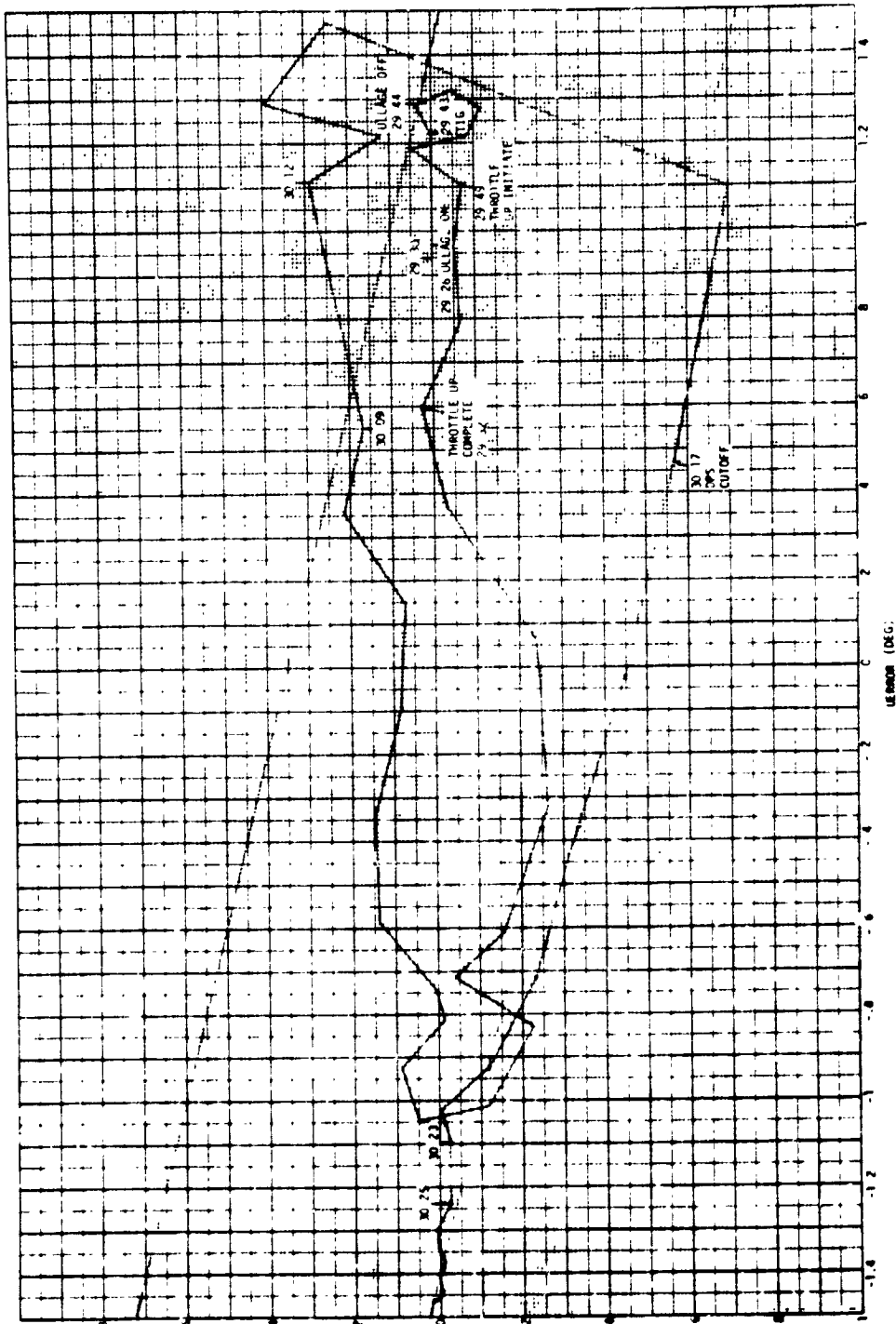
Figure 4-2 MCC 2 Burn
U Axis Phase Plane Plot

PRECEDING PAGE BLANK NOT FILMED

4-39
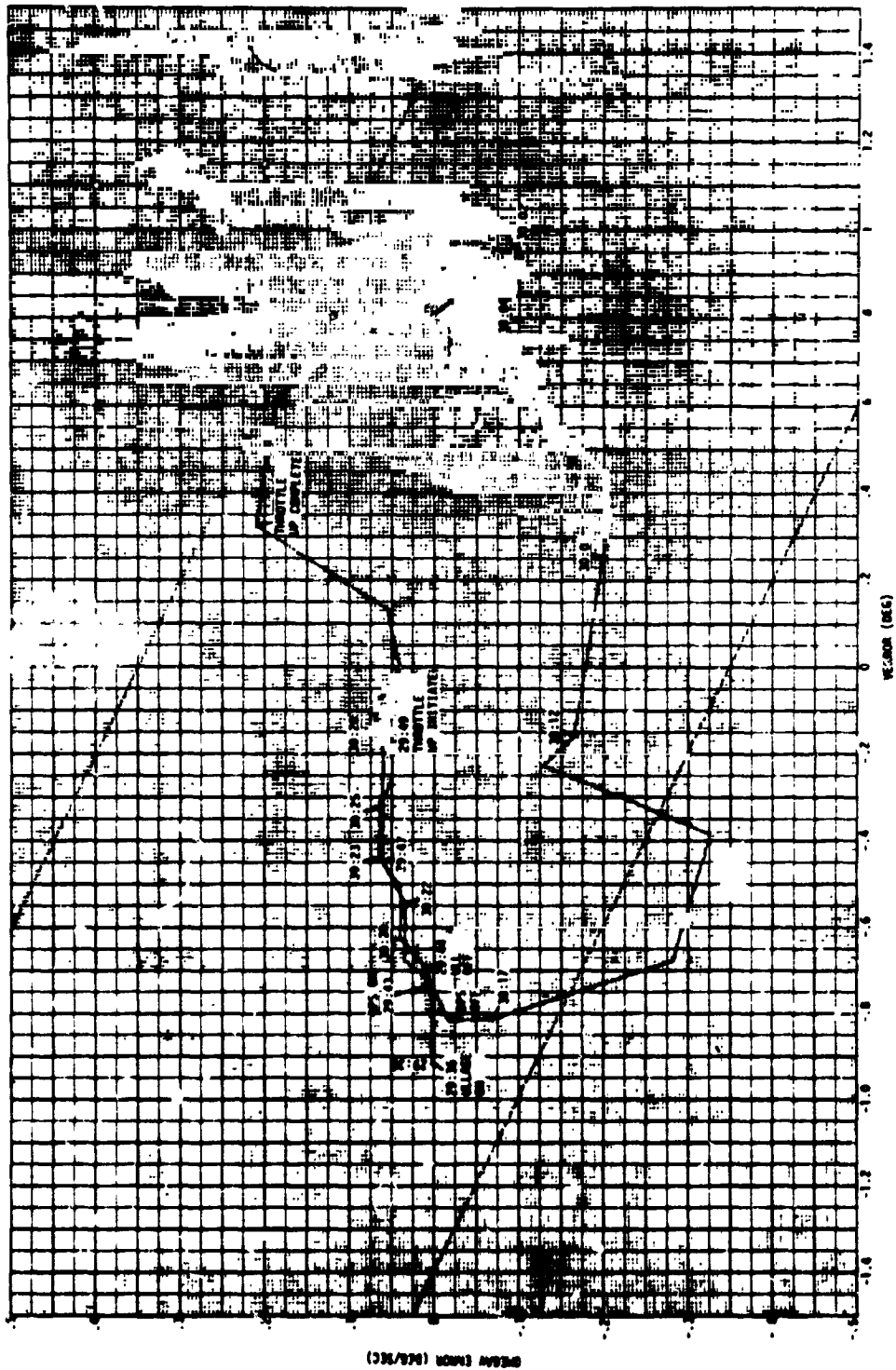
Figure 4-3 MCC2 Burn V Axis Phase Plane Plot
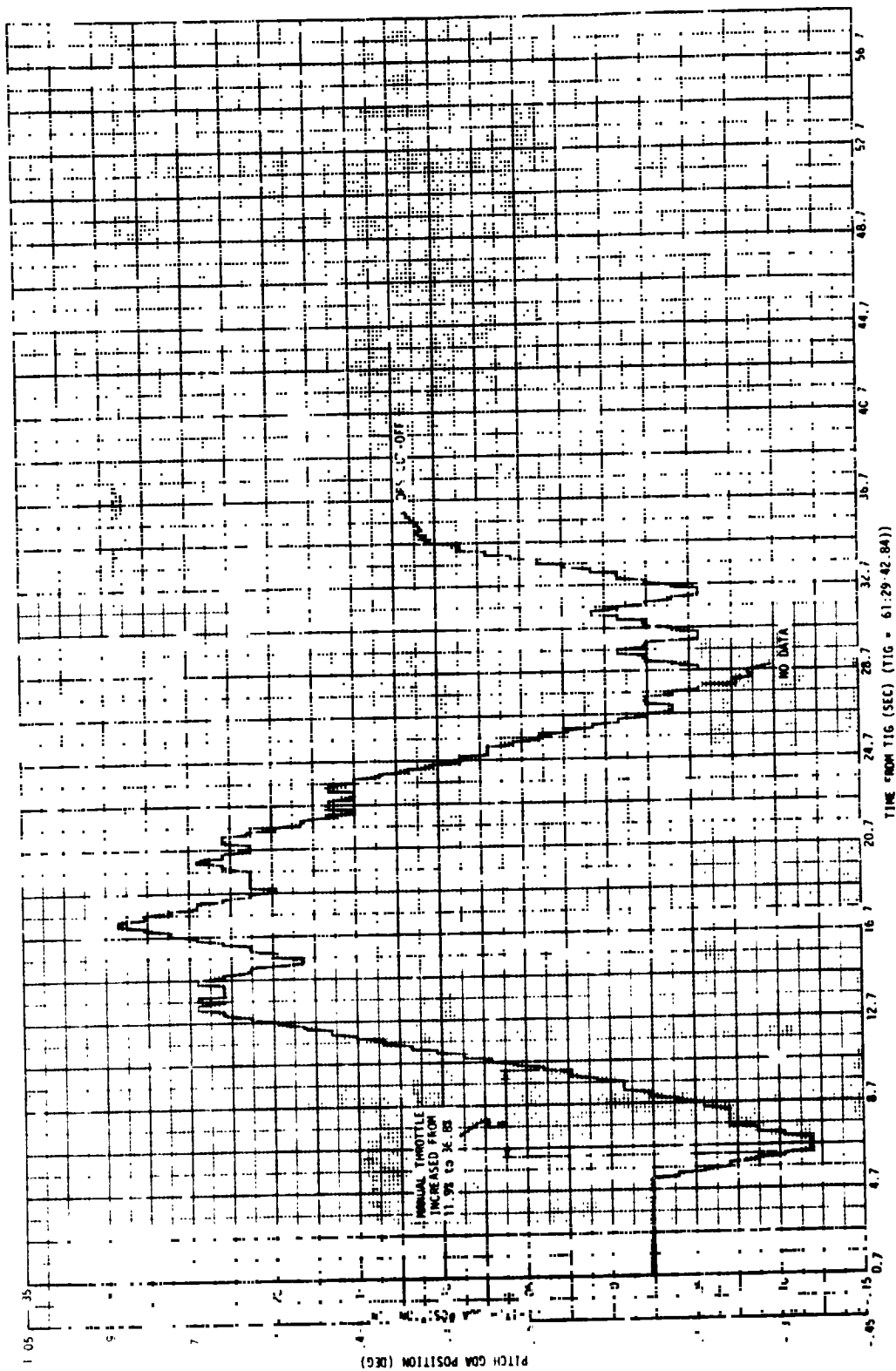
Figure 4-4   MCC2 Burn Pitch GDA
Position

4-43
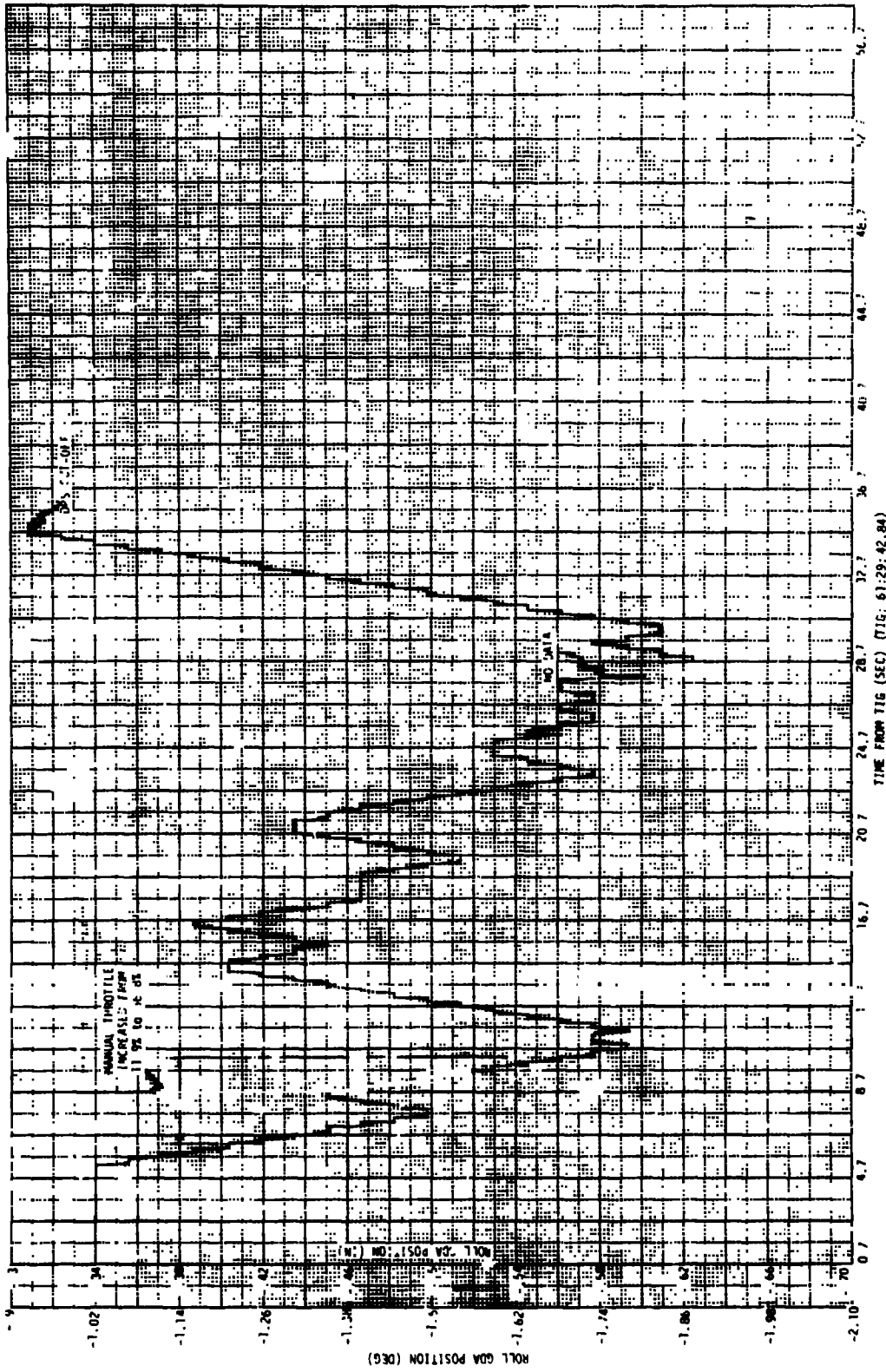
Figure 4-5 MCC2 Burn Roll GDA
Position

4-45

PERROR (DEG)

OMEGAP ERROR (DEG/SEC)
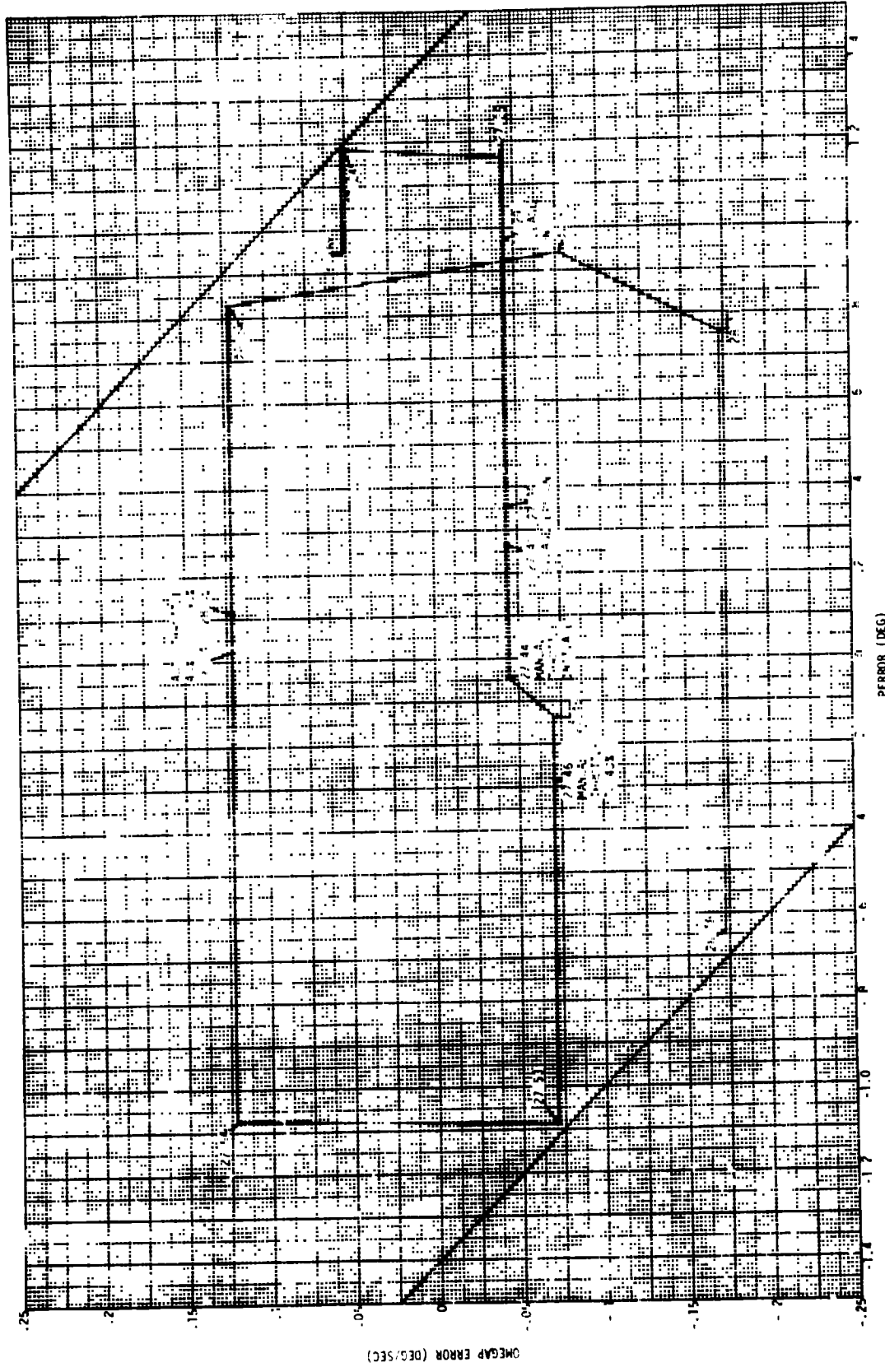
Figure 4-6 TEI Burn From Prior to Burn
Initiation Through Throttle-
Up-P Axis Phase Plane Plot

4-47
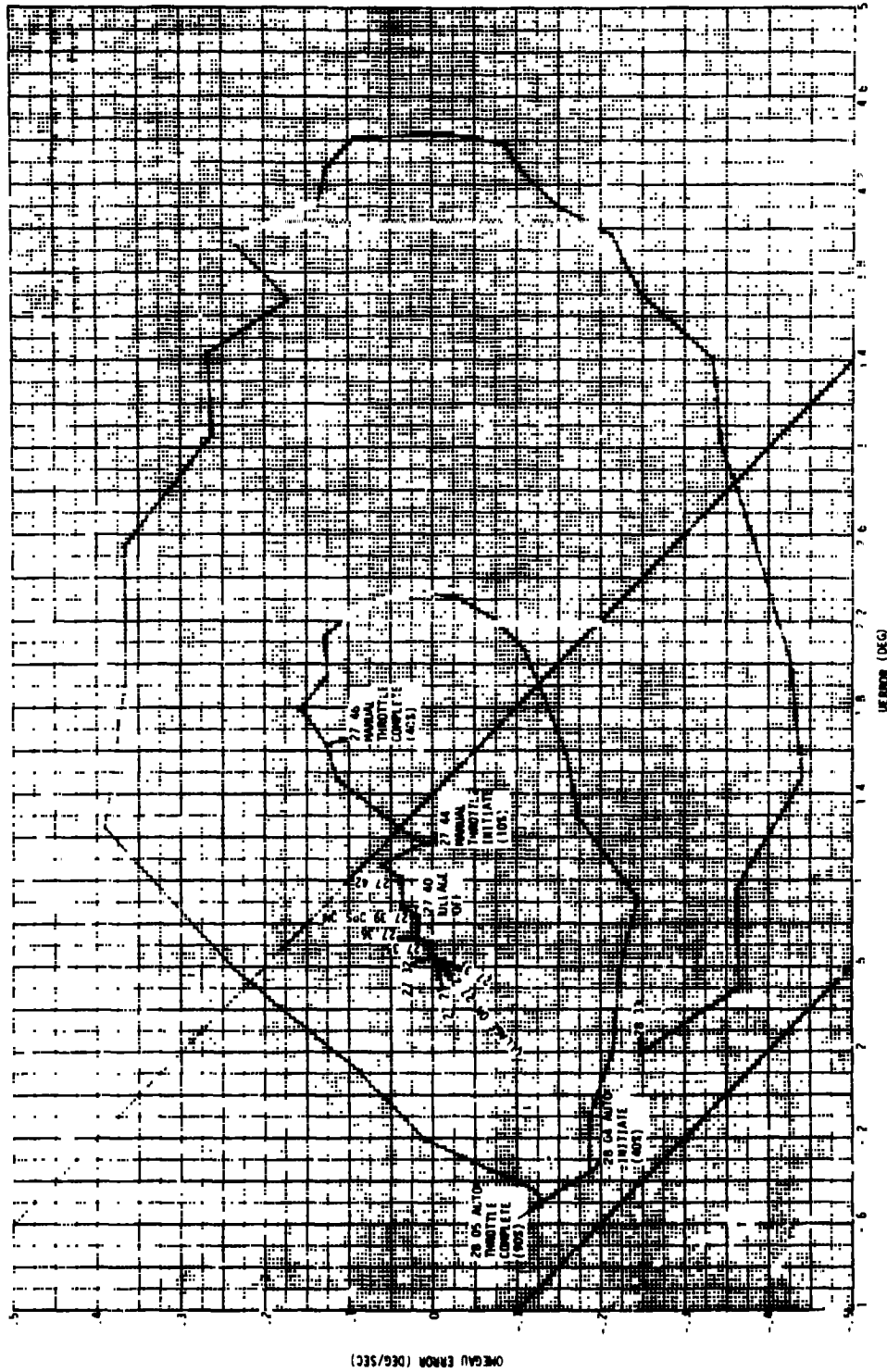
Figure 4-7 TEI Burn from Prior to
Burn Initiation through
Throttle-up—U Axis Phase
Plane Plot

4-49
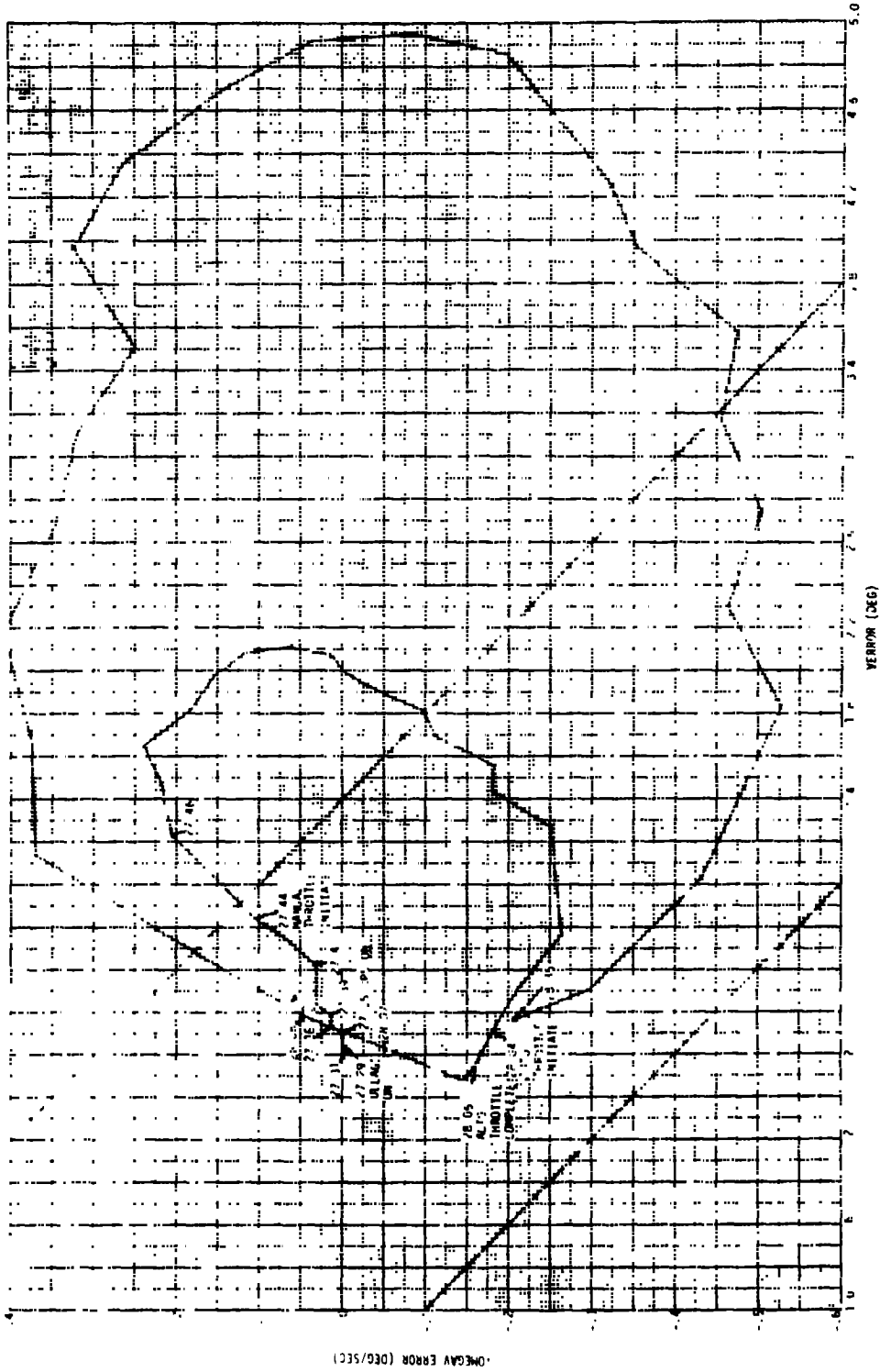
Figure 4-8 TEI Burn from Prior to
Burn Initiation through
Throttle-Up-V Axis Phase
Plane Plot

4-51
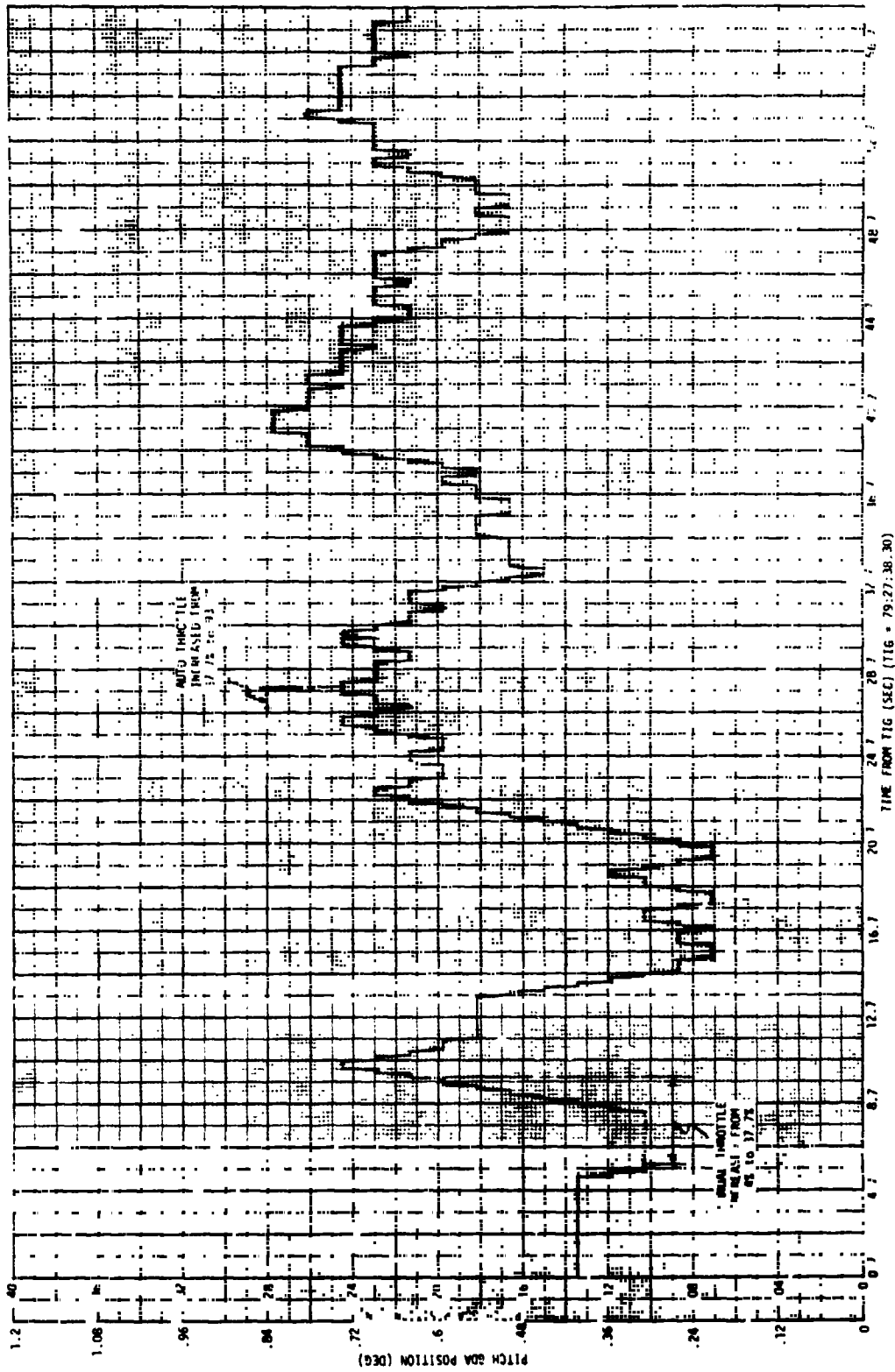
Figure 4-9   TEI Burn Pitch GDA
Position Through Throttle-Up

4-53
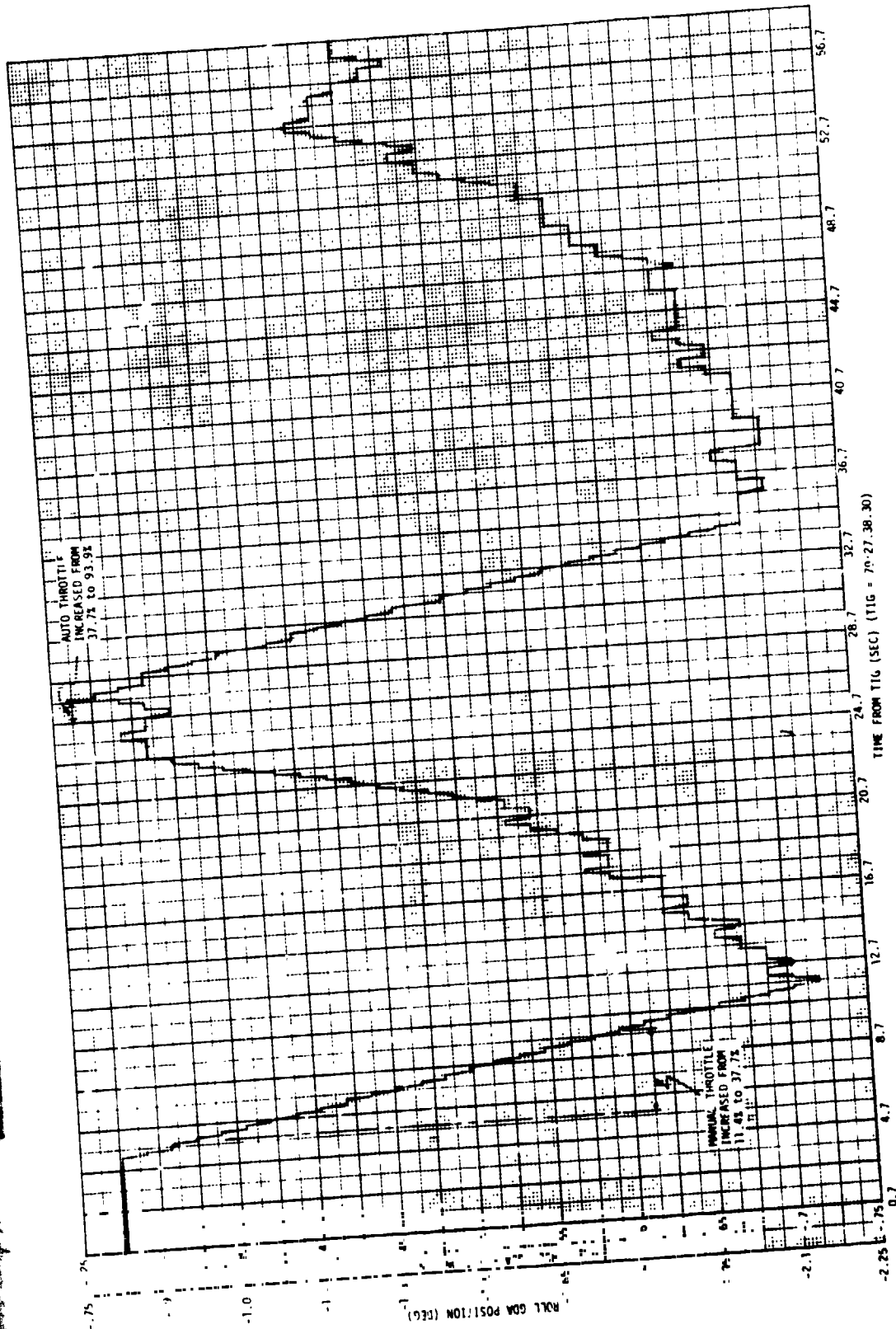
Figure 4-10   TEI Burn Roll GDA
Position Through
Throttle-Up

4-55
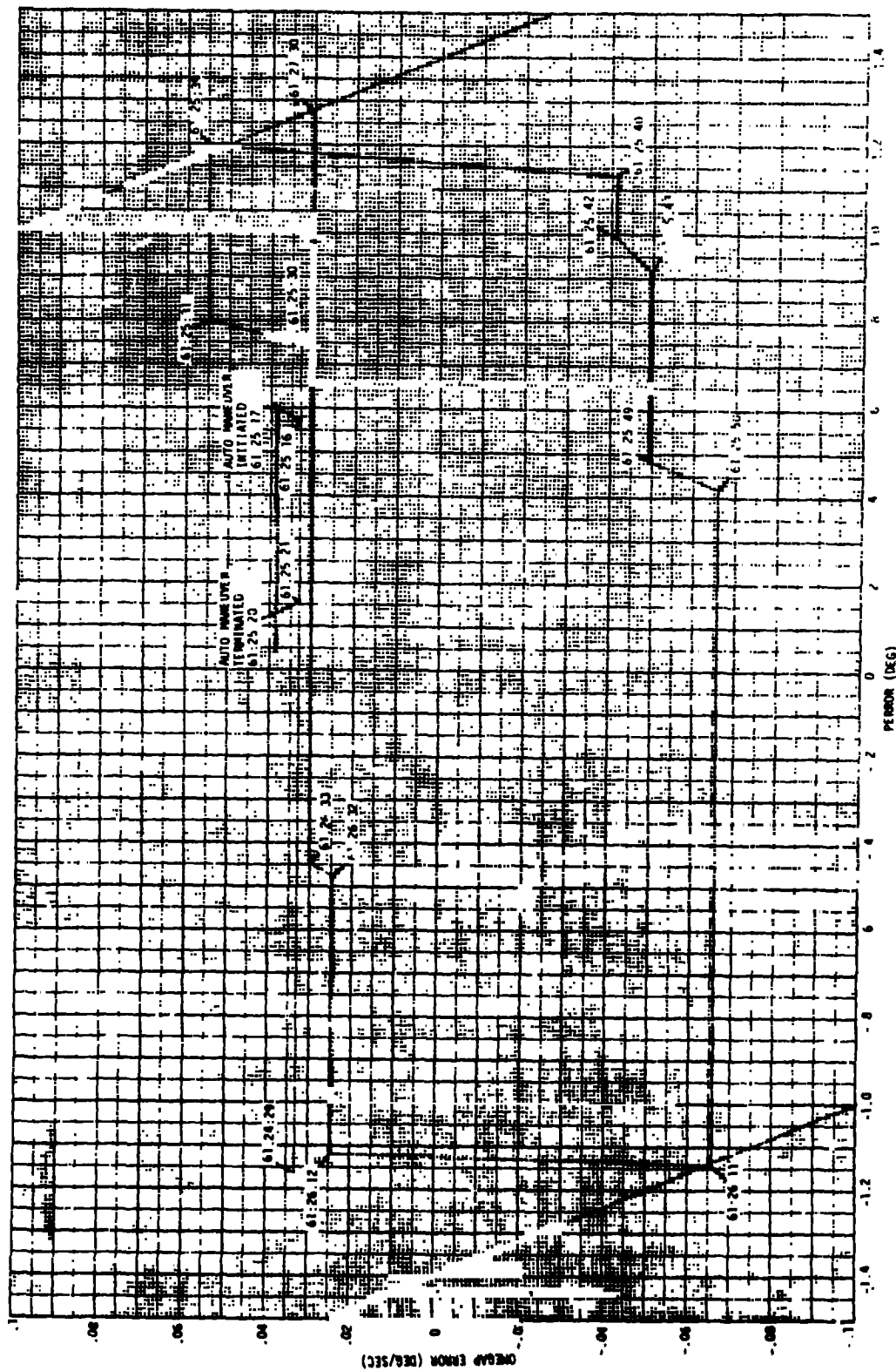
Figure 4-11   LM/CSM Configuration
               Auto Maneuver and
               Attitude Hold-P Axis
               Phase Plane Plot

4-57
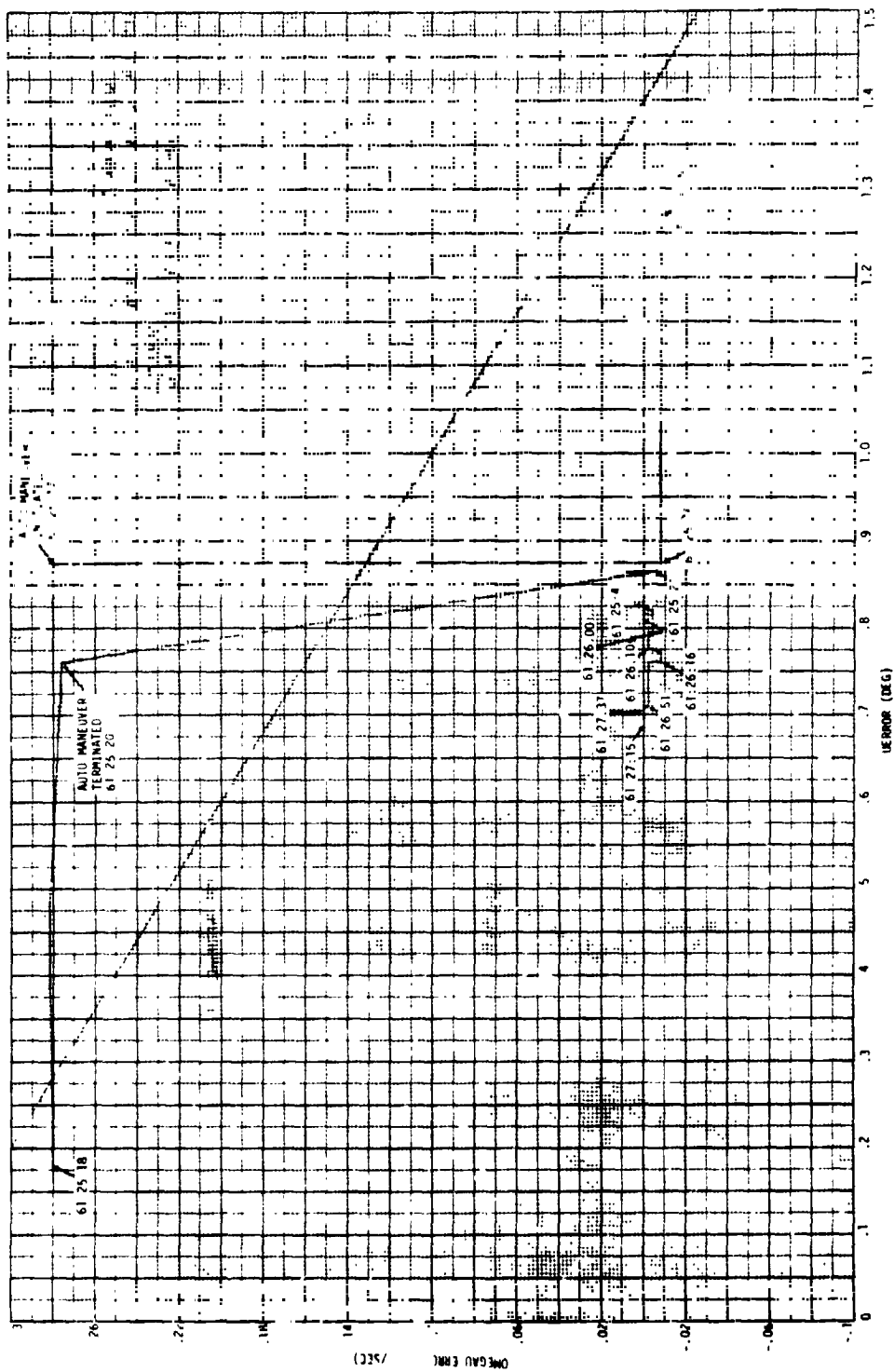
Figure 4-12   LM/CSM Configuration
Auto Maneuver and Attitude
Hold-U Axis Phase Plane Plot

4-59
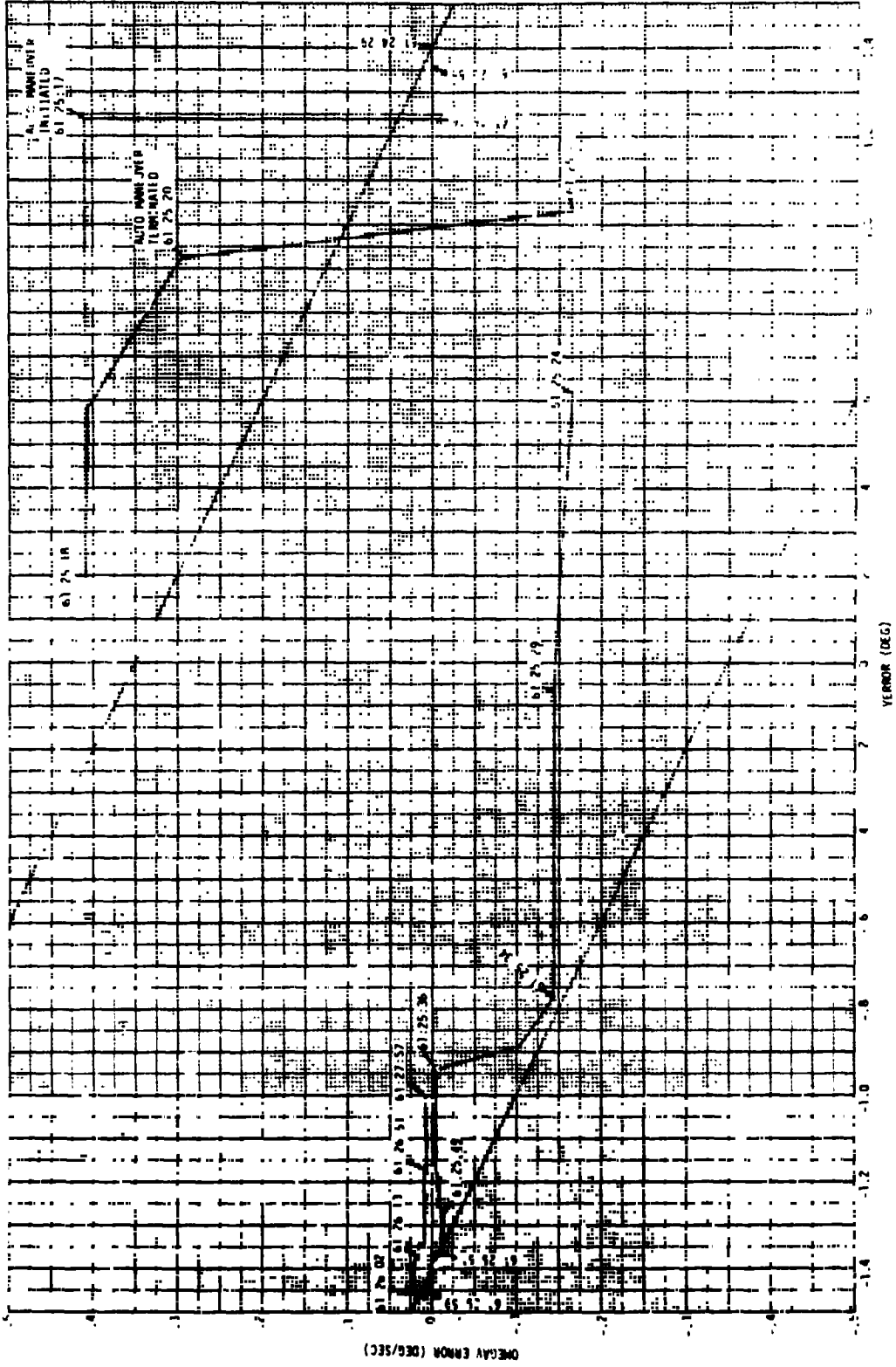
Figure 4-13 LM/CSM Configuration Auto
Maneuver and Attitude Hold
V Axis Phase Plane Plot

4-61
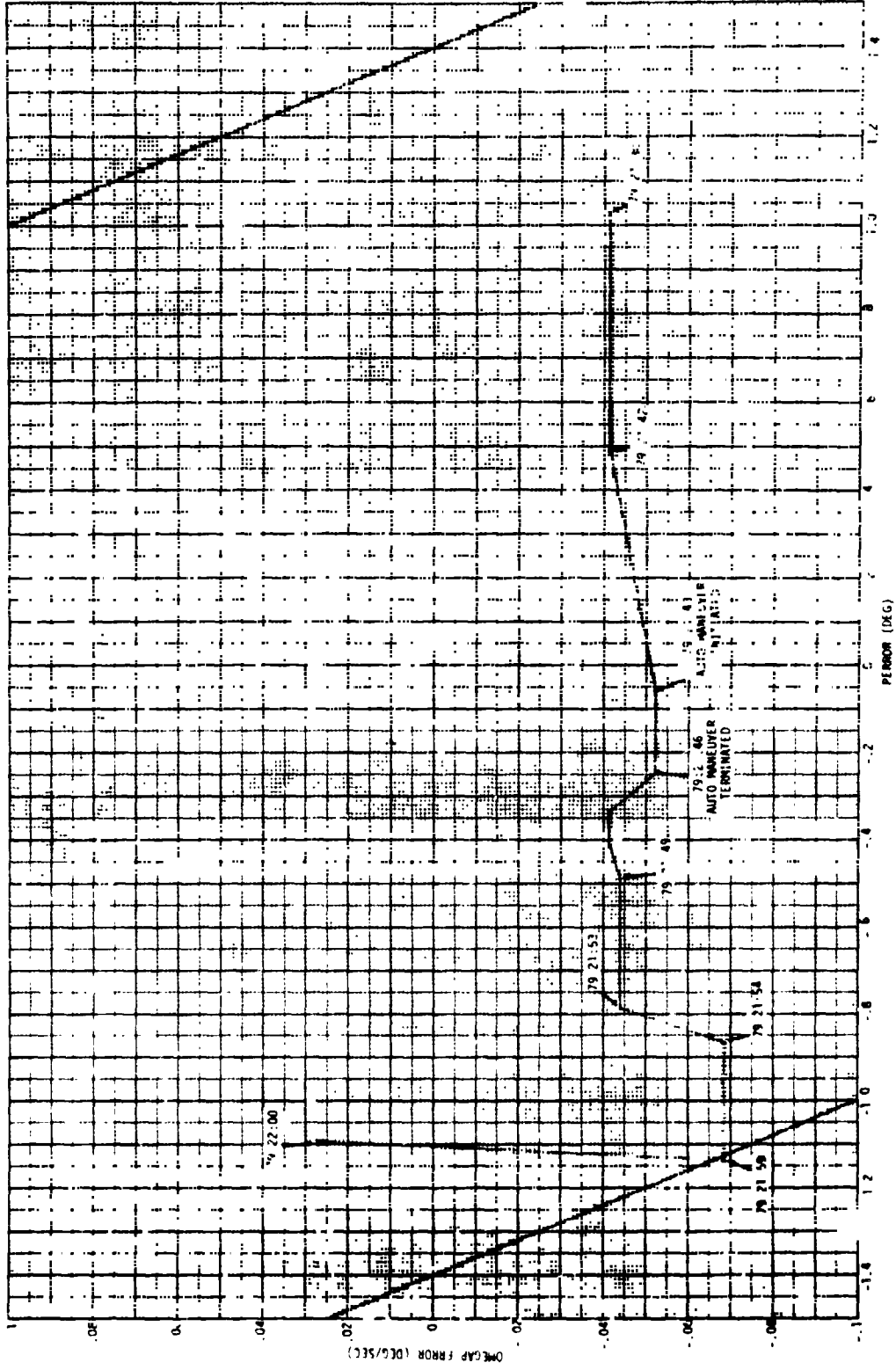
Figure 4-14 LM/CSM Configuration Auto
Maneuver—P Axis Phase
Plane Plot

4-63
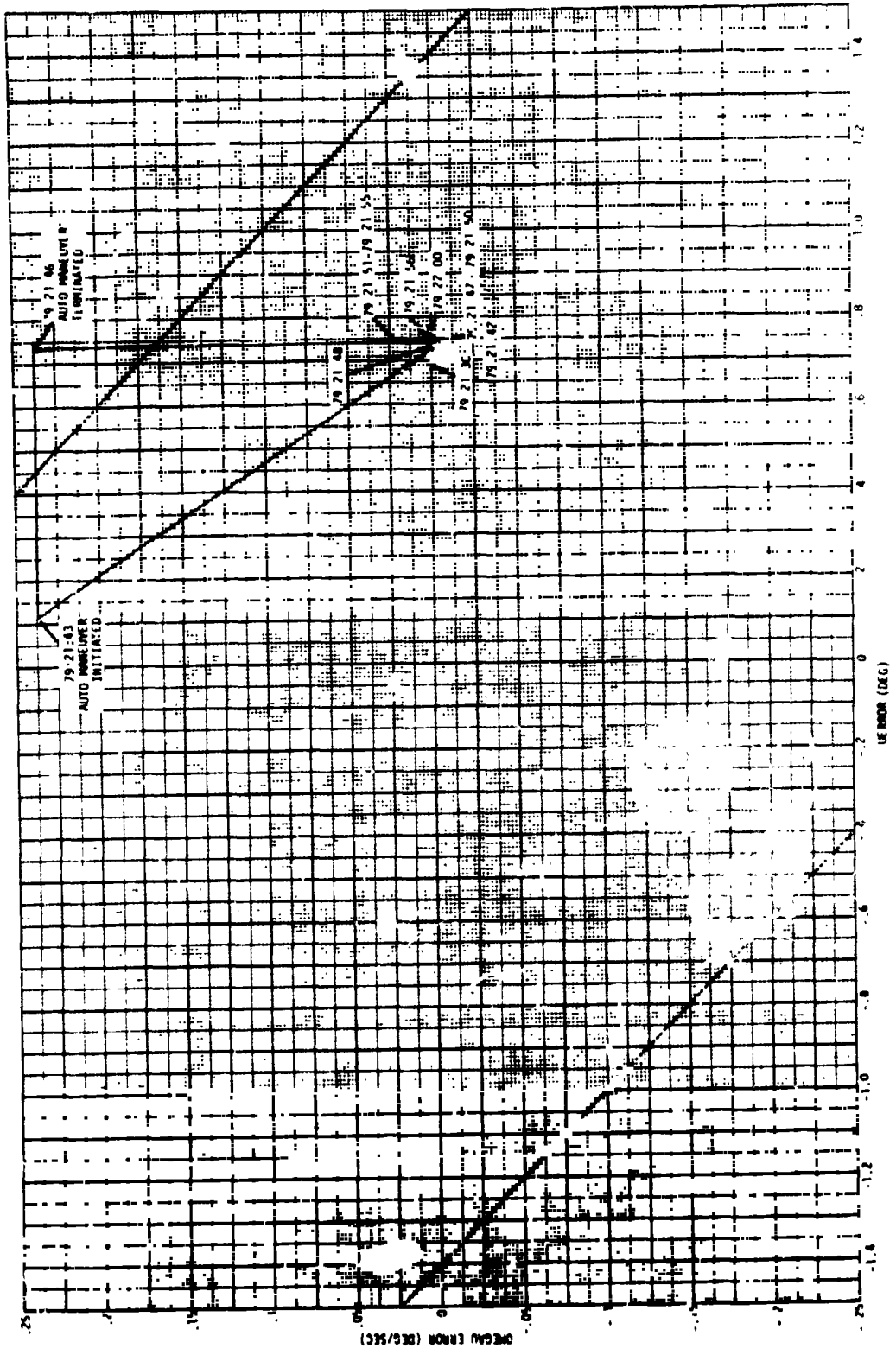
Figure 4-15 LM/CSM Configuration Auto
Maneuver-U Axis Phase
Plane Plot

4-65
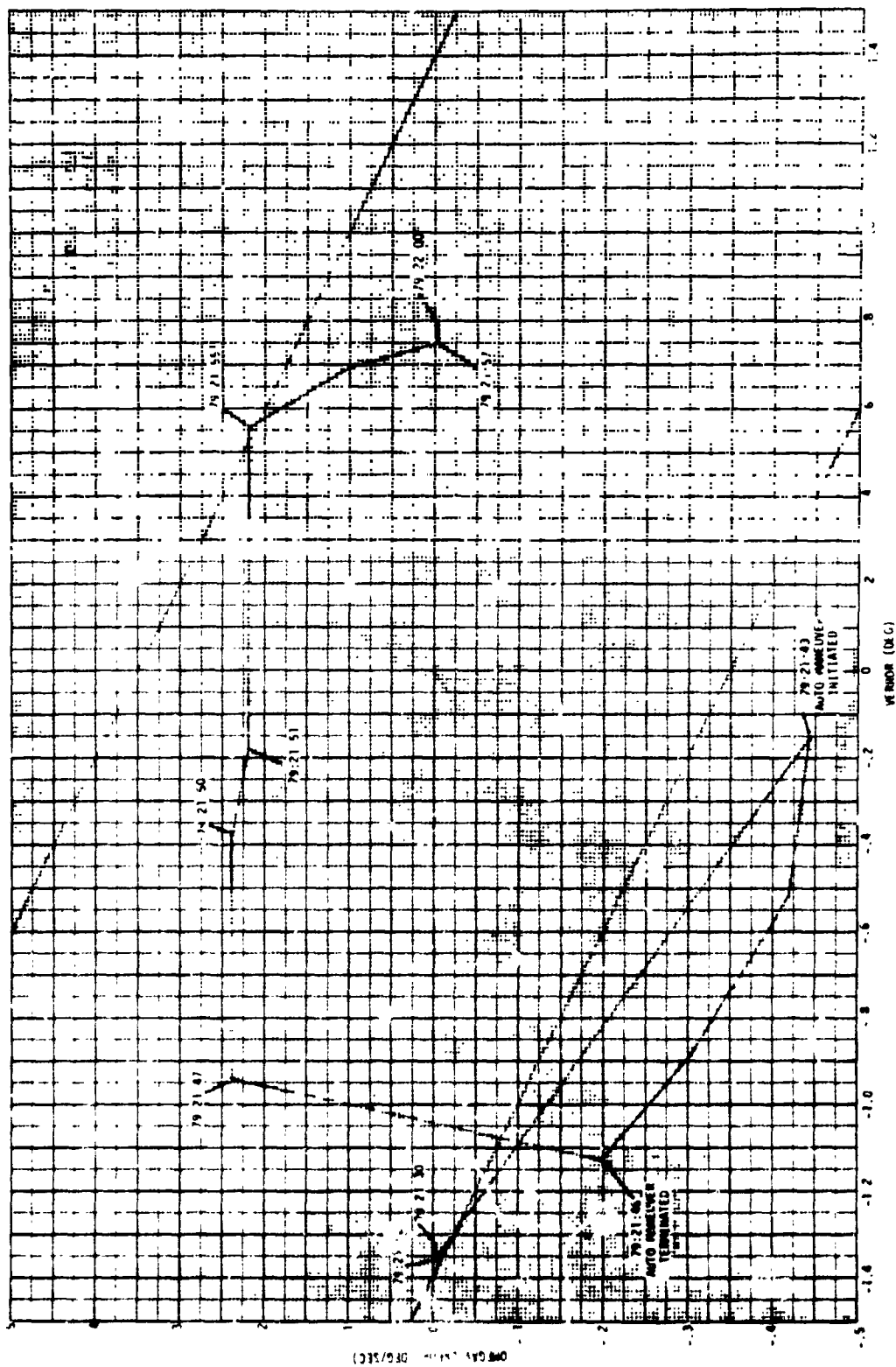
Figure 4-16   LM/CSM Configuration Auto
Maneuver—Y Axis Phase Plane
Plot

4-67
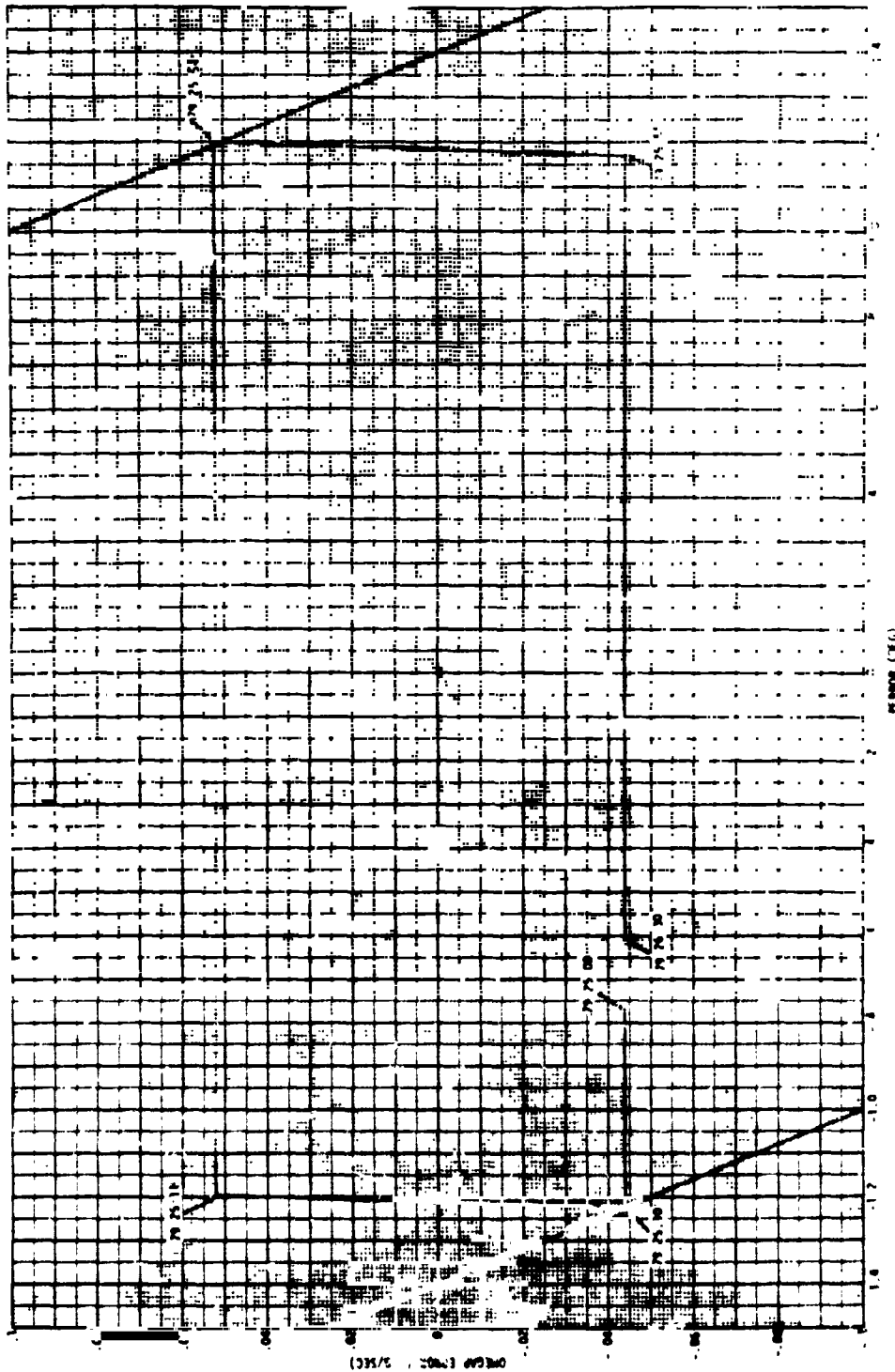
Figure 4-17 LM/CSM Configuration
Attitude Hold-P Axis
Phase Plane Plot

4-69

Figure 4-18 LM/CSM Configuration
Attitude Hold-U Axis
Phase Plane Plot

4-71

Figure 4-19 LM/CSM Configuration
Attitude Hold-V Axis
Phase Plane Plot

4-73

Figure 4-20 LM/CM Configuration
Manual Maneuver and
Attitude Hold-P Axis
Phase Plane Plot

4-75

Figure 4-21 LM/CM Configuration Manual
Maneuver and Attitude Hold
U Axis Phase Plane Plot

4-77
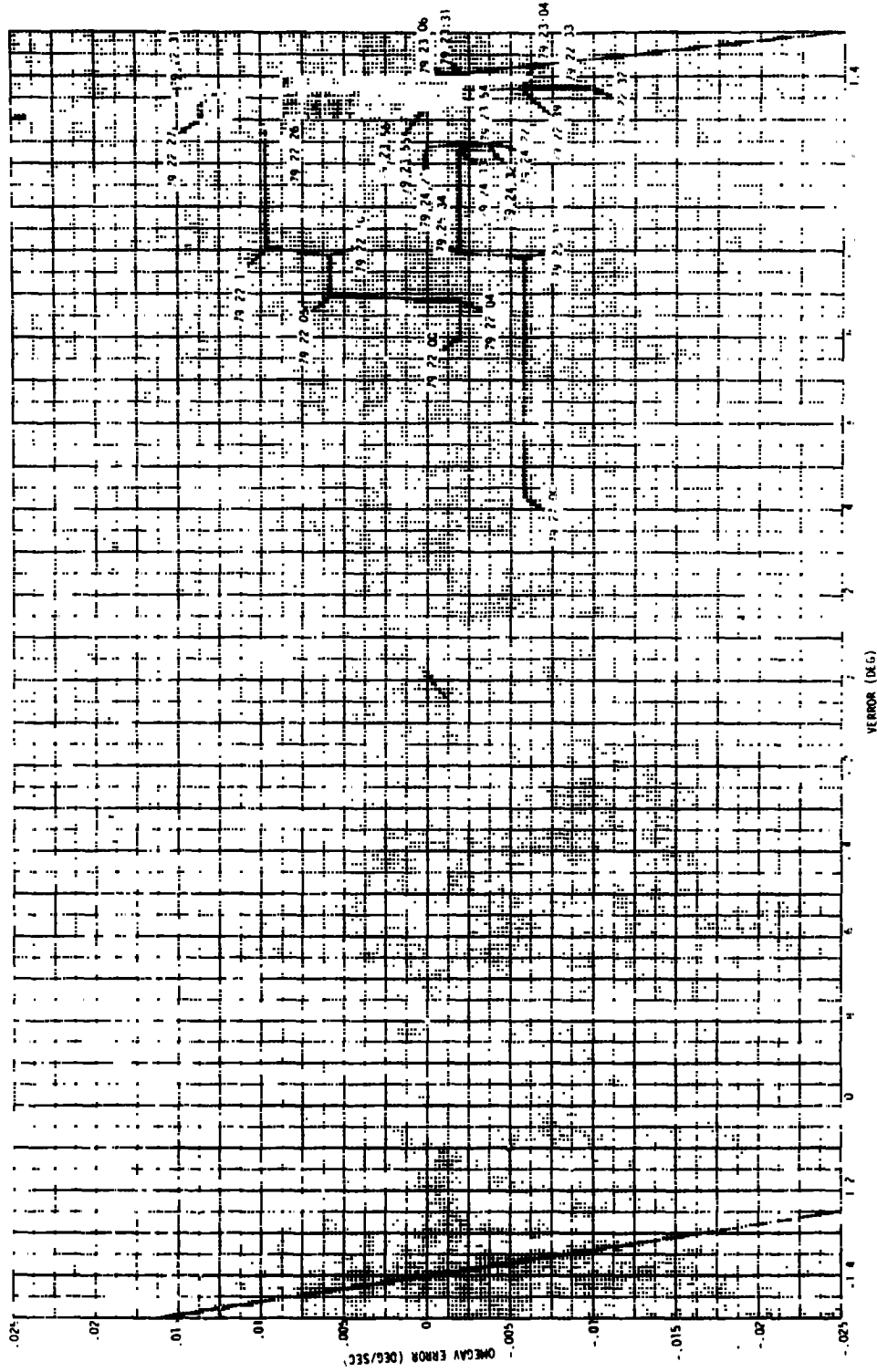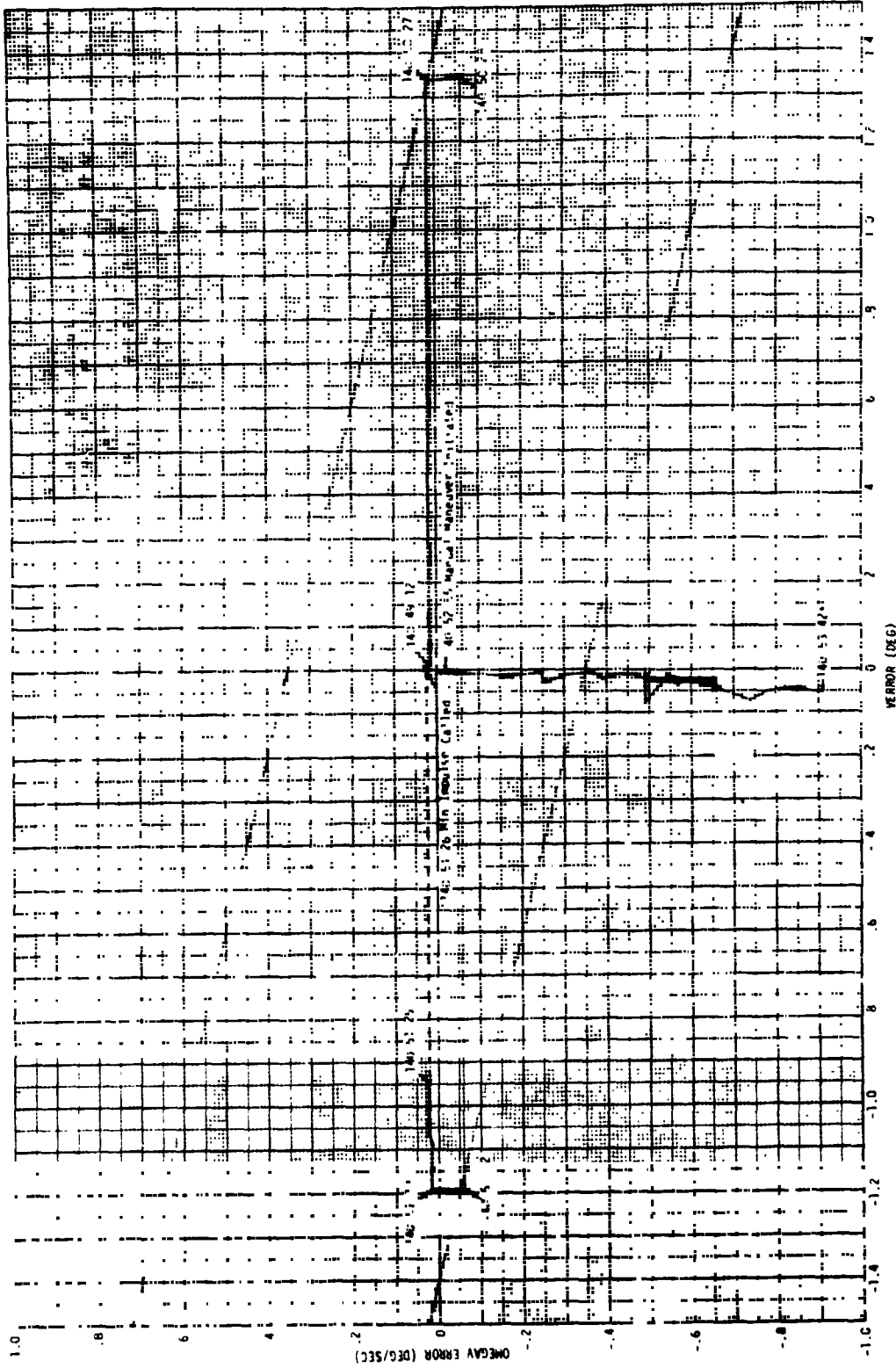
Figure 4-22 LM/CM Configuration Manual
Maneuver and Attitude Hold
V Axis Phase Plane Plot

4-79
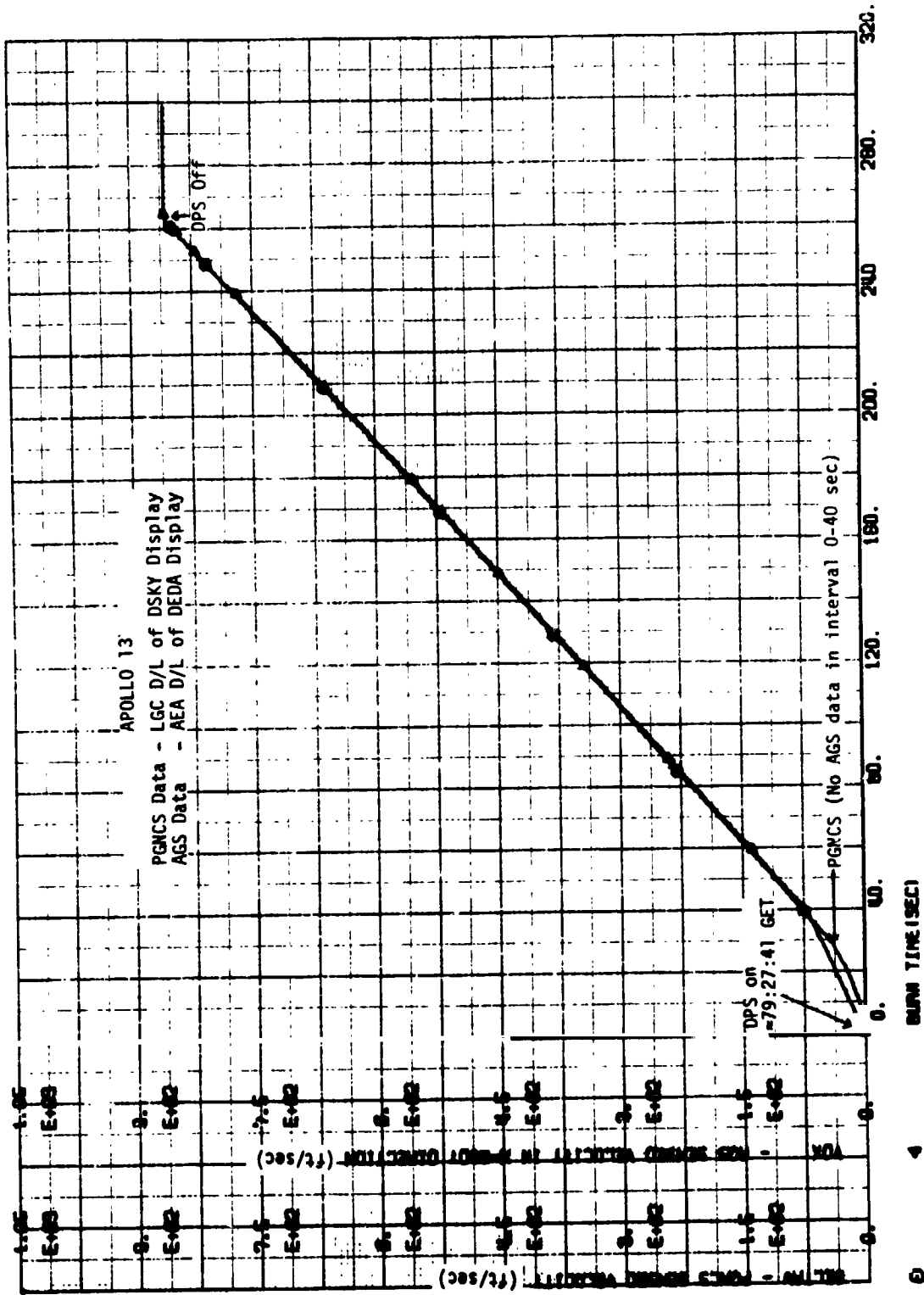
Figure 4-23   AGS/PGNCS Sensed Velocity
Comparison During TEI Burn
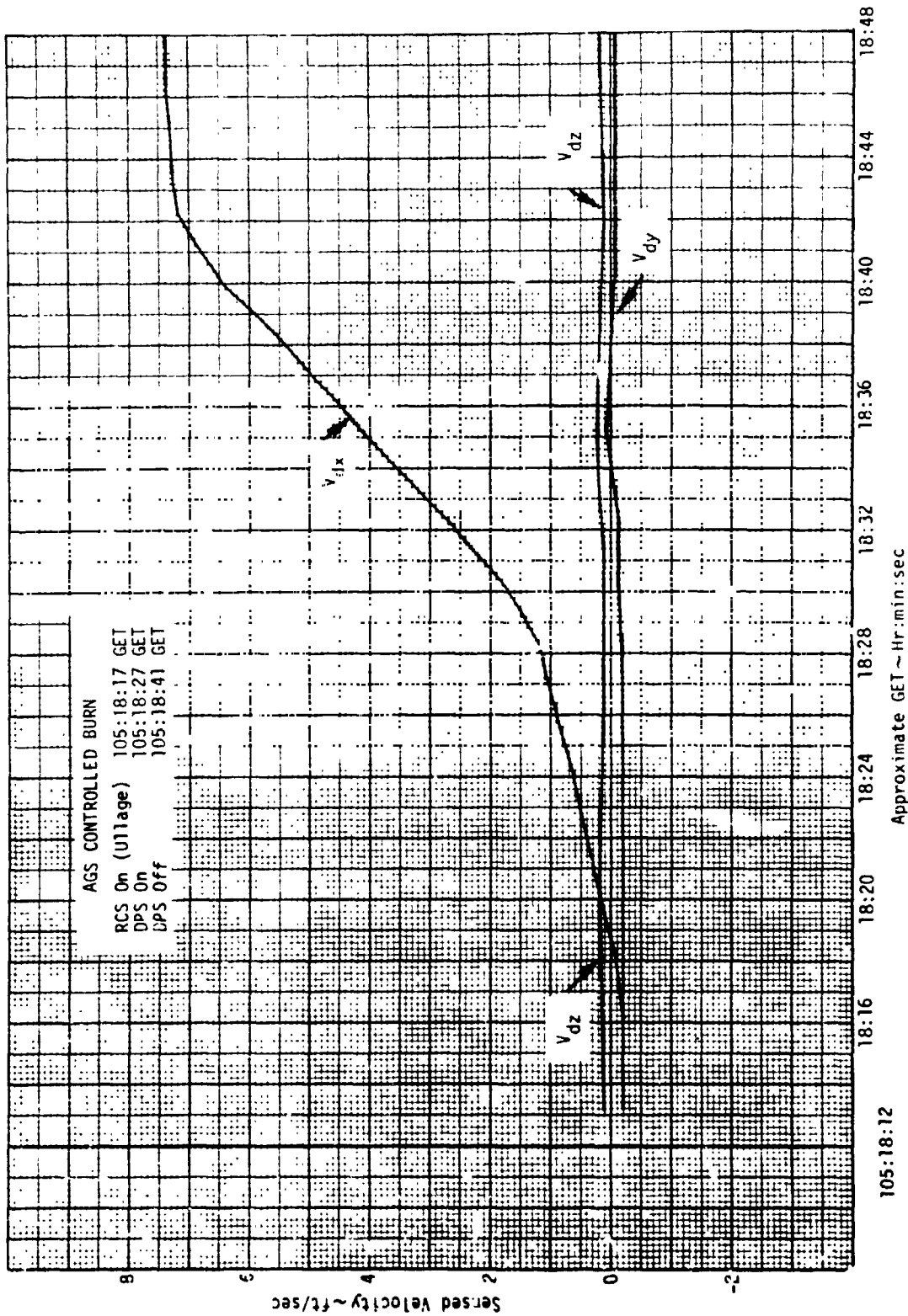
Figure 4.24   AGS Sensed Velocity Along
Body Axes During MCC-3 Burn

4-82
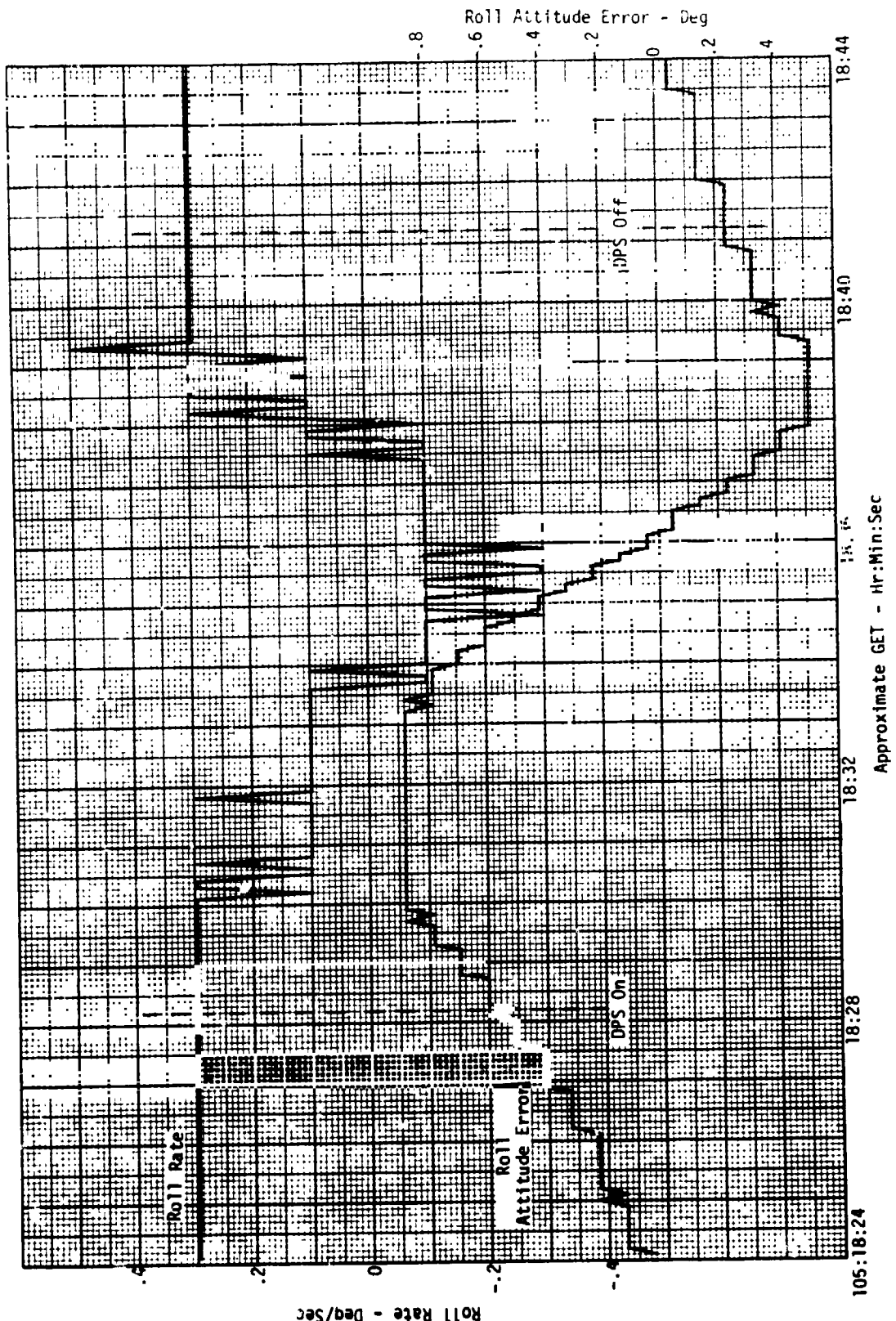
Figure 4-25   Roll Rate and Attitude Error
During MCC-3 (AGS Controlled)
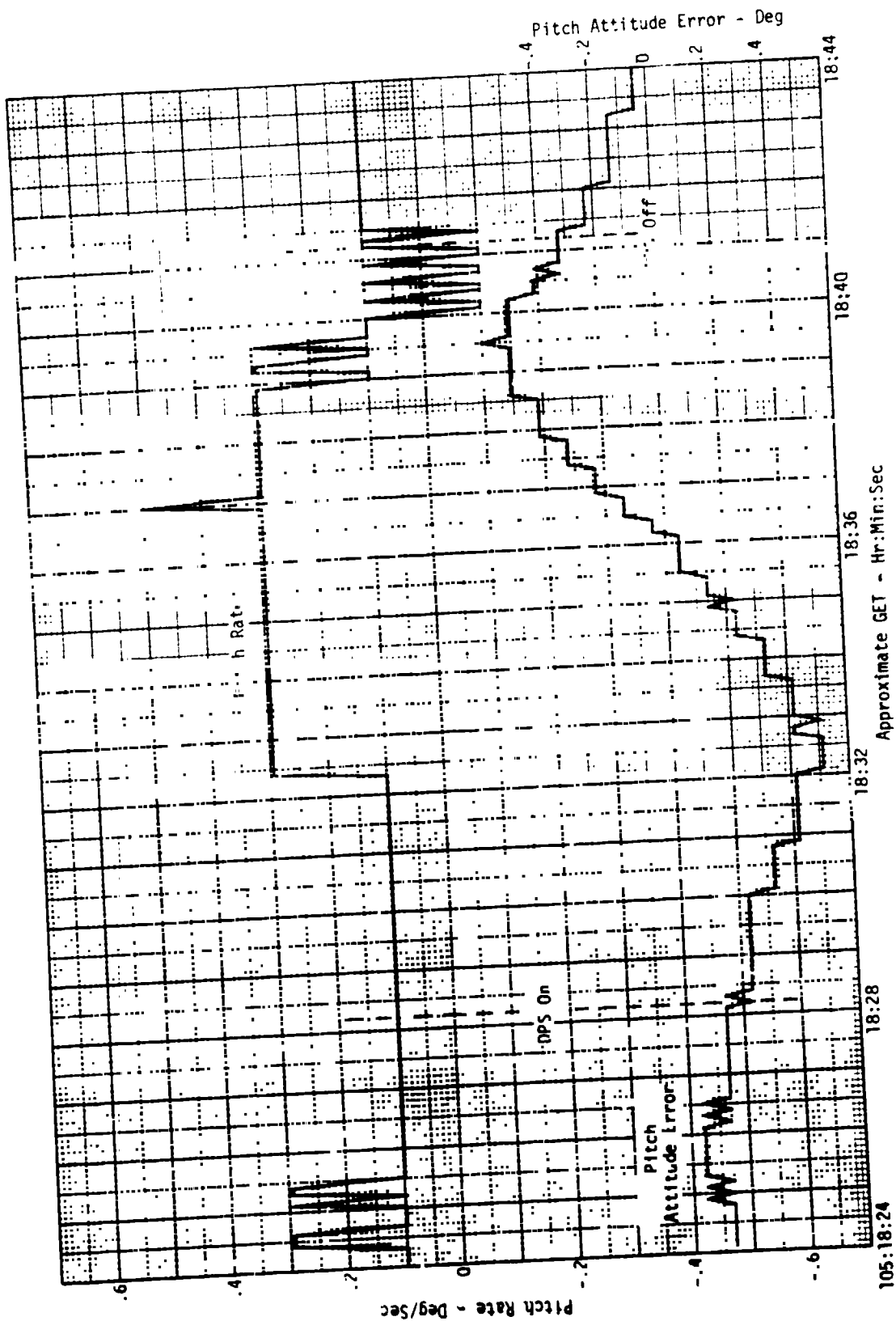
Figure 4-26   Pitch Rate and Attitude Error
               During MCC-3 (AGS Controlled)
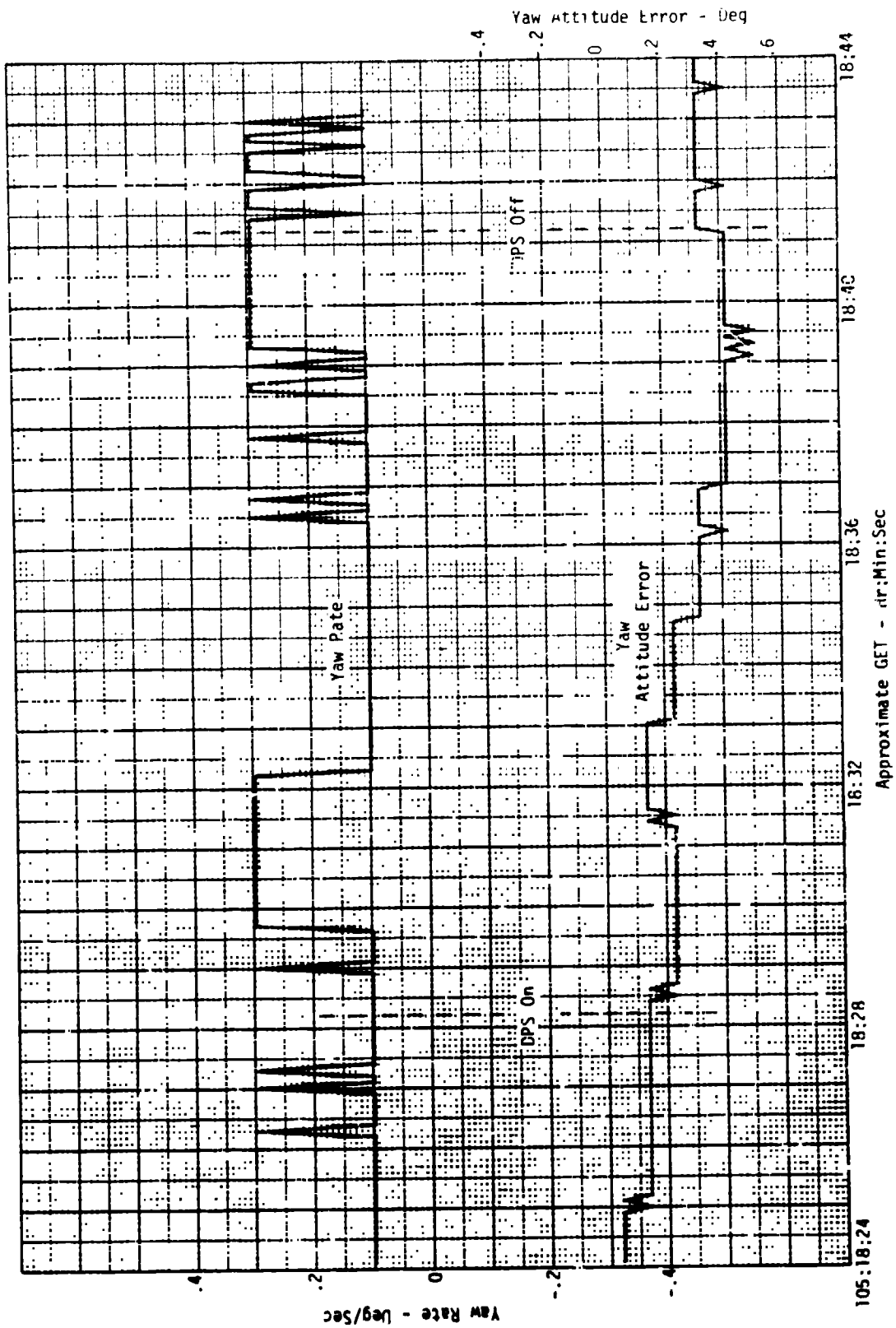
Figure 4-27   Yaw Rate and Attitude Error
During MCC-3 (AGS Controlled)
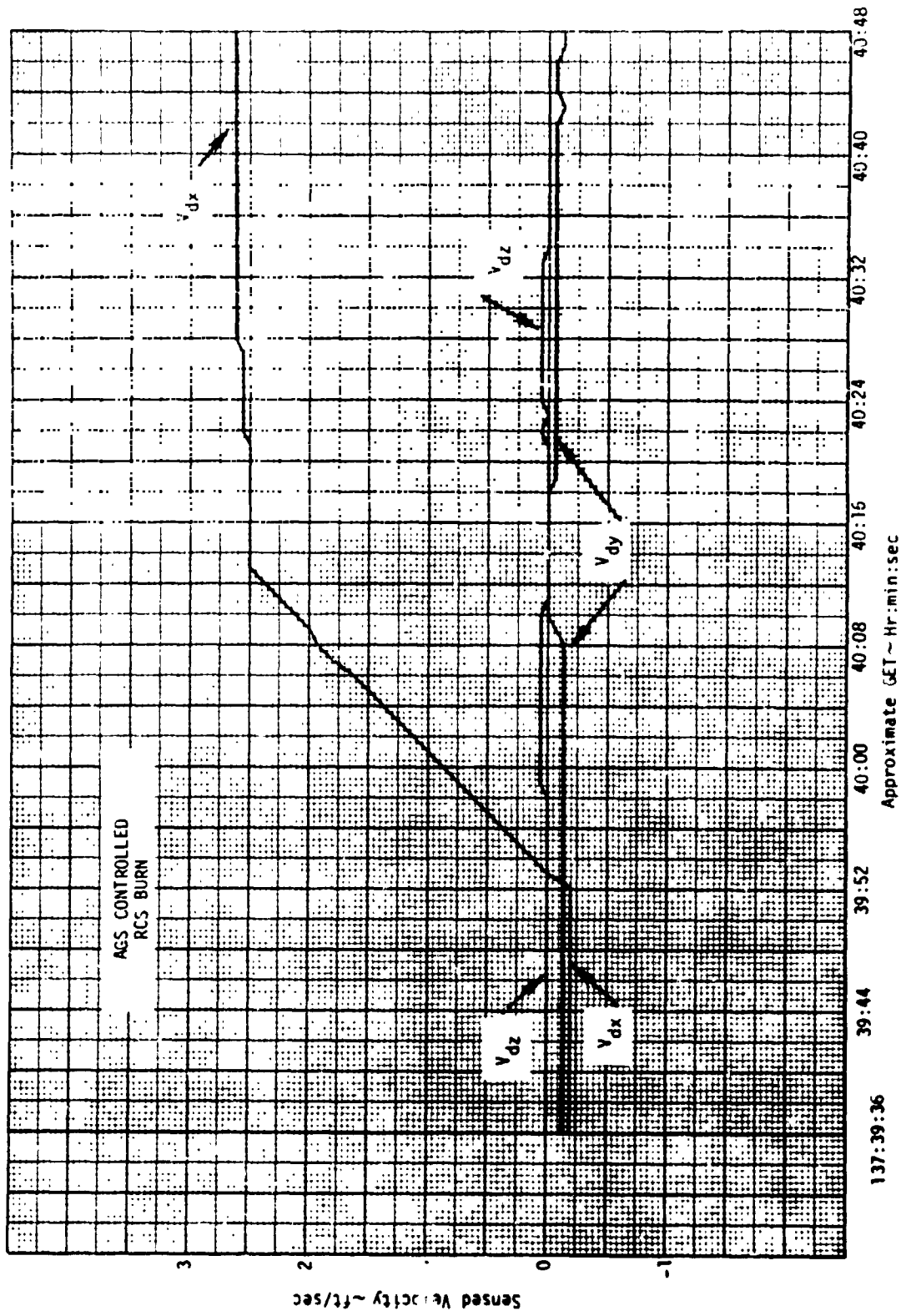
Figure 4-28   AGS Sensed Velocity Along
Body Axes During MCC-4 Burn
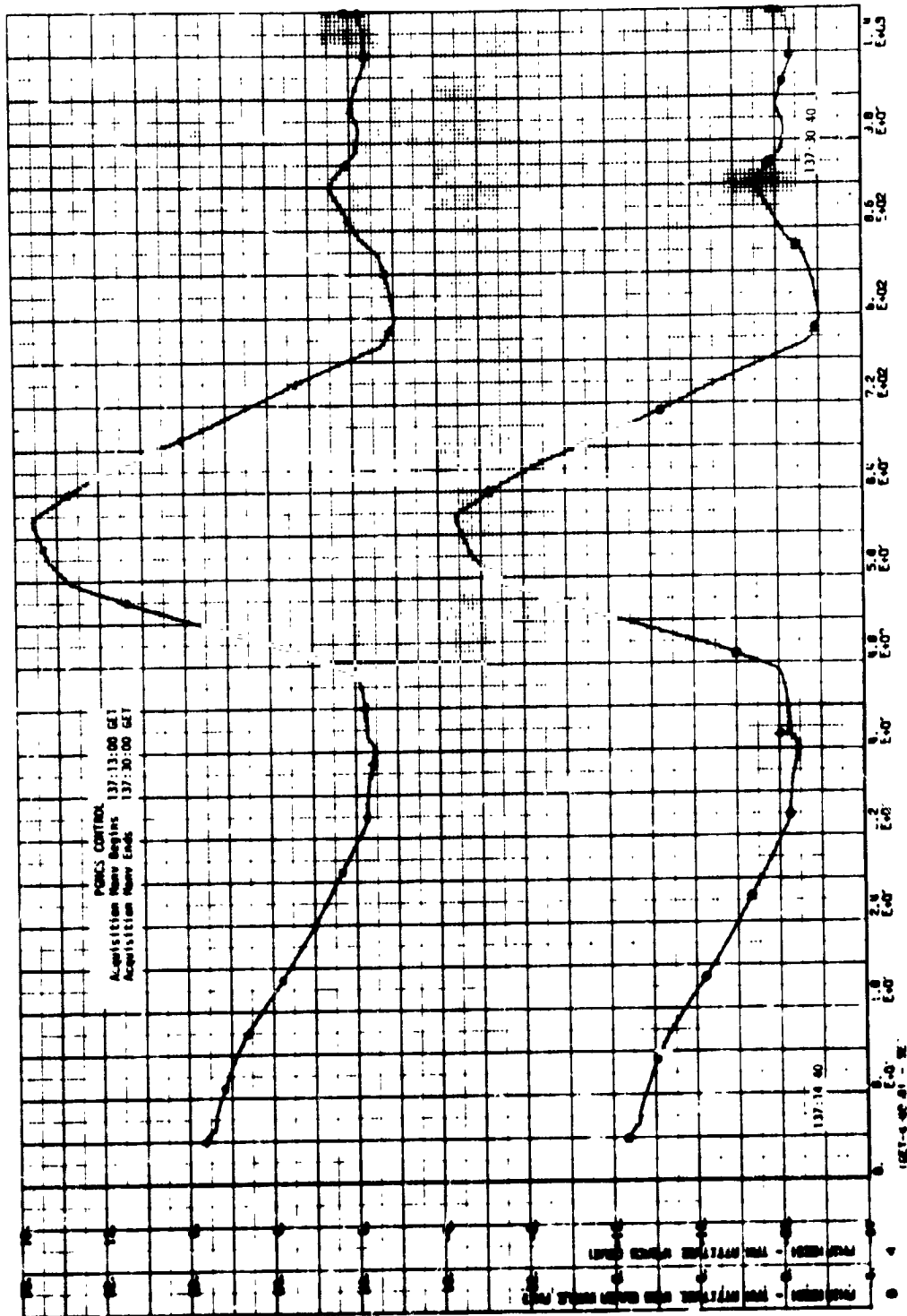
Figure 4-29   Acquisition of Yaw
Attitude for MCC-4 Burn

4-87
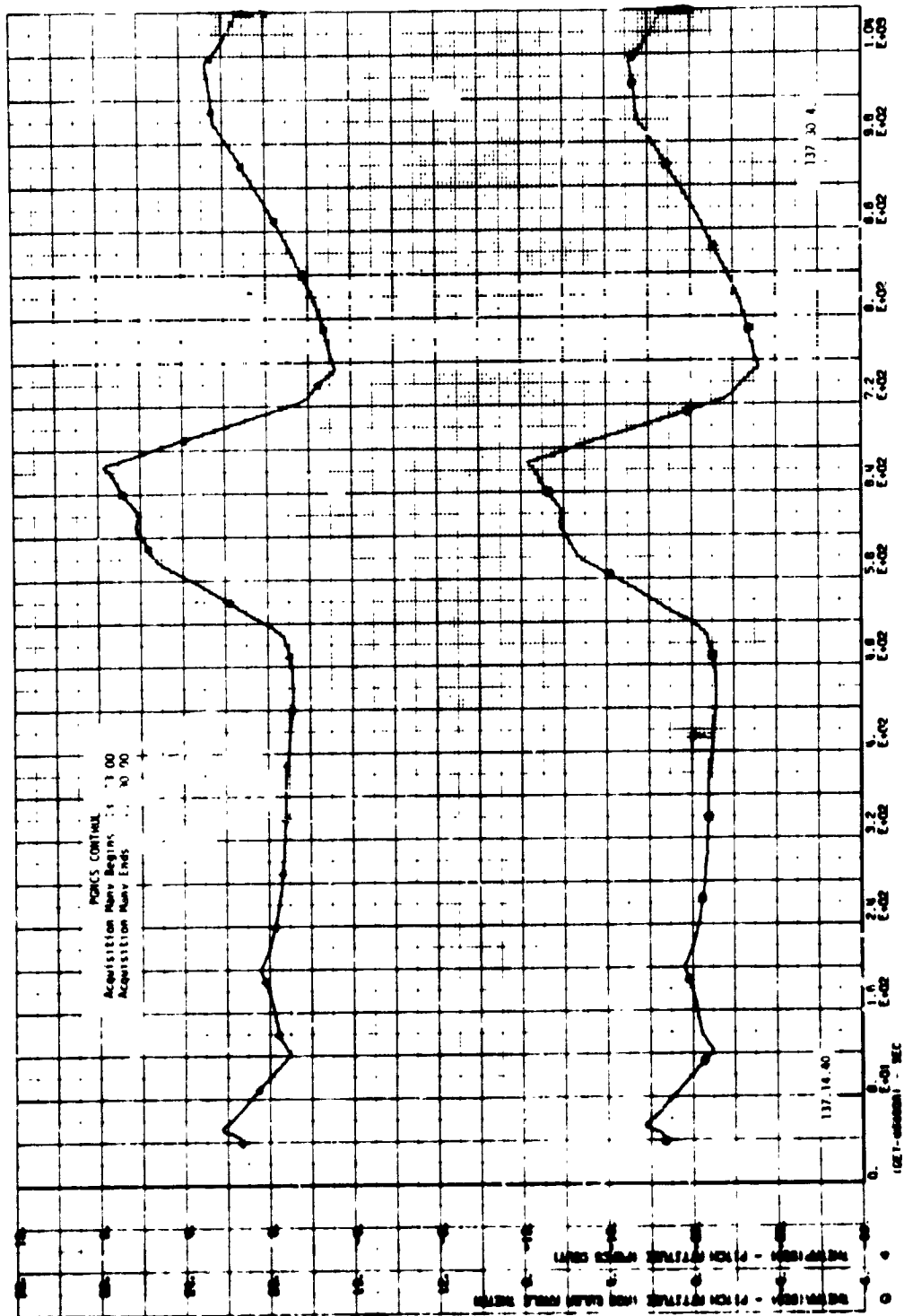
Figure 4-30   Acquisition of Pitch
                Attitude for MCC-4 Burn
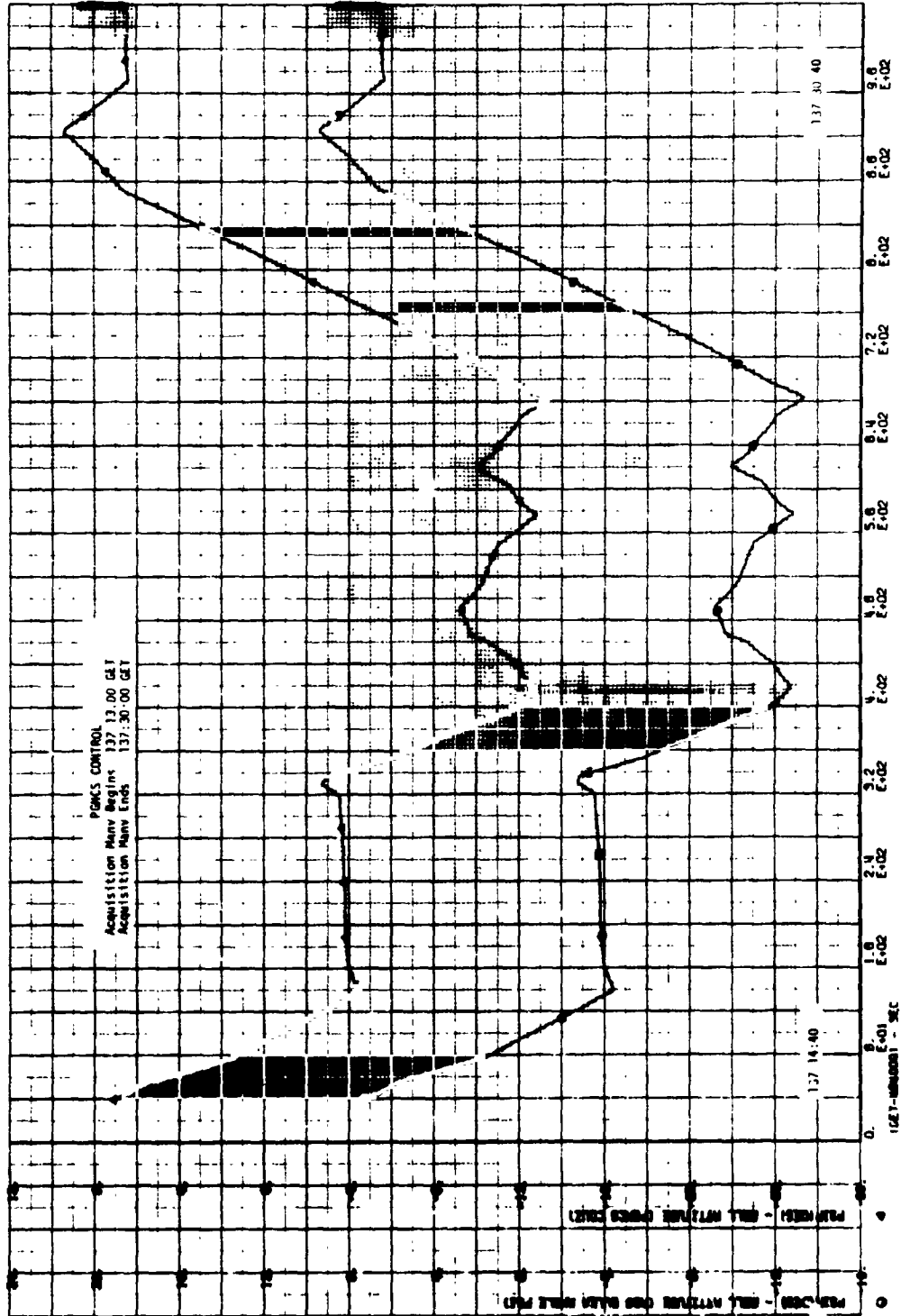
Figure 4-31   Acquisition of Roll
              Attitude for MCC-4 Burn
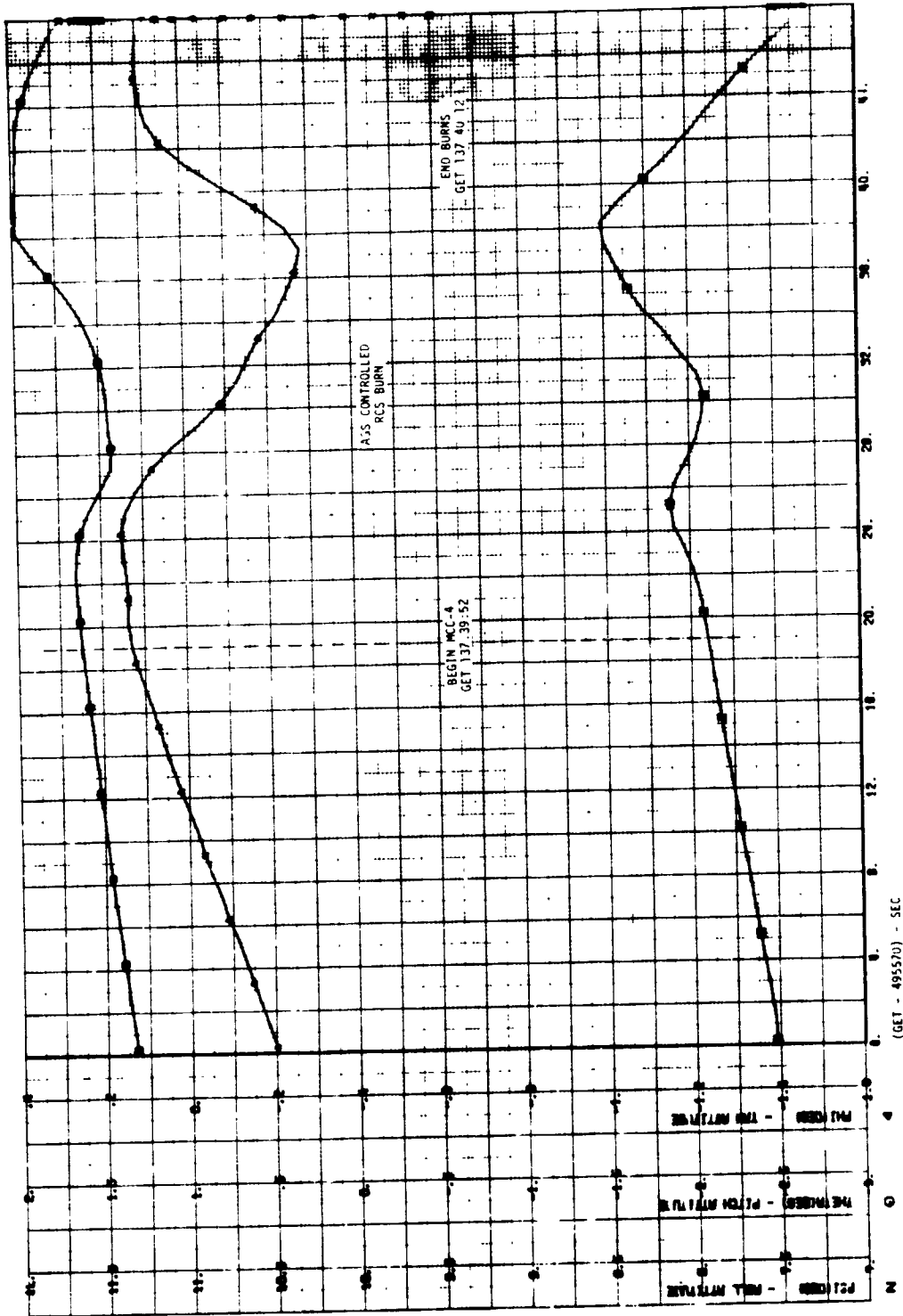
Figure 4-32   Spacecraft Attitude During
MCC-4 Burn (AGS Euler Angles)
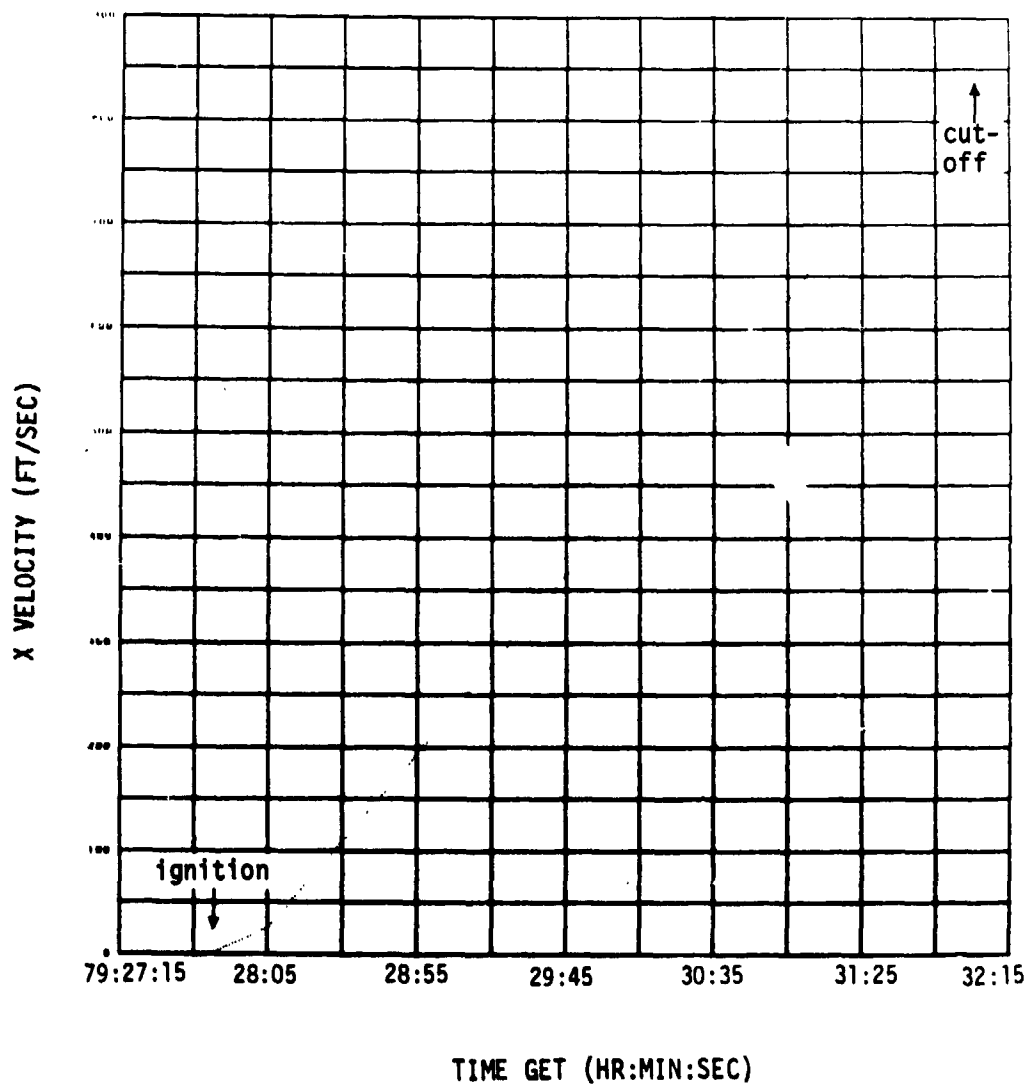
FIGURE 4-33   ACCUMULATED X-AXIS SENSED VELOCITY
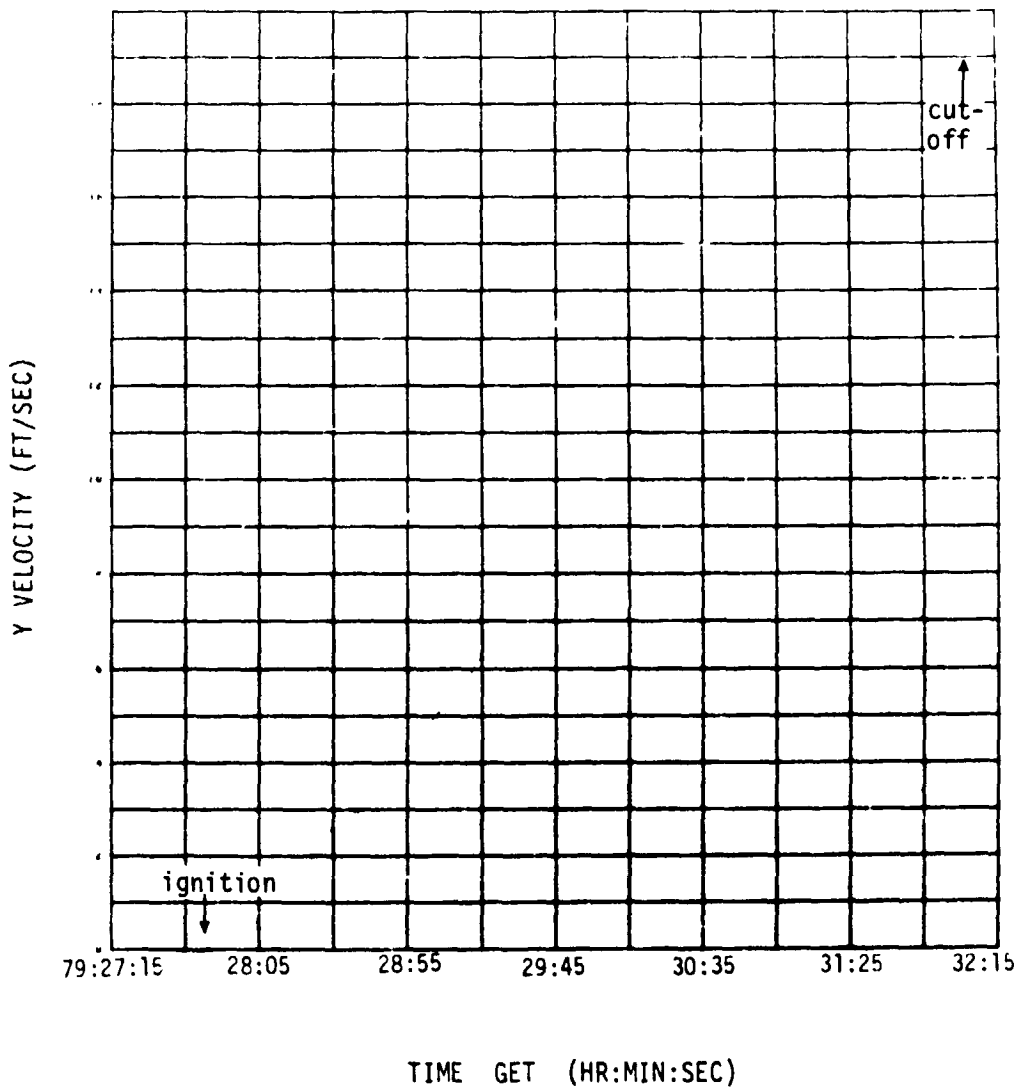
FIGURE 4-34 ACCUMULATED Y-AXIS SENSED VELOCITY
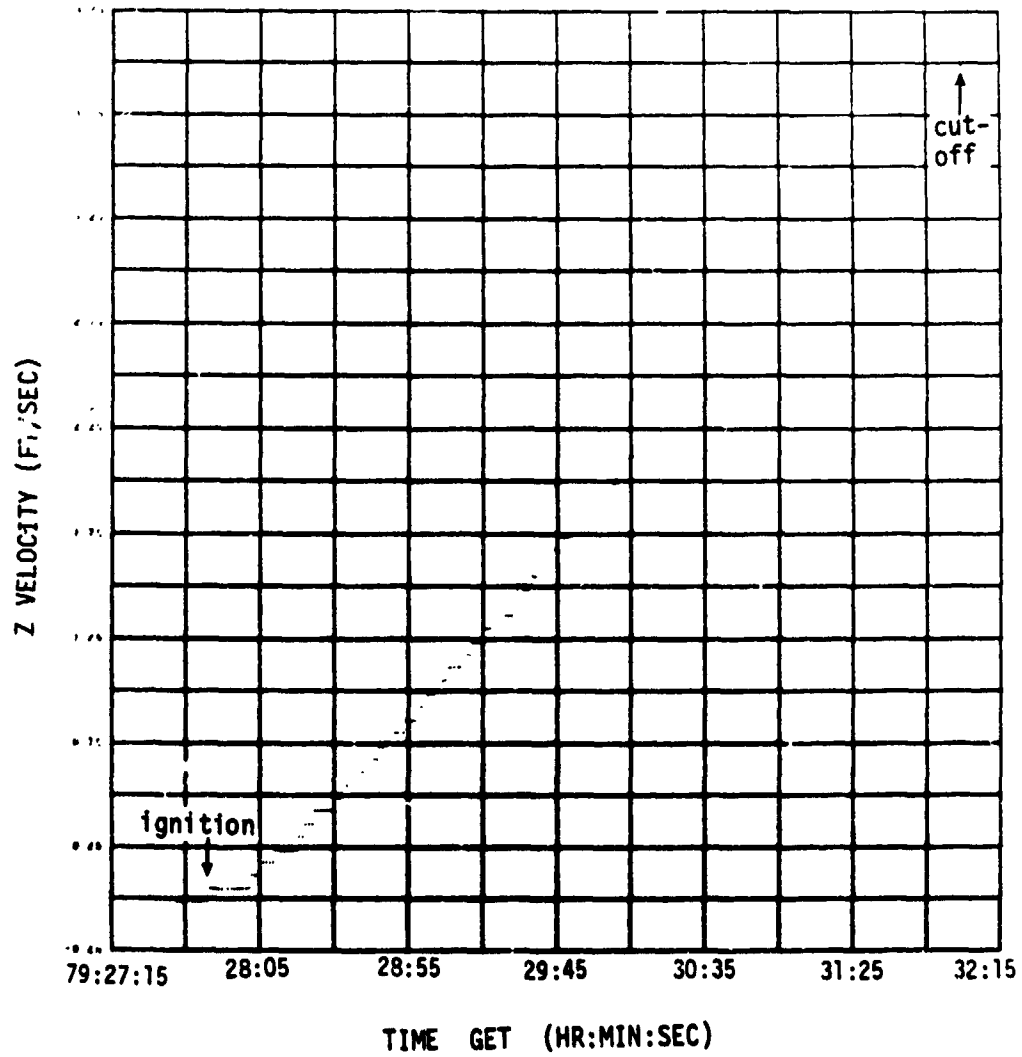
FIGURE 4-35   ACCUMULATED Z-AXIS SENSED VELOCITY
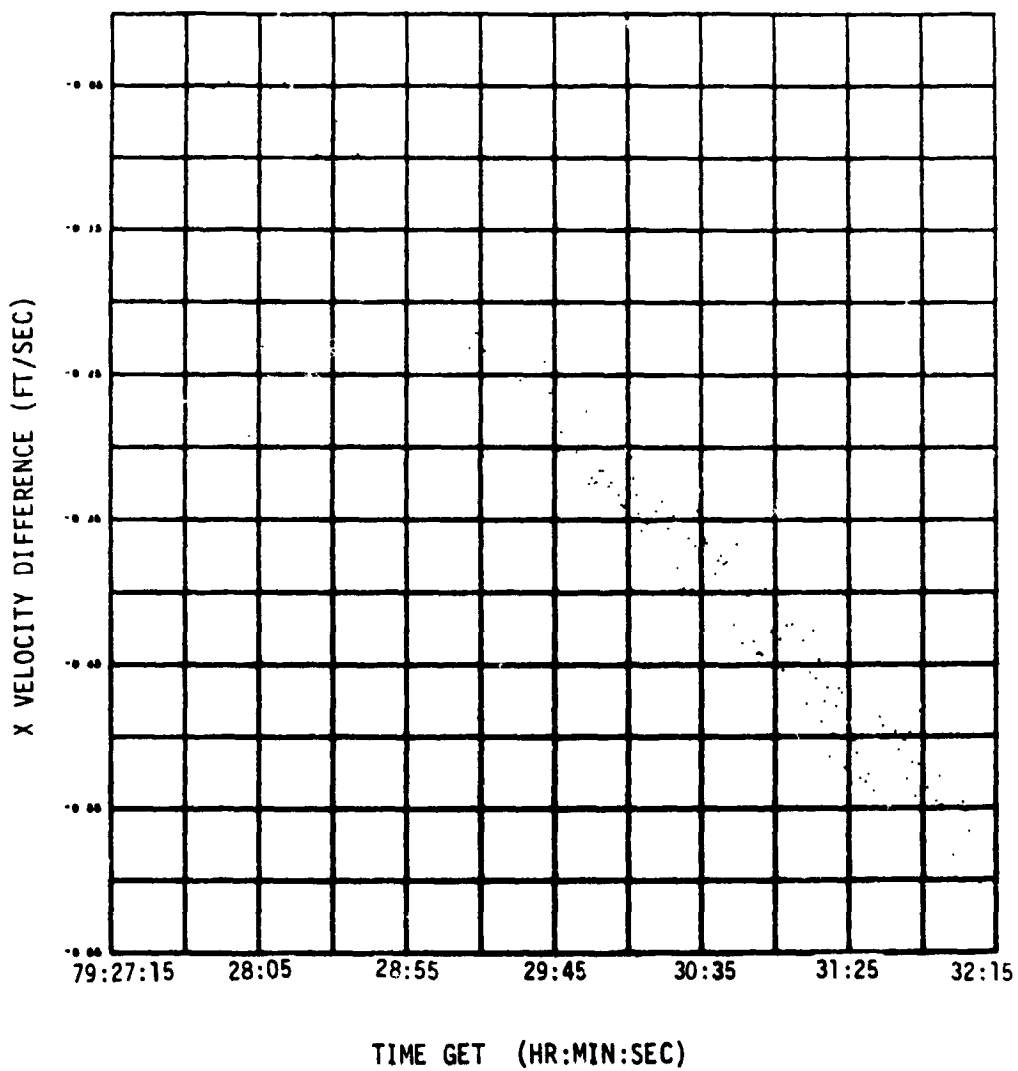
FIGURE 4-36   X AXIS VELOCITY DIFFERENCES
(NO AGS COMPENSATION)
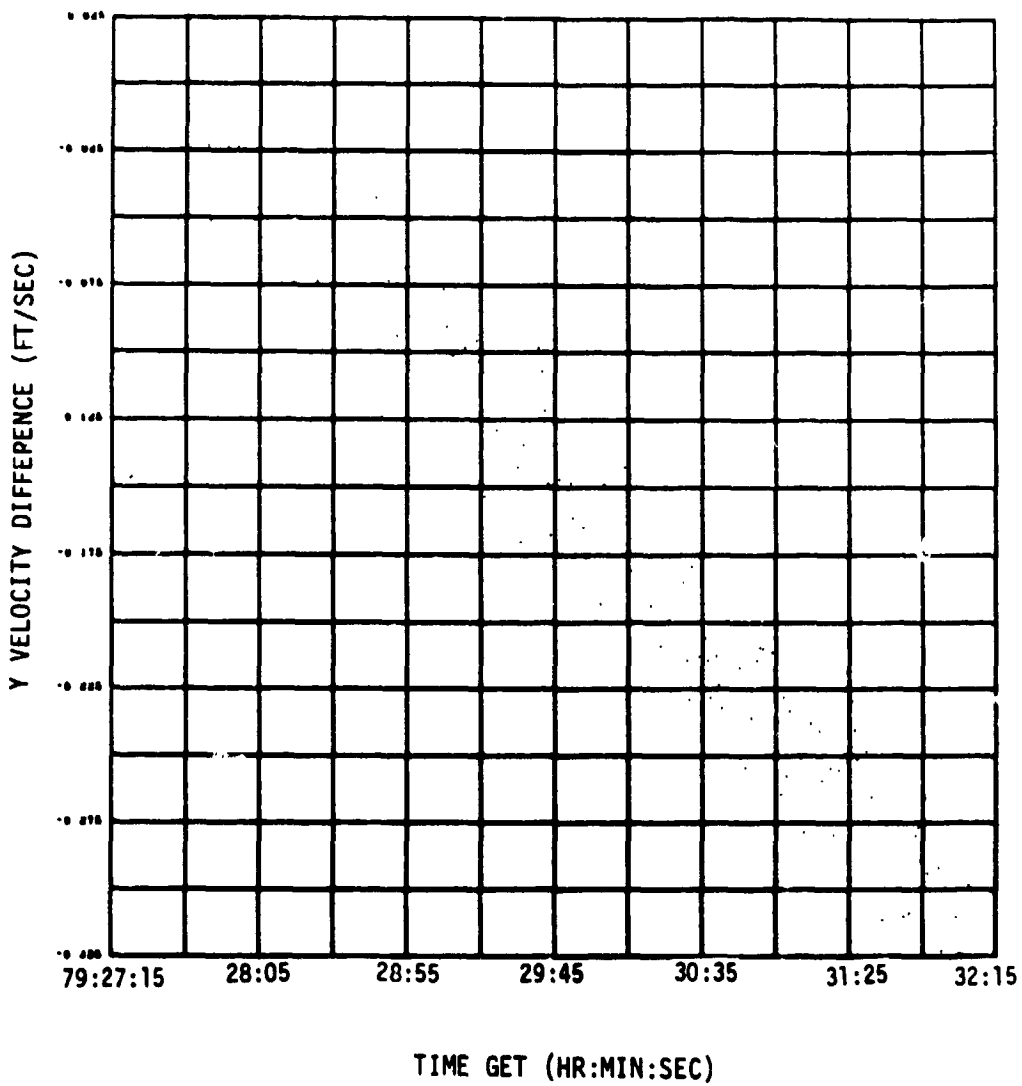
FIGURE 4-37   Y AXIS VELOCITY DIFFERENCES
(NO AGS COMPENSATION)
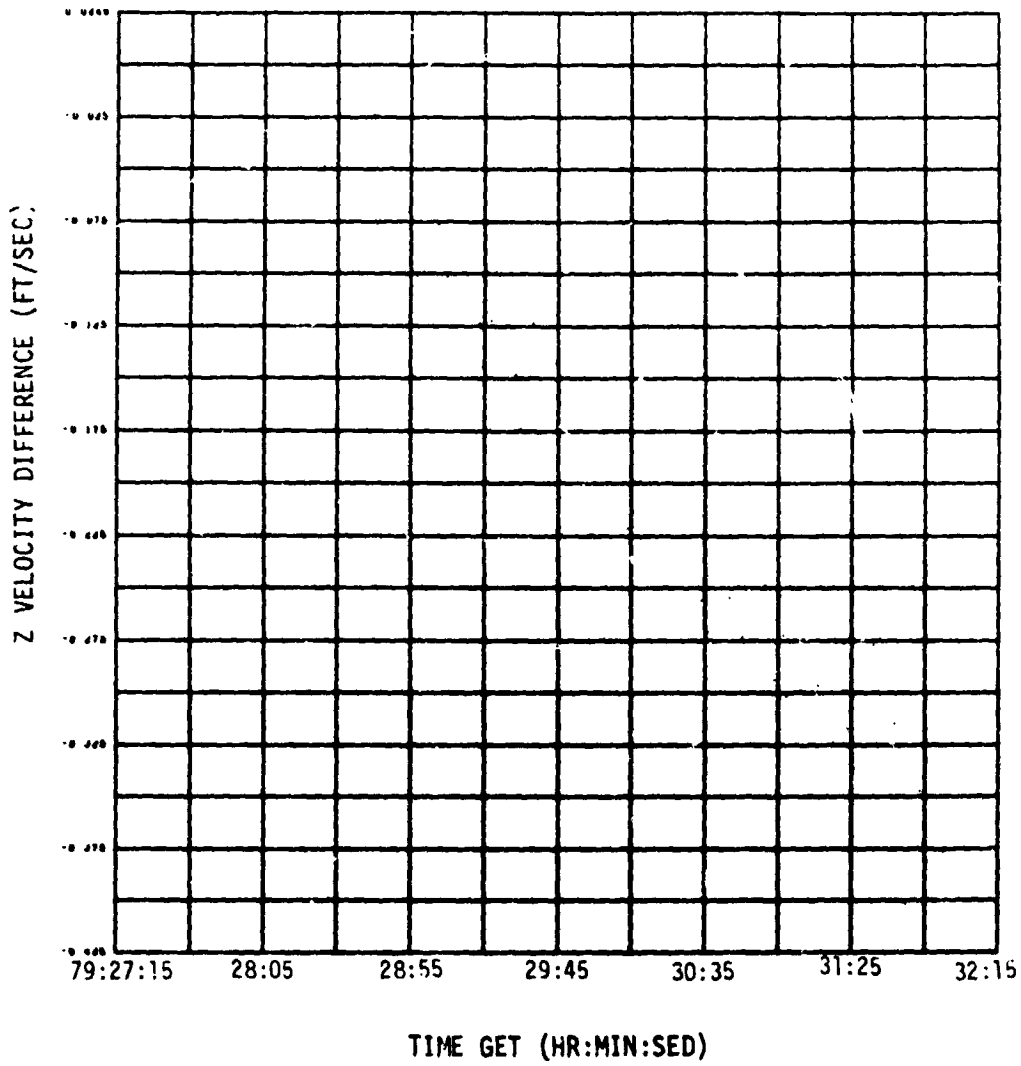
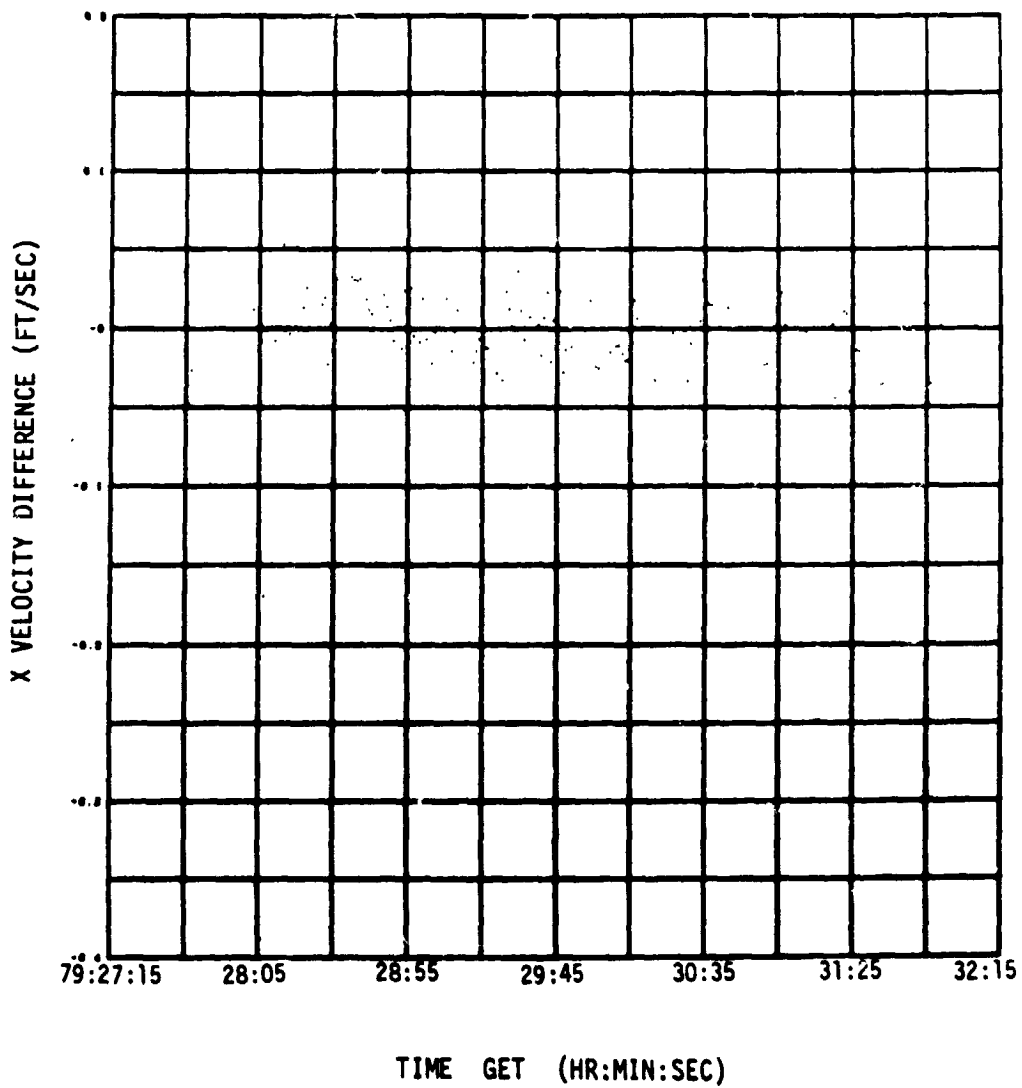FIGURE 4-38   Z AXIS VELOCITY DIFFERENCES
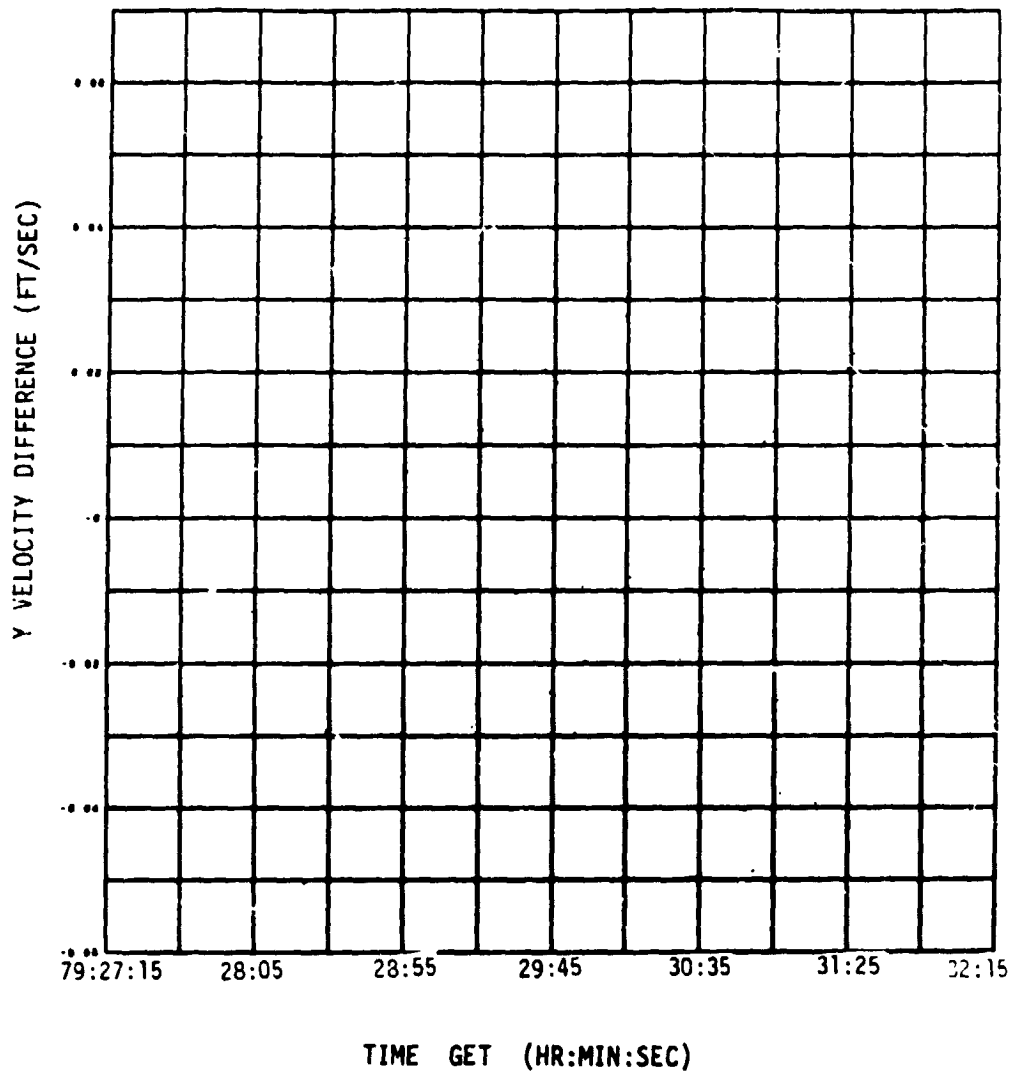(NO AGS COMPENSATION)

4-96

FIGURE 4-39   X AXIS VELOCITY DIFFERENCES (COMPENSATED FOR
               AGS ACCELEROMETER ERRORS)

FIGURE 4-40   Y AXIS VELOCITY DIFFERENCES (COMPENSATED
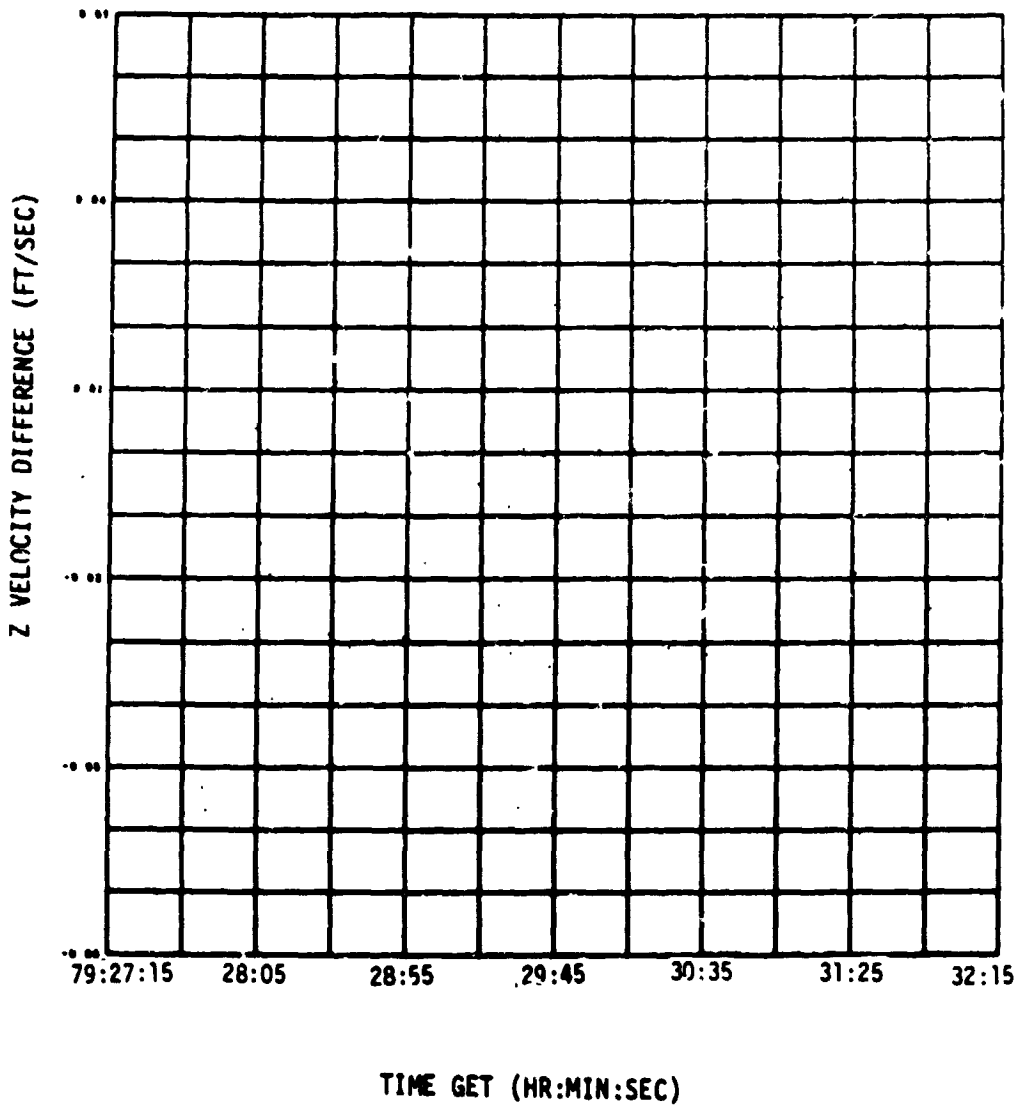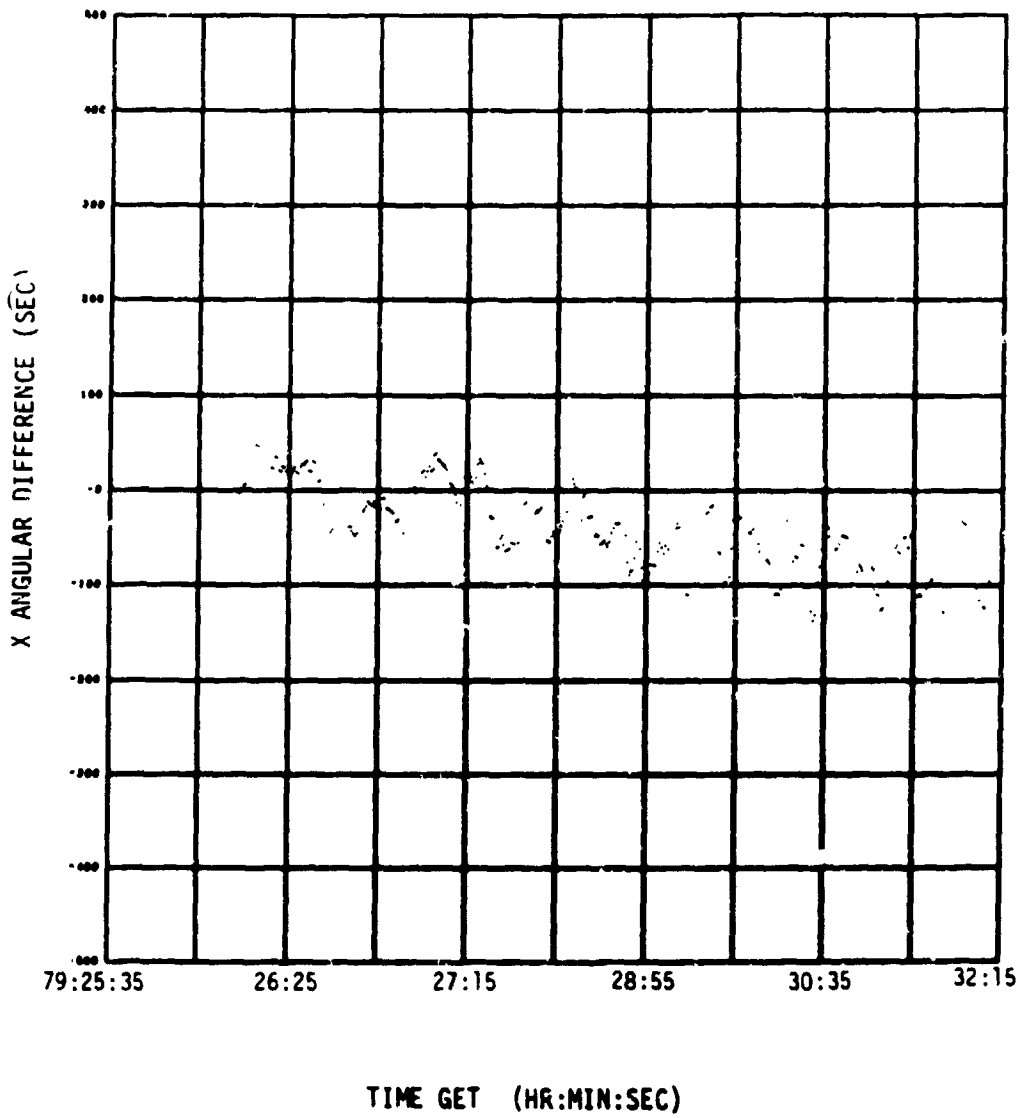FOR AGS ACCELEROMETER ERRORS)

4-98

FIGURE 4-41   Z AXIS VELOCITY DIFFERENCES (COMPENSATED
FOR AGS ACCELEROMETER ERRORS)

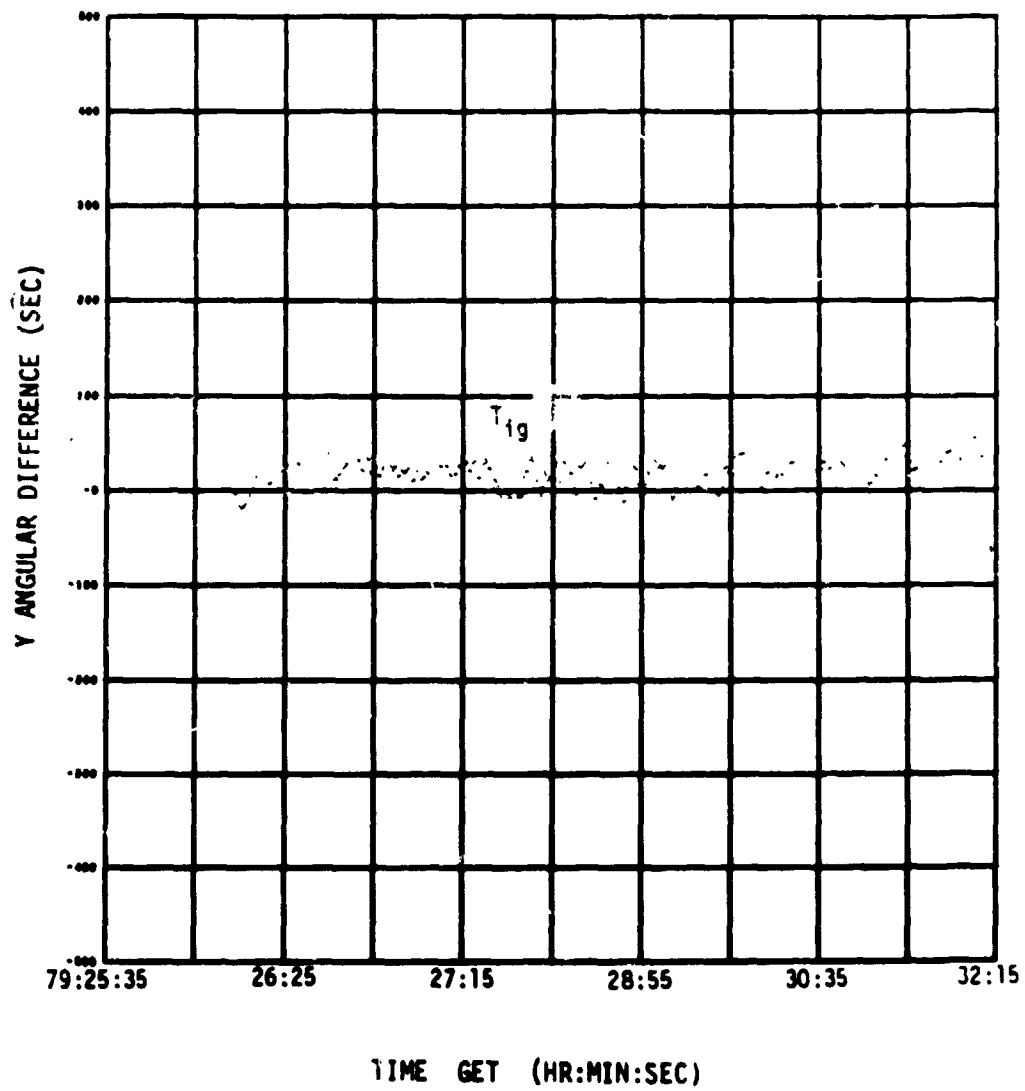FIGURE 4-42   AGS/PGNCS ANGULAR DRIFT - X BODY
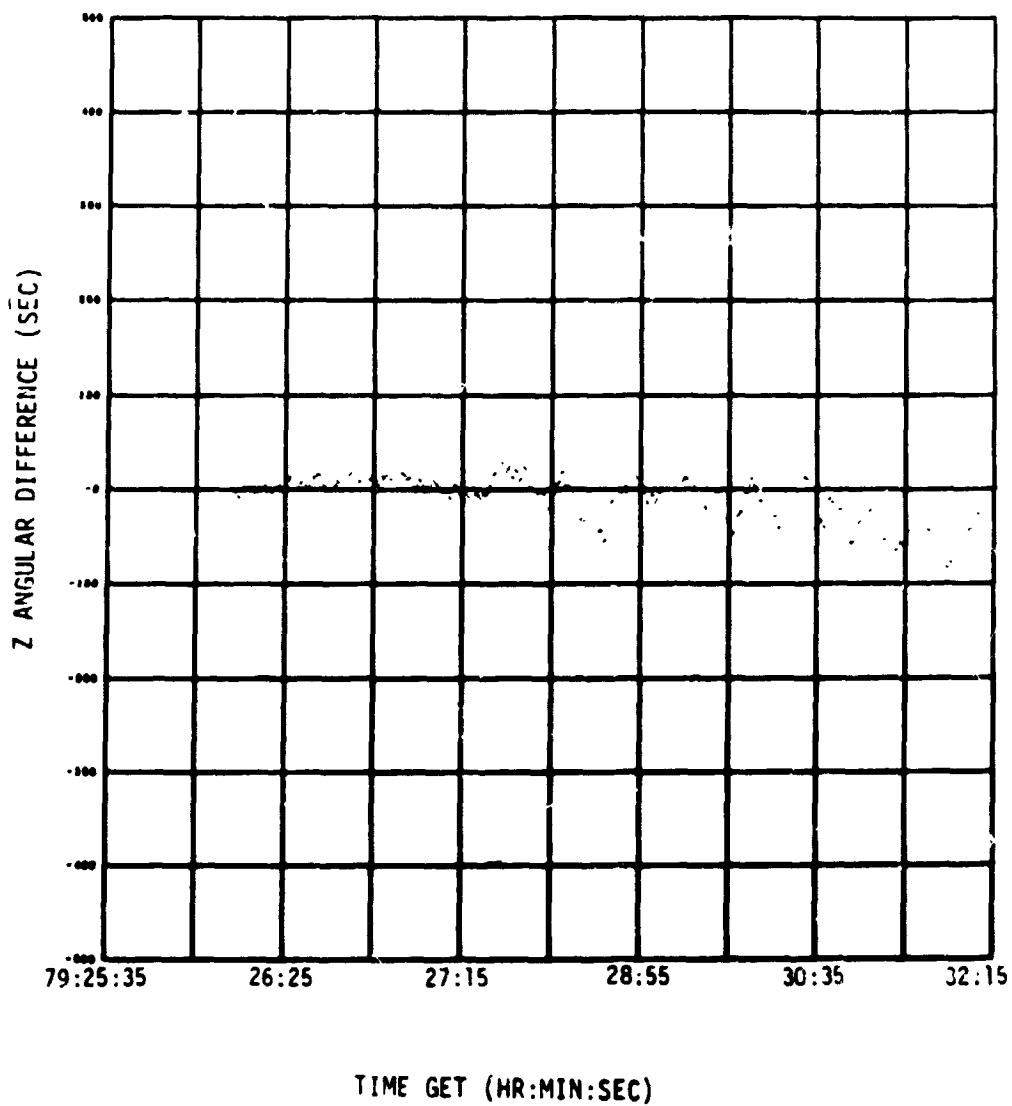
FIGURE 4-43   AGS/PGNCS ANGULAR DRIFT - Y BODY

FIGURE 4-44 AGS/PGNCS ANGULAR DRIFT Z BODY

5.0 SEPARATION MANEUVERS

Prior to re-entry there were two separation maneuvers to extricate the CM from the LM/CM/SM stack.

5.1 SM SEPARATION FROM THE LM/CM

Service module separation was performed by applying a positive X body velocity using the LM RCS thrusters, firing the separation latches, and then applying a retro ΔV using the LM RCS thrusters. The pre-planned maneuver called for 0.5 fps of positive ΔV_X followed by a negative 0.5 fps ΔV_X. LM IMU sensed ΔV at the time of separation indicated approximately 0.7 fps was applied in the positive direction and a subsequent 1.9 fps was applied in the retro direction. Approximately one minute later the retro velocity was decreased by 0.3 fps leaving a net inertial velocity of approximately .9 fps applied to the LM/CM stack and 1.6 fps of relative velocity between the SM and the LM/CM stack.

5.2 LM SEPARATION FROM THE CM

LM separation from the CM was performed by leaving the CM/LM tunnel partially pressurized, firing the latches, and allowing the trapped gas to force the two vehicles apart. A similar type of separation occurred on Apollo 10 between CSM and LM at LM jettison. On Apollo 10, however, the tunnel pressure was approximately 80% higher than on Apollo 13. From the Apollo 10 data, LM separation velocity was determined and then considering the lower tunnel pressure, an impulse was calculated for Apollo 13. Applying the analytical impulse to CM and LM, an estimated ΔV of 2.15 fps and 0.86 fps was calculated for CM and LM, respectively. Actual experienced ΔV at separation was 1.88 fps and 0.65 fps for CM and LM, respectively, indicating good agreement with the estimated impulse. The sensed vectors at separation are derived below.

5.2.1 LM ΔV

After bias correction, PIPA counts telemetered from the LGC indicate the following inertial thrust velocity changes during the 2 second interval 141:30:00.16 to 141:30:02.16 GET bracketing the time of LM jettison.

$$\Delta V_x = -.294 \text{ ft/sec}$$

$$\Delta V_y = .555 \text{ ft/sec}$$

$$\Delta V_z = -.169 \text{ ft/sec}$$

The gimbal angles at the time of separation were: CDUX = -156.1707 deg; CDUY = -31.4429 deg; CDUZ = 57.4145 deg yielding a direction cosine matrix which transforms from platform to body.

$$\Delta \overline{V}_{body} = \begin{bmatrix} -0.65 \\ -0.017 \\ -0.003 \end{bmatrix} \text{ ft/sec}$$

AGS telemetry data shows $V_{BX} = -.625$ during the 1 second interval 141:29:59.85 GET confirming the LM IMU data.

5.2.2 CM ΔV

Since the CMC telemetry was in low-bit-rate (data available at 1/5 the normal sample rate) during separation, it was necessary to compute 10 second DELV's from the available state vector data. Gimbal angles near the center of the 10 second computations cycle were used to transform the inertial accelerations into CM Body Coordinates.

The CM showed evidence of some venting for about 40 seconds after the separation event.

From the reconstructed thrust accelerations it appears that the CM experienced the following velocity change across the separation period:

$$\Delta V_x \text{ (body)} = -1.54 \text{ ft/sec}$$
$$\Delta V_y \text{ (body)} = 0.42 \text{ ft/sec}$$
$$\Delta V_z \text{ (body)} = 0.99 \text{ ft/sec}$$

The CM DSKY display of thrust velocity in body coordinates (V16 N83) during the LM separation maneuver differed significantly from the derived values above due to the large Z PIPA bias error that existed. Application of this Z-PIPA bias error greatly reduces the discrepancy between the magnitudes of the reconstructed and of the DSKY displayed ΔV (from 4.19 ft/sec to 1.98 ft/sec). The remaining 1.08 ft/sec discrepancy is unexplained.

REFERENCES

1. MSC Internal Note, "Apollo 13 Mission Report," 1970.

2. NASA SNA-8-D-027, "CSM/LM Spacecraft Operational Data Book," Vol. III (Mass Properties), Revision 2, 20 August 1969.

3. P. Pantason, Grumman IOC No. LAV-500-853, "Effects of RCS Jet Thruster Plume Reflectors on LM Attitude Control Authority," 17 March 1969.

4. MIT/IL R-567, "Guidance System Operational Plan for Manned LM Earth Orbital and Lunar Missions Using Program Luminary 1C (Rev 130)," Section 3 (Digital Autopilot), Revision 3, October 1969.